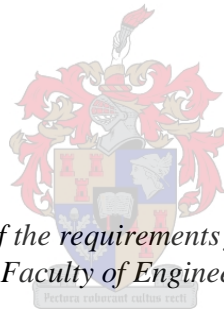


# Software to Aid in the Detailed Design of Tall Post-tensioned Concrete Wind Turbine Towers

by  
Derrick van Schalkwyk



*Thesis presented in fulfilment of the requirements for the degree of Master of Civil Engineering (Research) in the Faculty of Engineering at Stellenbosch University*

Supervisor: Dr. GC van Rooyen

March 2017

# Declaration

By submitting this thesis electronically, I declare that the entirety of the work contained therein is my own, original work, that I am the authorship owner thereof (unless to the extent explicitly otherwise stated) and that I have not previously in its entirety or in part submitted it for obtaining any qualification.

Date: .....March 2017.....

# Abstract

In engineering practice, the process associated with the detailed design of wind turbine towers is often an overwhelming task. This is particularly the case when using sophisticated Finite Element Method (FEM) software to model and analyse wind turbine towers, as these packages generally have significant computational modelling requirements.

The aim of this study is to design custom software specific to tall post-tensioned concrete wind turbine towers, to aid in the detailed design process. Focus is placed on designing software to be computationally inexpensive and user friendly, while still being able to produce accurate analysis results.

To do this, a simplified two-dimensional finite element model, only consisting of 4 Degree of Freedom (DOF) beam elements, is used to represent the wind turbine tower. Although the tower model is simplified significantly, the complexity of the tower is captured using a composite cross section model, which is able to consider nonlinear material properties. The cross section analysis methodology is also designed to consider the effects of internal post-tensioning applied to the tower.

A FEM modal analysis is implemented to calculate the tower frequencies. The model is also analysed using the Stiffness Method and Moment Area Method to obtain tower deflections. Furthermore, iterative numerical approaches are presented in conjunction with these analysis techniques to consider second order effects. By integrating the cross section analysis methodology with the structural analysis techniques, accurate beam element properties, normal stresses and deflections are calculated.

Various case studies are included in this study using the developed methodology and compared to results obtained from literature or existing software as verification. The tests are conducted using a graphical user interface (GUI). The GUI is designed to guide the user through the entire process of analysing a Wind Turbine Generator (WTG) tower, aiding in the model setup, generation of loads on the tower, performing analyses and providing relevant analysis output information.

It has been found that the implemented analysis techniques yield accurate results while significantly less computational effort is expended when compared to sophisticated FEM software.

# Samevatting

In die ingenieurspraktyk is die gedetailleerde ontwerp van windturbine torings dikwels 'n oorweldigende taak. Dit is veral die geval wanneer gesofistikeerde Eindige Element sagteware gebruik word om windturbine torings te modelleer en analiseer, omdat hierdie pakette hoë numeriese modellering vereistes het.

Die hoofdoel van hierdie projek is om sagteware te ontwerp om ondersteuning te bied tydens die gedetailleerde ontwerp proses van hoë nagespande beton windturbine torings. Fokus word geplaas op die ontwerp van gebruikersvriendelike sagteware met relatiewe lae numeriese modellering vereistes, terwyl dit steeds in staat is om akkurate resultate te lewer.

Vir hierdie doel is 'n vereenvoudigde tweedimensionele eindige element model, wat slegs bestaan uit balk elemente met vier vryheidsgrade elk, ontwikkel om 'n windturbine toring te modelleer. Hoewel die toring model aansienlik vereenvoudig is, is die kompleksiteit van die toring vasgevang met behulp van 'n saamgestelde dwarsnit model, wat in staat is om nie-lineêre materiaaleienskappe in ag te neem. Die dwarsnit analise metodiek is ook ontwerp om die effek wat interne voorspanning op 'n toring het in ag te neem.

'n Eindige Element Metode (EEM) modale analise is geïmplementeer om die toring frekwensies te bereken. Die model is ook geanaliseer met behulp van die Styfheidsmetode en Moment Area Metode om toring defleksies te bepaal. Verder word iteratiewe, numeriese benaderings beskryf wat geïntegreer word met bogenoemde analisetegnieke om tweede orde effekte in ag te neem. Deur die integrasie van die dwarsnit analise metode met die struktuuranalise tegnieke, kan akkurate balk element eienskappe, normaalspannings en defleksies bereken word.

Verskeie gevallestudies is ingesluit in hierdie studie met die doel om die ontwikkelde metodiek se resultate te vergelyk met dié verkry vanuit die literatuur of bestaande sagteware. Die toetse word uitgevoer met behulp van 'n grafiese gebruikerskoppelvlak. Die koppelvlak is ontwerp om die gebruiker te lei deur die hele ontwerpproses van die windturbine toring, insluitende die opstelling van die model, die plasing van laste op die toring, die uitvoering van analises en die verskaffing van relevante analiese resultate.

Daar is gevind dat die geïmplementeerde analisetegnieke akkurate resultate lewer, terwyl die ontwikkelde sagteware aansienlik minder tyd en numeriese vereistes het in vergelyking met gesofistikeerde EEM sagteware.

# Acknowledgements

I would like to thank Dr. van Rooyen for being a fantastic mentor. He was inspirational throughout this study, and he guided me to success with patience and a willingness to help.

I would also like to thank Stellenbosch University Department of Civil Engineering for providing funds for the project, and once again for Dr. van Rooyen for his help in arranging the funds.

To my family and friends, thank you for your love and support. You provide me with stability and keep me balanced, and make everything I do more worthwhile.

I would like to thank the Lord for guiding me and keeping me during this study. Looking back now, it feels like everything fell into place perfectly.

*“Behold, I am doing a new thing; now it springs forth, do you not perceive it? I will make a way in the wilderness and rivers in the desert.”*

Isaiah 43:19.

# Contents

Chapter 1: Introduction.....	1
1.1 Background .....	1
1.2 Objectives.....	1
1.3 Methodology .....	2
1.4 Layout of this study.....	2
1.5 Scope .....	3
Chapter 2: Literature review .....	4
2.1 Introduction.....	4
2.2 Transportation difficulties of large wind turbine towers .....	5
2.3 Concrete towers that can overcome transportation difficulties.....	6
2.3.1 Post-tensioned concrete towers using pre-fabricated segments .....	7
2.3.2 Concrete-steel hybrid towers .....	7
2.3.3 Post-tensioned concrete towers using slip-formed construction .....	7
2.3.4 New concrete WTG tower initiative .....	8
2.4 Current software used to analyse wind turbine towers .....	9
Chapter 3: Software specific to wind turbine generators.....	12
3.1 Introduction.....	12
3.2 Simplification of WTG finite element model.....	12
3.3 Modelling of a Wind Turbine Tower.....	13
3.4 UML diagrams of developed software.....	15
3.5 Advantages of the software.....	19
Chapter 4: Cross section analysis .....	20
4.1 Introduction.....	20
4.2 The Model Column Method.....	20
4.2.1 Model Column Method Algorithm.....	21
4.2.2 Discretization of the cross section.....	21
4.2.3 Calculating the strain distribution over the cross section .....	22
4.2.4 Calculating the updated neutral axis and cross section properties .....	23

4.2.5	Calculating internal forces.....	25
4.3	Modelling of the reinforced concrete circular hollow section.....	26
4.4	Implemented nonlinear material models.....	27
4.4.1	Tension stiffening.....	28
4.4.2	Stress-strain relationship for concrete.....	29
4.4.3	Stress-strain relationship for reinforcing steel .....	32
4.5	Algorithm developed to calculate the cross section properties .....	36
4.6	Verification of cross section analysis results .....	37
Chapter 5:	Vibration Analysis .....	40
5.1	Introduction.....	40
5.2	FEM modal analysis.....	41
5.2.1	Derivation of the eigenvalue problem.....	42
5.2.2	Stiffness and mass matrix formulation .....	43
5.3	Vortex induced transverse vibrations .....	44
5.4	Verification of frequency analysis output.....	47
Chapter 6:	Wind Loading.....	51
6.1	Introduction.....	51
6.2	Summary of implemented codes and guidelines .....	52
6.3	SANS 10160-3:2011 .....	52
6.4	IEC 61400-1 (2005) .....	53
6.4.1	Extreme wind speed model.....	55
6.5	ASCE 7-10 (2010) .....	56
6.5.1	Velocity pressure calculation procedure.....	56
6.5.2	Design wind force calculation procedure.....	58
6.6	Sensitivity to vibration according to BetonKalender.....	61
Chapter 7:	Deflection and Internal Stress Analysis.....	63
7.1	Introduction.....	63
7.2	Internal Moment and Shear Force calculations .....	64
7.3	Moment Area Method for deflection calculation.....	64
7.4	Direct Stiffness Method for deflection calculations .....	67

7.5	Geometric and Physical Nonlinear Analysis .....	68
7.6	Verification of Analysis results .....	70
7.6.1	Linear Material Properties Analysis Comparison and Verification .....	70
7.6.2	Geometric and Physical Nonlinear Analysis Comparison and Verification.....	72
7.7	Case study: 120m High RC Tower.....	76
Chapter 8:	Modelling of a Post-tensioned Concrete Tower.....	79
8.1	Introduction.....	79
8.1.1	External unbonded prestressing tendons.....	79
8.1.2	Internal grouted prestressing .....	80
8.2	Methodology developed to consider internal grouted post-tensioning .....	81
8.2.1	Cross section model used to consider post-tensioning.....	81
8.2.2	Algorithm developed to consider post-tensioning.....	81
8.2.3	Implemented material model for prestressing steel .....	82
8.3	Case studies.....	83
8.3.1	Case study A: Individual tower segment post-tensioning (C35/45 concrete) .....	83
8.3.2	Case study B: Individual tower segment post-tensioning (C50/60 concrete) .....	85
8.4	Comments on case study results .....	86
Chapter 9:	Graphical User Interface.....	87
9.1	Introduction.....	87
9.2	User Manual .....	88
9.2.1	Model setup.....	88
9.2.2	Performing analyses .....	90
Chapter 10:	Conclusions and recommendations.....	95
10.1	Summary.....	95
10.2	Conclusions.....	95
10.3	Recommendations .....	96
References	.....	97

# List of Figures

Figure 2.1: Steel tower diameter constraints during transport (U.S. Department of Energy, 2015).	5
Figure 2.2: Turbine blade transportation obstacle (U.S. Department of Energy, 2015)	6
Figure 2.3: Slip-form system description (Energy world, 2008)	8
Figure 2.4: New concrete WTG tower initiative (Dvorak, 2016)	9
Figure 2.5: 8-Node brick element used to mesh a wind turbine tower (Way, 2014)	10
Figure 2.6: 8-Node quadrilateral curved shell element (Diana 9.4.4, 2012)	10
Figure 3.1: 4DOF beam element used in the FE model	13
Figure 3.2: Components of a wind turbine tower (Way, 2014)	13
Figure 3.3: Discretization of a WTG model	15
Figure 3.4: General UML diagram of developed software	16
Figure 3.5: UML diagram of reinforced concrete circular hollow cross section (a)	17
Figure 3.6: UML diagram of reinforced concrete circular hollow cross section (b)	18
Figure 3.7: UML diagram of reinforced concrete tower segment and beam element	19
Figure 4.1: Comparison between radial and horizontal elements on a circular hollow section	22
Figure 4.2: Typical cross section subject to a moment and axial load	25
Figure 4.3: Modelling of a reinforced concrete CHS	27
Figure 4.4: Tension stiffening effect (Piles Machinery, 2013)	28
Figure 4.5: Tension Stiffening effect for different percentages of reinforcing steel (Grünberg & Göhlmann, 2013)	29
Figure 4.6: Nonlinear stress-strain curve for concrete, according to Eurocode 2	32
Figure 4.7: Idealized and design stress-strain diagrams used for reinforcing steel in compression (EN 1992-1-1:2004, 2004)	32
Figure 4.8: Demonstration of how the developed software finds the curvature for a given moment	37
Figure 4.9: Comparison of the cross section analysis results generated by the developed software to the example found in BetonKalender (Grünberg & Göhlmann, 2013)	38
Figure 5.1: Example of a Campbell diagram for a three bladed wind turbine (Manwell, et al., 2009)	40
Figure 5.2: Relationship between the Strouhal number and Reynolds number (Techet, 2005)	46
Figure 5.3: Relationship between the Strouhal number and the ratio of the tower height to the tower top diameter (DNV/Risø, 2002)	46
Figure 5.4: Test 4 mode shapes generated by the developed software	49
Figure 5.5: Test 4 mode shapes generated by Prokon	50
Figure 7.1: Moment Area Method Theorem 1 visualisation (BridgeArt.net, 2016)	65
Figure 7.2: Moment Area Method Theorem 2 visualisation (BridgeArt.net, 2016)	65
Figure 7.3: Moment area method	67

Figure 7.4: Additional moment due to P-delta effects (Van Zyl, 2014) .....	69
Figure 7.5: Schematization of the test model used to verify the analysis results when only linear material properties are considered .....	71
Figure 7.6: Two configurations of the implemented material models (Walls, 2016) .....	73
Figure 7.7: Implement test model (Walls, 2016) .....	73
Figure 7.8: Deflection comparison of Test 1 with increasing end moment with $E_0 = 200\text{GPa}$ and $\beta = -1000$ .....	74
Figure 7.9: Deflection comparison of Test 1 with increasing end moment with $E_0 = 20\text{GPa}$ and $\beta = -50$ .....	74
Figure 7.10: Deflection comparison of Test 2 with increasing end moment, lateral and axial loads with $E_0 = 200\text{GPa}$ and $\beta = -1000$ .....	75
Figure 7.11: Deflection comparison of Test 2 with increasing end moment, lateral and axial loads with $E_0 = 20\text{GPa}$ and $\beta = -50$ .....	76
Figure 8.1: Unguided (left) vs. corbel-guided (right) external prestressing tendons according to Grünberg & Göhlmann (2013). Image obtained from a journal by Von Der Haar & Marx (2015) ...	80
Figure 8.2: Idealized and design stress-strain diagrams for prestressing steel. Obtained from Eurocode 2 (EN 1992-1-1:2004, 2004) .....	82
Figure 9.1: How to specify input parameters using the GUI.....	88
Figure 9.2: Entering generator input parameters using the GUI .....	89
Figure 9.3: Entering wind loading input parameters using the GUI .....	89
Figure 9.4: The GUI displaying a simple representation of the WTG tower and input parameters .	90
Figure 9.5: Performing a modal analysis using the GUI.....	91
Figure 9.6: Performing a structural analysis using the GUI.....	92
Figure 9.7: Illustration of GUI after the successful completion of a structural analysis.....	92
Figure 9.8: An illustration of the tower deflection along with the analysis output information .....	93
Figure 9.9: Illustration of warning message along with suggestions on the amount of post-tension steel required to avoid yielding.....	94
Figure 9.10: Illustration of success message after the post-tension forces have successfully been applied to the tower.....	94

# List of Tables

Table 4.1: Strength and deformation characteristics for concrete (EN 1992-1-1:2004, 2004).....	31
Table 5.1: Strouhal numbers for various cross sections (EN 1991-1-4:2005, 2005) .....	47
Table 5.2: Deflection analysis test model details .....	48
Table 5.3: Frequency modal analysis output verification .....	48
Table 5.4: Time required to perform modal analysis tests .....	50
Table 6.1: Basic parameters for wind turbine classes (IEC 61400-1:2005, 2005).....	54
Table 6.2: Terrain Exposure Constants (ASCE 7-10, 2010) .....	58
Table 6.3: Calculation procedure of the structural factor, $C_f$ , for chimneys, tanks, rooftop equipment and similar structures (ASCE 7-10, 2010) .....	61
Table 7.1: Comparison of the deflections (in mm) obtained from the Prokon analysis to the implemented analysis techniques .....	72
Table 7.2: % Difference of the results obtained from the implemented analysis techniques to the results obtained by Prokon.....	72
Table 7.3: Lateral wind loads acting on the tower.....	76
Table 7.4: Input parameters of the model used in the case study.....	77
Table 7.5: Deflection comparison (mm) of the various implemented analysis techniques.....	77
Table 7.6: Base moment (MNm) comparison between the various implemented analysis techniques .....	78
Table 7.7: Computation time (seconds) comparison between the various implemented analysis techniques .....	78
Table 8.1: Case study A: Second order nonlinear analysis results before individual tower segment post-tensioning .....	84
Table 8.2: Case study A: Second order nonlinear analysis results after individual tower segment post-tensioning .....	84
Table 8.3: Case study B: Second order nonlinear analysis results before individual tower segment post-tensioning .....	85
Table 8.4: Case study B: Second order nonlinear analysis results after individual tower segment post-tensioning .....	85

# Nomenclature

## Abbreviations

DOF – Degree of Freedom  
 EWM – ICE 61400-1 Extreme Wind Speed Model  
 FEM – Finite Element Method  
 GUI – Graphical User Interface  
 SLS – Serviceability Limit State  
 ULS – Ultimate Limit State  
 UML – Unified Modelling Language  
 WTG – Wind Turbine Generator

## Roman Upper Case

$A_k$  – Area of the  $k^{\text{th}}$  element being investigated ( $\text{m}^2$ )  
 $A_f$  – ASCE 7-10 projected area normal to the wind ( $\text{m}^2$ )  
 $C_f$  – ASCE 7-10 force coefficient  
 $C_s C_d$  – Structural factor  
 $E_{com}$  – Tangent modulus of elasticity of concrete (GPa)  
 $E_{cm}$  – Secant modulus of elasticity of concrete (GPa)  
 $E_k$  – Young's modulus of elasticity of the  $k^{\text{th}}$  element being investigated (GPa)  
 $E_p$  – Design value of modulus of elasticity of prestressing steel (GPa)  
 $E_s$  – Young's modulus of elasticity of reinforcing steel (GPa)  
 $F$  – ASCE 7-10 design wind force (N)  
 $G_f$  – ASCE 7-10 gust effect factor  
 $I_k$  – Second Moment of Inertia of the  $k^{\text{th}}$  element being investigated ( $\text{m}^4$ )  
 $I_{ref}$  – IEC 61400-1 expected value of the turbulence intensity  
 $K_d$  – ASCE 7-10 directionality factor  
 $K_z$  – ASCE 7-10 velocity pressure exposure coefficient  
 $K_{zt}$  – ASCE 7-10 topographical factor  
 $M(h)$  – Internal moment at height  $h$  (Nm)  
 $M_{P-\delta,h}$  – P-delta moment at height  $h$  (Nm)  
 $M_z$  – Applied moment (Nm)  
 $N_x$  – Applied axial force (N)  
 $Q$  – ASCE 7-10 background response

$R$  – ASCE 7-10 resonant factor

$V$  – ASCE 7-10 basic wind speed (m/s)

$V(h)$  – Shear force at height  $h$  (N)

$V_{cri}$  – Critical wind speed (m/s)

$V_{ref}$  – IEC 61400-1 reference wind speed (m/s)

### Roman Lower Case

$c'$  – Shifted neutral axis position, measured relative to the datum position (m)

$f_{cm}$  – Mean value of the concrete cylinder compressive stress (MPa)

$f_{ctk;0.05}$  – Characteristic tensile stress of concrete with a 5% chance of being exceeded (MPa)

$f_{ctd}$  – Design tensile strength of concrete (MPa)

$f_{ctm}$  – Mean tensile strength of concrete (MPa)

$f_{pk}$  – Characteristic tensile strength of prestressing steel (MPa)

$f_{p0.1k}$  – Characteristic 0.1% proof-stress of prestressing steel (MPa)

$f_{yk}$  – Characteristic yield strength of the reinforcing steel (MPa)

$g_Q$  – ASCE 7-10 peak factor for background response

$g_R$  – ASCE 7-10 peak factor for resonance

$g_V$  – ASCE 7-10 peak factor for wind response

$q_z$  – ASCE 7-10 velocity pressure (Pa)

$St$  – Strouhal number described below

$\omega_i$  – The  $i^{th}$  natural frequency of the tower (Hz)

### Greek symbols

$\alpha_{Ed}$  – Design modular ratio

$\beta_t$  – Coefficient that considers the influence of the duration of the loading or repeated loading

$\varepsilon_s$  – Strain in the reinforcing steel (m/m)

$\varepsilon_{c1}$  – Concrete strain associated with peak compressive stress (m/m)

$\varepsilon_k$  – Concentric strain (m/m)

$\varepsilon_{srd}$  – Design strain corresponding to the appearance of the first crack (m/m)

$\varepsilon_{ud}$  – Design strain of reinforcing or prestressing steel at maximum load (m/m)

$\varepsilon_{uk}$  – Characteristic strain of reinforcing or prestressing steel at maximum load (m/m)

$\kappa_z$  – Curvature of the  $k^{th}$  element being investigated ( $m^{-1}$ )

$\rho_s$  – Ratio of the area of reinforcing steel to the area of the concrete

$\sigma_k$  – Stress of the  $k^{\text{th}}$  element being investigated (Pa)

$\sigma_{sr}$  – Stress leading to the appearance of the first crack in the concrete (MPa)

$\gamma_c$  – Partial factor of safety for concrete

# Chapter 1: Introduction

## 1.1 Background

As die global wind industry trends to taller wind turbine towers to gain access to stronger, steadier winds, designs other than the typical tubular steel tower become an economical solution. Recent studies have shown that when tower hub heights exceed 100m, concrete and concrete-steel hybrid towers become less expensive in terms of material costs (Way, 2014). Transport limitations also pose a problem with steel towers when diameters exceed 4.5m. Currently in South Africa, the trend is also moving to taller wind turbine towers, such as the 138MW Gouda Wind Facility, which makes use of 100m concrete towers (ACCIONA Energy, 2016).

With the South African wind industry still in its infancy, most South African wind farm projects rely on specialist engineering companies abroad to design the wind turbine towers. DCD, a manufacturing and engineering company, manufactured the first 80m tubular steel tower in South Africa, which was under licence from the German engineering company, Aerodyne (DCD Mining and Energy, 2016). Nordex SE, a German wind turbine company that designs, sells and manufactures wind turbines, entered into an agreement with Spanish wind turbine makers, Acciona Windpower (Kahn, 2016). Together they formed a consortium with the South African construction group, Aveng, among other partners, which developed the Gouda Wind Facility (Creamer media reporters, 2015). The towers constructed at the Gouda Wind Facility were designed in house by Acciona Windpower in Pamplona, Spain (Cook, 2016).

Currently, no official design code exists that gives guidance on the design of wind turbine towers in South Africa. If a South African structural engineer should attempt to design a safe and economical wind turbine tower, the engineer is faced with the task of combining various codes and guidelines. The modelling of the tower poses the next difficulty. Although various Finite Element Method (FEM) software packages exist which could be used to analyse a wind turbine tower, the process of setting up the model could become very complex and time consuming. This is especially the case with post-tensioned reinforced concrete towers, where the modelling of the reinforcing alone could become expensive in the workplace environment.

## 1.2 Objectives

The overall objective of this study is to design suitable software to aid in the detailed design of tall post-tensioned reinforced concrete wind turbine towers. The software should be designed to be computationally inexpensive and user friendly, while maintaining the ability to generate accurate results compared to existing commercial software.

## 1.3 Methodology

To achieve the aim of this study, a short literature study is performed in order to better understand the wind turbine tower designs that could be incorporated to replace the traditional tubular steel towers. The literature review also includes data of how wind turbine generators (WTG) have been analysed in past studies using general purpose FEM software and the complexity associated with this task.

Object modelling is then used to develop software specifically for the analysis of tall post-tensioned concrete towers. Focus is placed on the modelling of the tower geometry so that a finite element (FE) model can be generated that accurately simulates the actual tower. A graphical user interface (GUI) is developed to aid the user in setting up the FE model. Wind loads are also generated and added to the FE model based on the inputs from the user, through the use of the GUI. The GUI is also designed to generate relevant output associated with each type of analysis. To contribute to the convenience of the software, the developed software tools are integrated so that input parameters are updated automatically when changes are made to the model.

During the finite element formulation, the element properties are obtained by a cross section analysis, which is performed at various heights along the tower. In the cross section analysis, physical nonlinearities associated with each material comprising the cross section are considered. The cross section analysis technique is also extended to include the effects of internal grouted post-tensioning. The FE model is then analysed to provide the user with principal design stresses, tower deflections and tower fundamental frequencies. Geometric nonlinearities associated with the tower are taken into account through the implemented structural analyses.

Various case studies are included throughout this study for verification purposes, which compare the results of the developed software to that of existing commercial software.

Eclipse Integrated Development Environment (IDE) is used as the software development environment for this study. Java version 8 is used as computing language. JavaFX is used to develop the graphical user interface (GUI).

## 1.4 Layout of this study

Due to the nature of this study, it is sensible to address every chapter independently. For every chapter, literature is included that gives a background to the subject. From the various methods discussed in the literature, a suitable approach is chosen and implemented. At the end of every chapter, the implemented methods are verified by comparing the results to the results obtained from existing software or proven approaches.

## 1.5 Scope

This study focusses specifically on the analysis of the towers of onshore WTGs. The analysis of the tower foundation and soil properties are excluded from this study. A fixed connection at the base of the tower is thus assumed for all of the analyses performed in this study. The study includes a proposal on how to obtain the external wind loading on the tower, but excludes the determination of loads acting on the blades and nacelle. The software is designed so that the user should provide the generator loads. The generator loads are then added to the FE model, along with the wind loads acting on the tower.

Due to wind turbine towers generally being classified as dynamically sensitive structures, design guidelines are given that provide guidance on how to ensure that the towers will not be susceptible to resonance effects. This is discussed in Chapter 6: Wind Loading. To aid in this, a FEM model analysis is implemented to calculate the fundamental frequency of the tower. A full dynamic analysis is excluded from this study, but dynamic effects are partially taken into account in the wind calculations.

Concerning the cross section analysis, the Euler-Bernoulli assumptions of plane sections remain plane must hold. Shear deformations are thus not considered.

The FE model is extended to consider the effects of post-tensioning. This study only considers the case where internal grouted post-tensioning is applied.

# Chapter 2: Literature review

## 2.1 Introduction

South Africa has significant potential for wind energy (Kahn, 2016). Favourable wind conditions particularly exist along the west and east coast, with average wind speeds reaching 8 m/s (meters per second) or greater. This is ideal for wind energy production (Way, 2014). With the largest tower in South Africa only reaching a hub height of 100m (Turbines.co.za, 2016), as opposed to European towers reaching hub heights of 135m, a significant amount of wind resources have not been utilised.

The advancement of wind turbine technology, construction methods and materials have unlocked wind resource areas, which were previously not considered as viable options due to the lack of consistent wind volumes. By reaching stronger, steadier wind speeds, the possible wind energy capacity has increased globally. The U.S. Department of Energy released a report stating that the advancement in turbine technology could lead to the generation of electricity in all fifty states (U.S. Department of Energy, 2015). The report also estimates that the technical potential for wind deployment in the U.S. can increase by 54% if tower hub heights are assumed to increase from 80m to 110m.

Tall wind turbine technology is already well rooted in Europe, which plays host to the tallest onshore tower in the world, namely, the E126 wind turbine. Manufactured by the German wind turbine manufacturer, Enercon, the E126 wind turbine stands at a hub height of 135m and has a rated power of 7.580MW (Enercon, 2015).

The erection of wind farms in South Africa not only contributes to countering the growing demand of uninterrupted electricity, but also has a significant benefit on the development of local communities. The Jeffrey's Bay wind farm for example, which reached commercial operations in 2014, implemented socio-economic and enterprise development programmes. Funded by a percentage of the project's operational revenues, these programmes aim to develop the skills needed to support the growth of the renewable energy industry in South Africa (Jeffrey's bay wind farm, 2016). During the construction of the wind farm, more than 700 people worked on site, of whom 45 percent were procured from the local community (South Africa info, 2014).

As of July 2016, the unemployment rate in South Africa stands at 26.6% (Trading Economics, 2016). The erection of wind farms could have a positive impact in providing careers and skill development opportunities. This is especially so in rural areas, where new wind farms could boost the local economy significantly.

## 2.2 Transportation difficulties of large wind turbine towers

The construction of tall WTGs pose many difficulties, most of which are associated with the transportation of its components to the construction site. Tower components are restricted to a height of 4.5m when transported on South African roads. This is the main disadvantage of the construction of tubular steel towers. Alternative means of increasing the stiffness of steel towers, such as increasing the wall thickness, are less effective and economical than increasing the diameter of the tower. This situation is illustrated in Figure 2.1. One way to overcome the transportation limit of steel towers is to fabricate half diameter segments of the tube and assemble it on site. This would however increase the cost of the project due to the design of the connections and the increase of construction time used to assemble the towers.

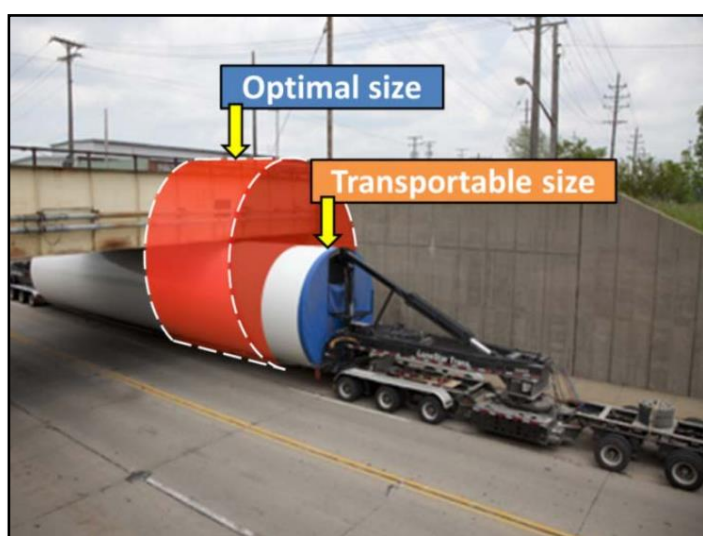


Figure 2.1: Steel tower diameter constraints during transport (U.S. Department of Energy, 2015).

With the increase in tower height, other components comprising the WTG, such as the nacelle, hub and blades, increase proportionally. These components could also cause transportation problems and could have a significant impact on the overall project cost. Figure 2.2 demonstrates how the transportation of large blades can become problematic. Blades are generally limited to 53m so that a reasonable turning radius can be maintained.



Figure 2.2: Turbine blade transportation obstacle (U.S. Department of Energy, 2015)

To attach the increasingly large non-structural components to the support structure, bigger mobile cranes are required. The mass of a 5-MW nacelle is approximately 173 tons, including the generator and gearbox. Due to the significant lift height and mass of these components, a large capacity crane is required (NREL, 2014). The transportation of larger crane classes to site poses a significant challenge. A 1,600-t crane, for example, has a width of nearly 13m. This is wider than a typical two-lane roadway, including shoulders. In addition to this, difficulties arise when these large cranes need to be manoeuvred in complex terrain on site. One solution that could partially solve this problem is to use two smaller cranes, rather than one big one. Using two cranes simultaneously roughly doubles the capacity of a single crane, and can increase stability during the hoisting of components (NREL, 2014). Other solutions suggest the idea of a “self-erecting” tower, in which tower components are transported to the top of the tower by means of a turbine lifting platform (TLP), which is attached to the side of the tower (D.H. Blattner & Sons Inc, 2003). In 2001, Valmont Industries Inc. demonstrated that a wind turbine could be constructed by only using small cranes, if any (Renewable Energy World, 2002). Valmont Industries Inc. produced a 60m (200ft) wind turbine tower in Nebraska using a TLP to lift a Vestas V-47, 660kW turbine to the top of the tower (Power engineering international, 2001).

### 2.3 Concrete towers that can overcome transportation difficulties

Concrete is a construction material used extensively throughout the world, and is especially favoured as construction material in South Africa. Although the use of concrete towers is still a relatively new concept in the wind industry, it is rapidly gaining popularity. A concrete WTG tower can either be constructed using pre-fabricated segments or in-situ, using slip-formed construction.

One of the biggest advantages of using concrete WTG towers is its transportability. Another advantage associated with concrete WTG towers, is the reduction of noise levels during turbine operation. This is due to the increased damping effect of concrete when compared to the high

stiffness of steel. It is also believed that the task of maintaining concrete towers is simpler than compared to steel towers (Way, 2014).

### 2.3.1 Post-tensioned concrete towers using pre-fabricated segments

There are various designs that have been developed to overcome some of the transportation difficulties mentioned above. Some have proven to be economic alternatives and are already being implemented, such as the E126 concrete towers designed by Enercon. The E126 tower is constructed out of pre-cast reinforced concrete segments small enough to be transported. The segments are then assembled on site and post-tensioned.

The 138MW Gouda Wind Facility in the Western Cape made use of a tower similar to that used to support the E126 wind turbine. As in the case with the E126 WTG, pre-cast sections were used to construct the towers at Gouda. Seventeen tower segments were used per tower, which reached a height of 100m once assembled. Self-compacting concrete was used, which allowed the fabrication of tower segments for nearly two towers per week. The tower segments were initially prestressed internally to resist cracking of the concrete during transportation, handling and erection. The completed towers were then post-tensioned externally once assembled on site (Cook, 2016).

### 2.3.2 Concrete-steel hybrid towers

Another alternative, in which the transportation difficulties associated with large diameter tower segments can be overcome, is by using concrete-steel hybrid towers. Concrete-steel hybrid towers are rapidly gaining popularity, due to its cost-effectiveness and simplicity (Way, 2014). These towers consist of a concrete bottom segment, constructed by either pre-cast segments or slip-formed construction. With no limit on the diameter of the concrete bottom segment, the necessary stiffness requirements can be obtained. The speed of construction is still maintained using the traditional steel top section, which can easily be mounted once the concrete segment is in place.

### 2.3.3 Post-tensioned concrete towers using slip-formed construction

The transportation of pre-cast tower segments can be avoided completely by cast-in-place towers, using slip-formed construction. Slip-forming is a construction technique that uses self-rising formwork so that a concrete structure can be cast with a single pour, creating a monolithic, jointless structure. This leaves only the raw materials used in the tower and foundation to be transported to site, along with the nacelle, hub and blades. Another advantage of slip-form construction is that post-tensioning only needs to be applied once, because initial prestressing applied for transport and handling purposes are not required.

The self-rising formwork used for slip-formed construction moves up at a rate of approximately 250mm per hour (Van Zyl, 2014). At this rate, it would take approximately three weeks to construct a tower of 120m tall. This is generally slower than the construction time using pre-cast segments, but has the advantage over pre-cast segment construction that crane costs are greatly reduced.

The slip-form system used for the construction of towers generally have three platforms, as illustrated in Figure 2.3. The uppermost deck is used to install reinforcement and facilitate the pouring of concrete. The hydraulic lifting system is usually supported by the middle platform. The middle platform is also regarded as the main deck, which provides locations where gates, ladder platforms and maintenance decks are formed. An area is also provided where steel reinforcing can be assembled and the concrete vibrated. The lower platform is used to inspect the newly exposed concrete to meet design specification and apply surface finishing (Ghonim, n.d.).

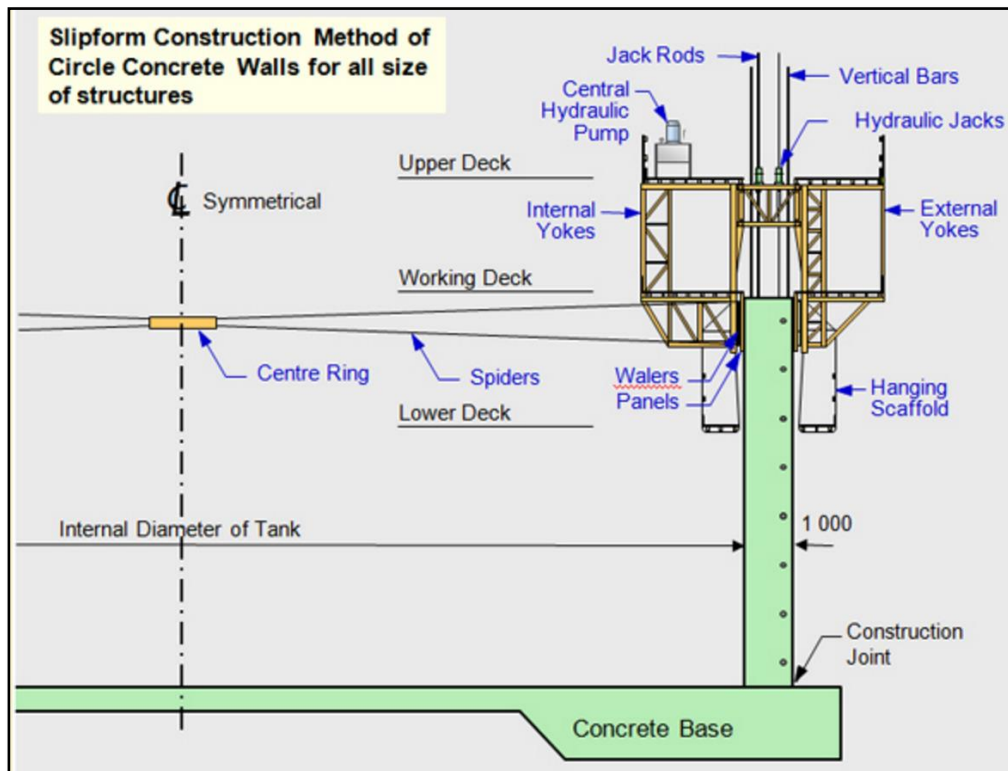


Figure 2.3: Slip-form system description (Energy world, 2008)

### 2.3.4 New concrete WTG tower initiative

A new concrete WTG tower concept, which utilises the key benefits of pre-cast and in situ construction, was developed by a team led by Prof. Johann Kolleggerr at the Institute of Structural Engineering at TU Wien. This concrete tower consists of pre-cast rectangular panels, which are transported to site and assembled on the ground to form double walled polygonal segments. These segments are then lifted on top of one another and filled with concrete (Dvorak, 2016). The simple shape and relatively light weight of the pre-cast components, reduce the stresses present during transportation and handling. This results in a reduction of reinforcing and wall thicknesses, compared to traditional pre-cast construction methods. Traditional pre-cast methods cast bigger, heavier segments, which require more reinforcing due to greater stresses arising during transportation and handling under own weight (Dvorak, 2016). The new tower initiative is illustrated in Figure 2.4.



Figure 2.4: New concrete WTG tower initiative (Dvorak, 2016)

## 2.4 Current software used to analyse wind turbine towers

Due to the protection of intellectual property, detailed information about tower designs currently used in the industry is difficult to obtain. Data regarding the modelling and analysis of WTGs was however obtained from recent studies conducted by two former M.Eng. (Research) students from the University of Stellenbosch.

Way conducted a study that compared material costs associated with steel, concrete and concrete-steel hybrid towers (Way, 2014). For this study, three towers of each material were modelled using the Abaqus Standard/CAE interface. The concrete towers and the concrete portions of the hybrid towers were modelled as post-tensioned. The post-tensioning was modelled as a concentric axial force, which was restricted to act perpendicularly to the cross section at the top of the tower. 8-Node hexagonal brick elements, with 3 degrees of freedom (DOF) per node, were used for all of the tower FE models (Way, 2014). Figure 2.5 demonstrates how a tower was meshed using 8-node brick elements.

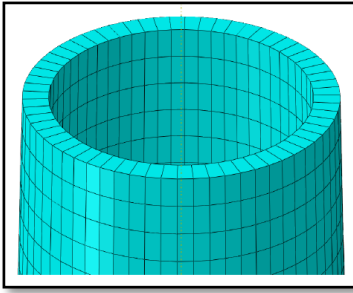


Figure 2.5: 8-Node brick element used to mesh a wind turbine tower (Way, 2014)

W.S. van Zyl conducted a study that focussed specifically on the design of tall concrete wind turbine towers. A significant part of this study consisted in modelling a 100m tall reinforced concrete wind turbine tower. This was done using a finite element package, known as Diana, which specializes in the nonlinear analysis of concrete and masonry structures (Van Zyl, 2014). Curved shell elements, consisting of either four or eight nodes per shell element, were used to model the tower structure. Every node consists of three translational and two rotational degrees of freedom. This element is illustrated in Figure 2.6. The study conducted by Van Zyl did not include the modelling and analysis of post-tensioned towers. Second order effects and nonlinear material properties were however included.

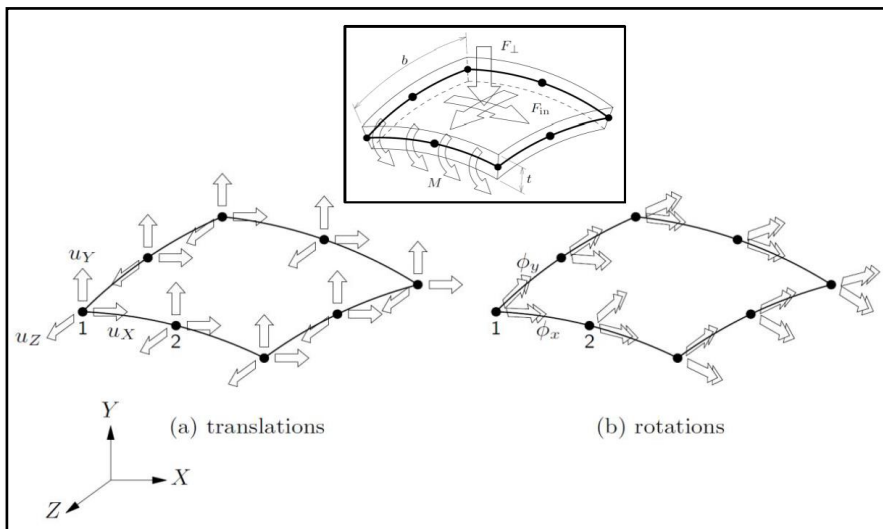


Figure 2.6: 8-Node quadrilateral curved shell element (Diana 9.4.4, 2012)

Although the software used in the studies mentioned above has the ability to generate very accurate results, computation time becomes a problem in the work environment. This is generally due to the high number of finite elements and degrees of freedom used in the FE models. Van Zyl and Way both performed modal analyses to obtain the natural frequencies of the WTG to verify that it does not coincide with the excitation frequencies induced by the blades. For both studies, the modal analysis took approximately two hours to complete. In the study conducted by Van Zyl, a nonlinear analysis was performed to accurately calculate the deflections and internal stresses. This analysis

initially took up to a week. After the model had been simplified, the computation time of the analysis decreased to approximately 8 hours (Van Zyl, 2016).

These software packages also have steep learning curves, making the operation of setting up the finite element model a time consuming one. According to Van Zyl (2016), once a user is familiar with Diana, setting up a wind turbine tower model in Diana could still take one to two weeks. During the study conducted by Way, the modelling of all nine towers took approximately three to four months using Abaqus, averaging in similar estimates given by Van Zyl (Way, 2016). After the model has been set up, wind loads are calculated and applied to the tower. When using general FEM software, wind loads are usually calculated using independent software packages such as Microsoft Excel. The calculated loads are then applied to the model manually. The lack of integration between these software packages could result in further time and effort added to the modelling process.

Although the information above is based on approximate figures from previous studies, it is provided to give an idea of the time required to model and analyse megastructures such as WTGs using complex FEM software. During the design process, it is common to modify the structure in the attempt to optimise the design. Modifying and re-analysing a WTG using complex FEM software could become very time consuming and uneconomical. This is especially the case with post-tensioned concrete towers, where an infinite number of combinations of input parameters exist.

# Chapter 3: Software specific to wind turbine generators

## 3.1 Introduction

In the attempt to increase the efficiency of the analysis process, the various areas contributing to the tediousness of the process have been identified. These inefficiencies are summarised below.

- Creating a FE model using general purpose FEM software;
- Adaptability of FE models in general purpose FEM software;
- Calculating and applying wind loads to the tower;
- Performing a FEM modal analysis; and
- Performing a FEM structural analysis to obtain internal stresses and tower deflections.

Two of the biggest factors contributing to the computation time during modal and structural analyses, are the number and complexity of finite elements used in the WTG model. The complexity refers to the number of degrees of freedom (DOFs), and whether linear or nonlinear interpolation is used between nodes. These two factors contribute to the size of matrix computations, which could take an excessive amount of time to solve when the number of DOFs become too large. Due to wind turbine towers having relatively simple geometry, the finite element model can be simplified significantly, provided that the complexity of the tower's physical attributes are considered elsewhere.

## 3.2 Simplification of WTG finite element model

The first way that the model can be simplified is by reducing the analysis to only consider two dimensions. This is a reasonable assumption, as WTGs generally consist of a symmetrical cross sectional shape. When bi-axial moments need to be considered, it is usually possible to use an interaction equation to reduce the bi-axial moments to a uniaxial moment.

Although three-dimensional shell and brick finite elements could be used to represent the geometry of the tower accurately, a large number of these elements are required to do so, as was seen in the studies conducted by Way (2014) and Van Zyl (2014). Furthermore, existing commercial software such as Abaqus and Diana are able to generate this kind of FE model. By utilising three-dimensional shell or brick elements in this study would thus be a replication of existing software.

The use of three-dimensional shell and brick finite elements are thus not considered as viable solutions. Instead, two-dimensional beam elements are used to model the WTG. The model is

simplified further by neglecting the axial degree of freedom, as the axial deflection is seen as minor importance compared to the rotational and lateral deflections. The axial forces in the tower are however considered in the cross section analysis, which is discussed in detail in Chapter 4: Cross section analysis. The cross section analysis also considers the complex physical characteristics of the materials comprising a reinforced concrete WTG tower, which is neglected in the FE model.

The finite element used in the modal and structural analyses of this study is illustrated in Figure 3.1.

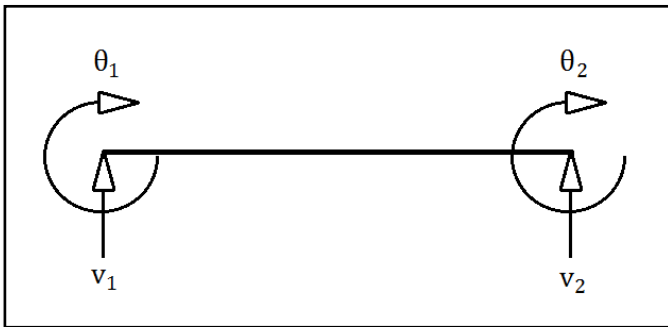


Figure 3.1: 4DOF beam element used in the FE model

### 3.3 Modelling of a Wind Turbine Tower

The WTG (wind turbine generator) system comprising the foundation, tower, generator and external loading is a complicated system to model. These components are illustrated in Figure 3.2. Due to the limited scope of this study, emphasis is placed on the modelling of the tower. The tower is thus modelled as a cantilever structure with a fixed base, neglecting the elastic effects of the foundation and soil. To demonstrate the expandability of the software, provision is made to model steel, concrete and hybrid towers.

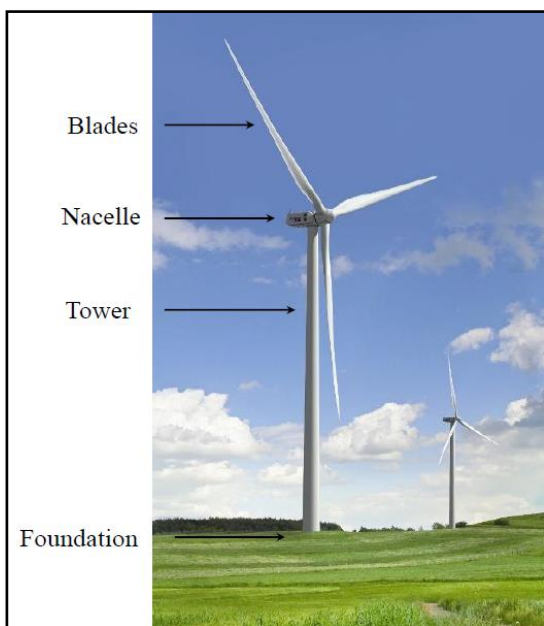


Figure 3.2: Components of a wind turbine tower (Way, 2014)

The WTG tower is discretised into a specified number of tower segments to model the geometry and material properties of the tower accurately. A tower segment represents a segment of the WTG tower with a uniform material and cross sectional shape. Provision is made to account for tapering diameters and wall thicknesses generally encountered in WTG towers. Considering a reinforced concrete tower segment with a circular hollow cross sectional shape, for example, the diameter and wall thickness may vary throughout the height of the tower segment, but the material properties and the amount of reinforcing steel is uniform. The specified exterior and interior concrete cover is also uniform throughout the entire tower segment.

Every tower segment is modelled by a series of 4DOF beam elements connected to each other by nodes. At every nodal position along the height of the tower, a cross section analysis is performed to determine the cross section properties at the particular node. The cross sectional properties (bending stiffness, axial stiffness and curvature) of a cross section are dependent on the internal loading and geometry of the cross section. Every beam element's properties is calculated as the average of its connecting nodal (cross sectional) properties. After the beam element's properties are calculated, the element stiffness matrix can be formulated.

The generator is modelled as a series of static loads and lumped mass at the top of the WTG tower. These loads include the concentrated horizontal load from the wind acting on the nacelle and blades, the moment and torsion.

The wind loading on the tower itself is modelled as a series of point loads acting on the nodes of the tower. The process of how the wind loading is obtained is discussed in detail in Chapter 6: Wind Loading. A schematization of how the tower is modelled and discretised is illustrated in Figure 3.3. Also demonstrated in Figure 3.3 is how the lateral wind loads and turbine loads are applied to the nodes of the beam elements.

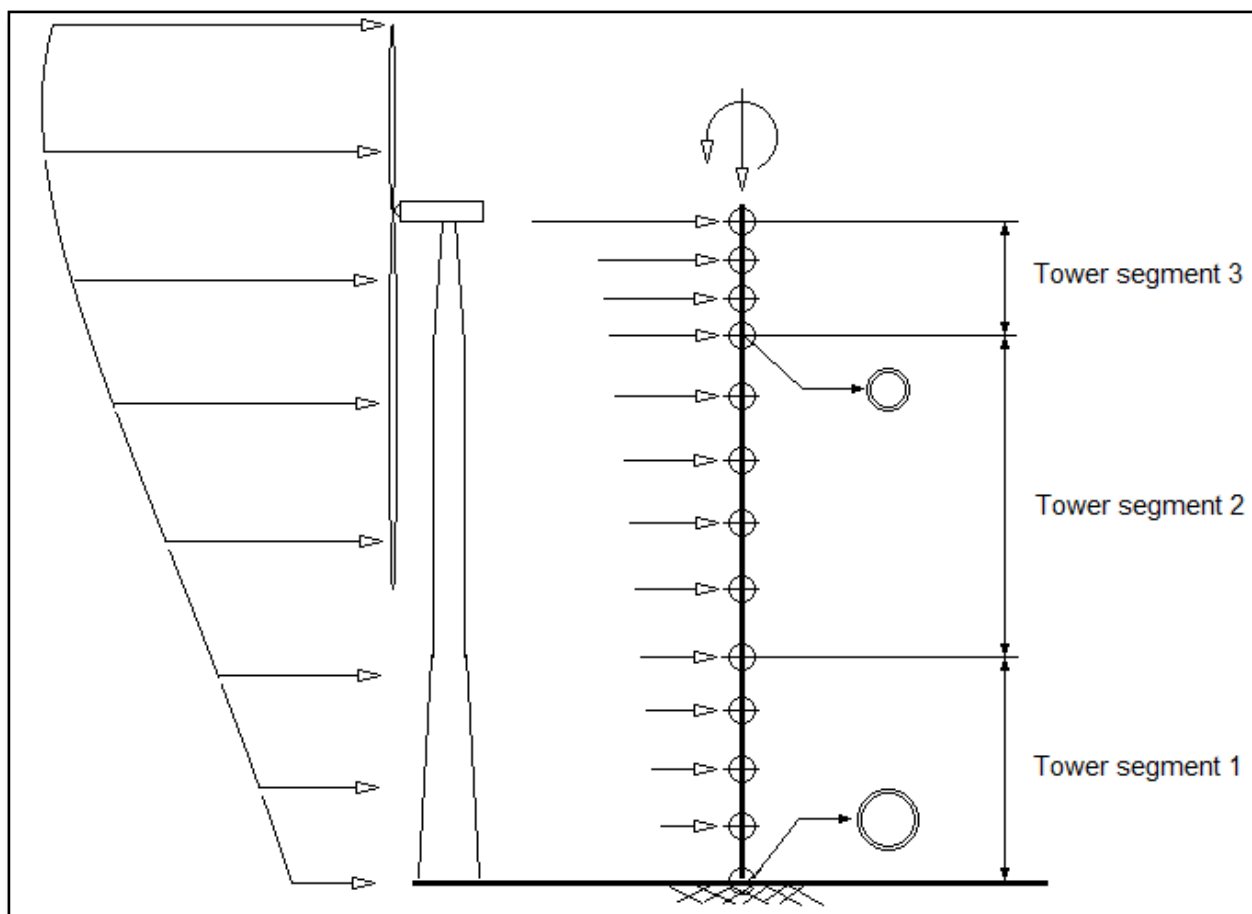


Figure 3.3: Discretization of a WTG model

### 3.4 UML diagrams of developed software

Demonstrated in the figures below are unified modelling language (UML) diagrams. These are included to provide a visualisation of the structure of the developed software. The first UML diagram illustrates the general structure of the WTG system model, consisting of generic *TowerSegment*, *Beam4DOF* and *CrossSection* classes. The UML diagrams in Figure 3.4 to Figure 3.7 illustrate the structure specific to post-tensioned concrete towers. Each of the blocks in the figures represent a Java *class*. When one class is connected to another by means of a line, a relationship between the two classes exist. When one class is connected to another by means of a line with an arrowhead, the class that is pointed to represents the *superclass*. In Figure 3.7, for example, the *ReinforcedConcreteTowerSegment* class points to the *TowerSegment* class, indicating that the *ReinforcedConcreteTowerSegment* class is a *subclass* of the *TowerSegment* superclass.

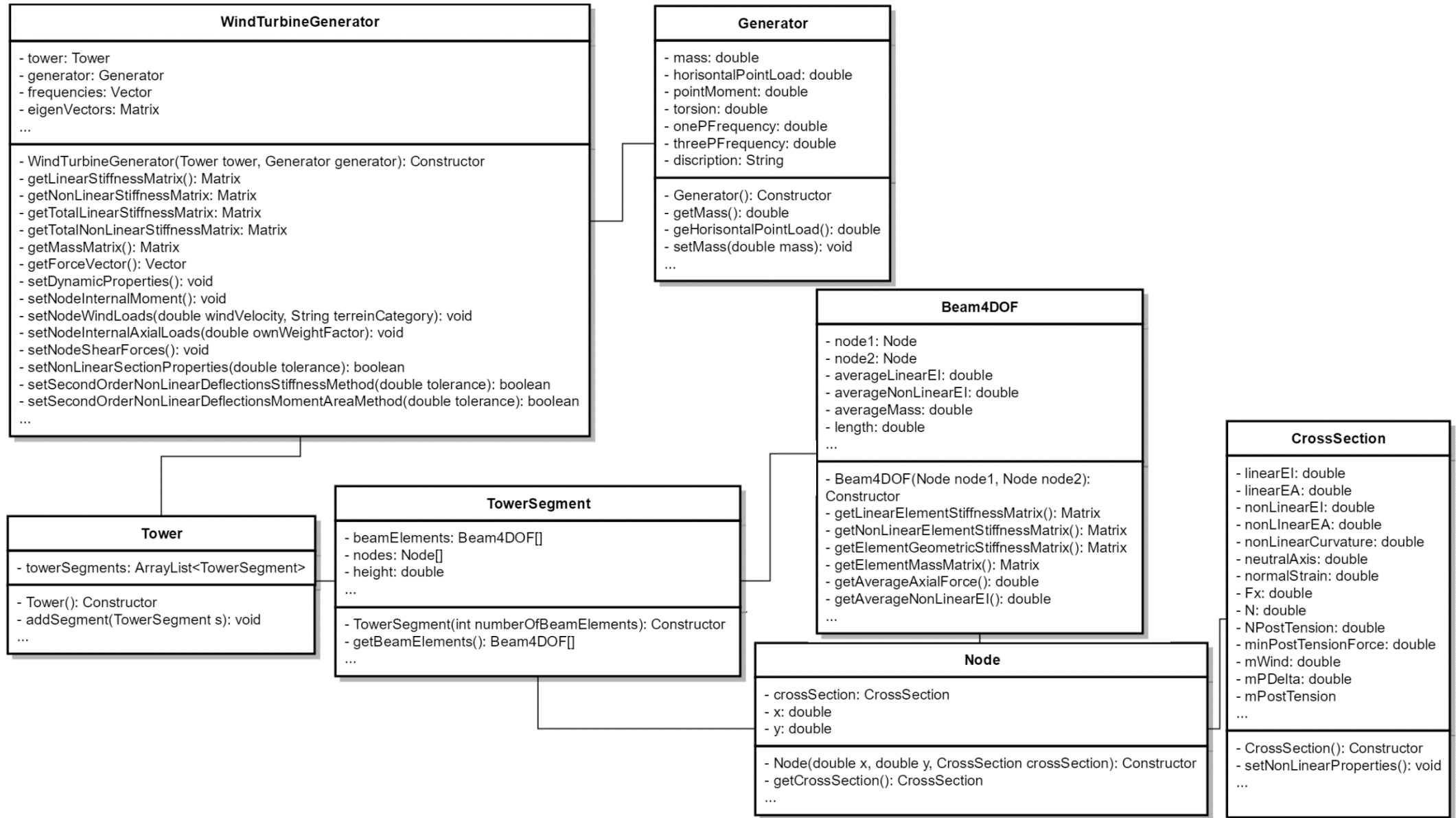


Figure 3.4: General UML diagram of developed software

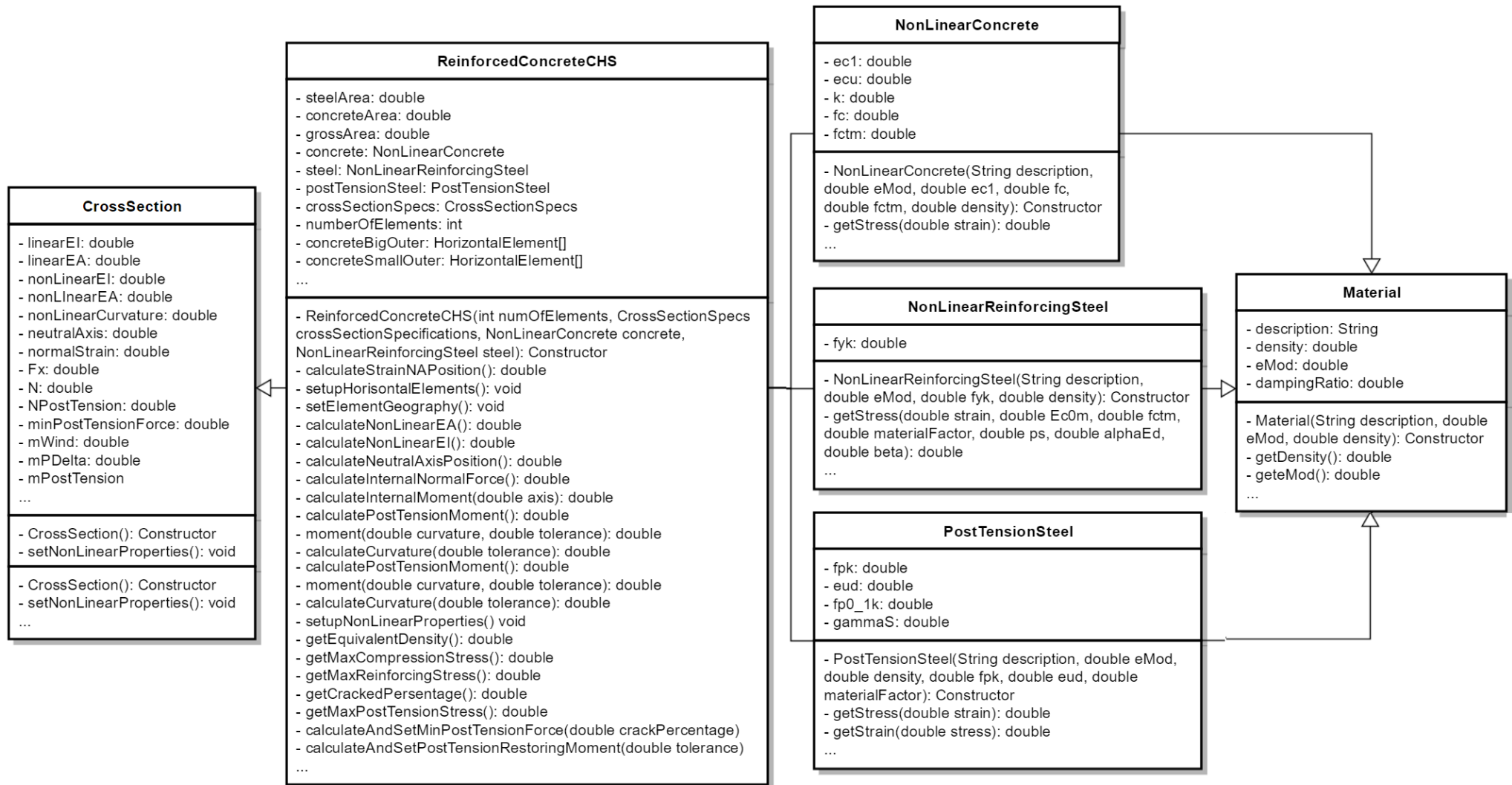


Figure 3.5: UML diagram of reinforced concrete circular hollow cross section (a)

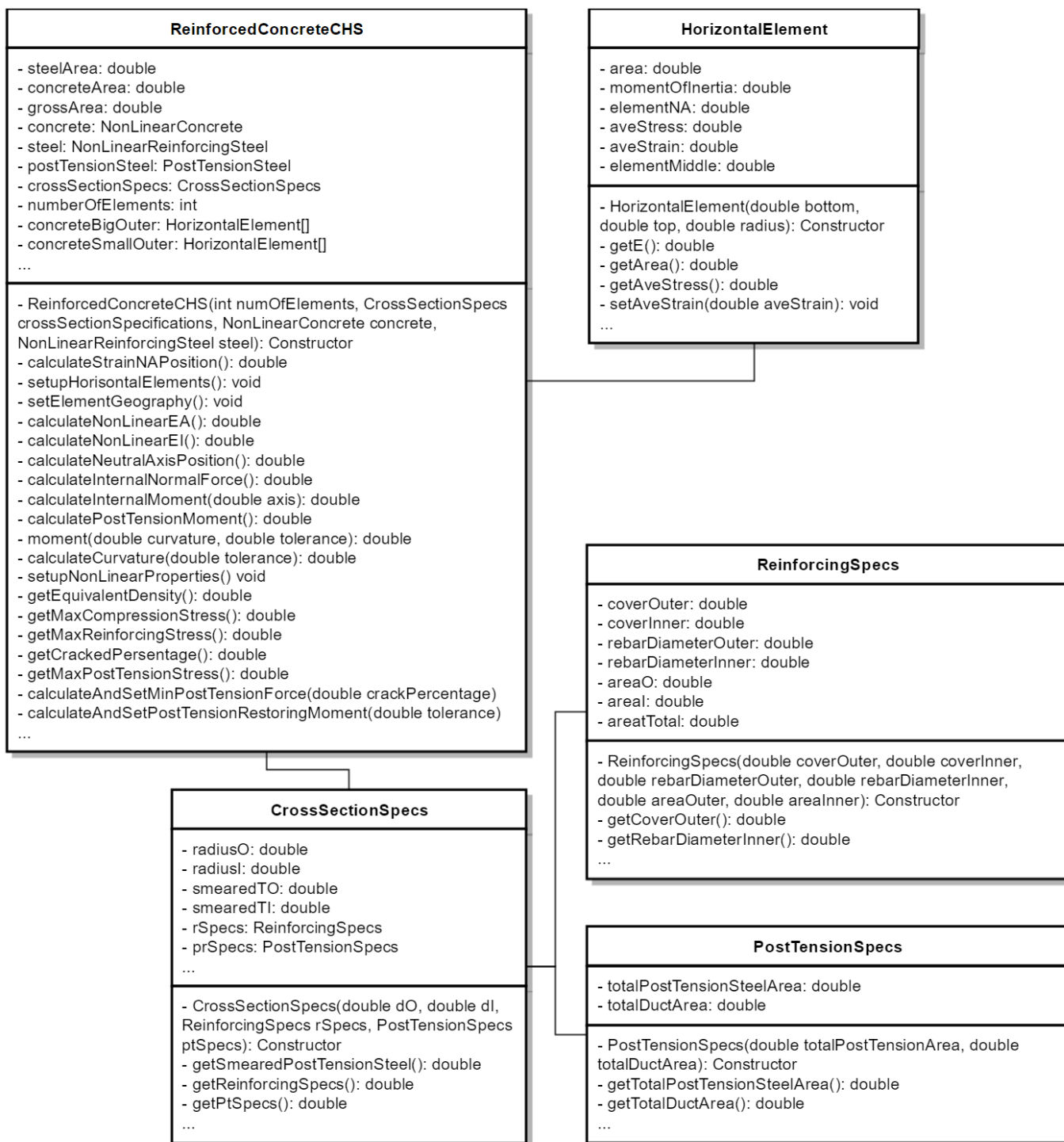


Figure 3.6: UML diagram of reinforced concrete circular hollow cross section (b)

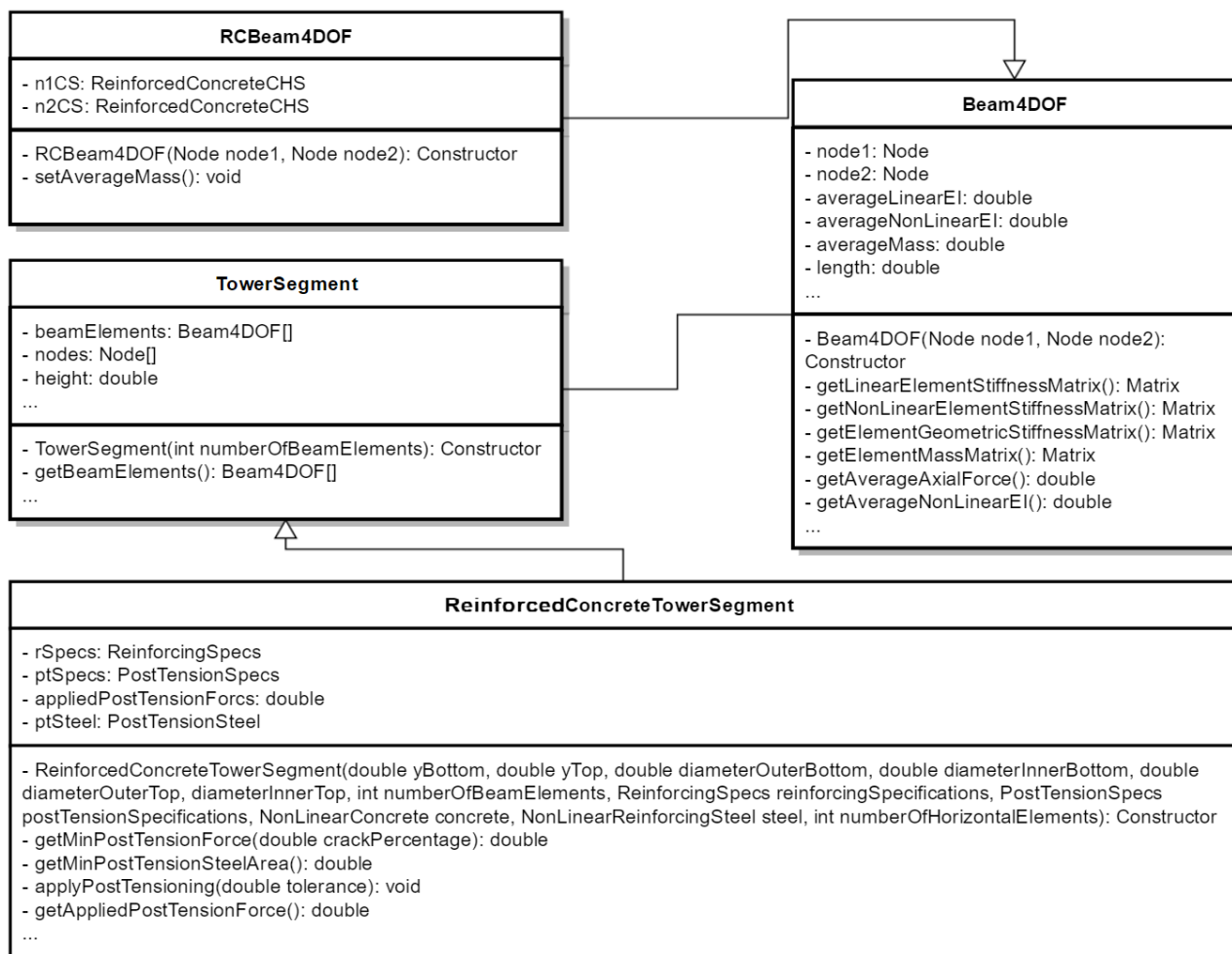


Figure 3.7: UML diagram of reinforced concrete tower segment and beam element

### 3.5 Advantages of the software

The main advantage of the software is that accurate models, which closely approximate the actual WTG, can be set up and analysed within 10 minutes.

The software automatically constructs finite elements after basic parameters are defined. These parameters describe properties associated with the bottom and top cross sections of the tower segment. The number of beam elements required for every tower segment is specified by the user, which has an influence on the accuracy of the analysis. By the use of interpolation, the beam elements enclosed by the top and bottom cross sections are generated. In this way, the tapering tower segments and varying cross section properties are considered.

Another advantage of the software is its adaptability. This is particularly useful during the modal analysis where the WTG frequencies are calculated. If it is found that the WTG's frequencies do not fall in the desired interval, the WTG's dimensions and mass distribution can be altered with ease. Different combinations of generators could also be tested using the software. The frequency analysis can be executed various times until the desired frequencies are obtained. This is a very important feature, which could save a significant amount of time during the initial design stages of the WTG.

# Chapter 4: Cross section analysis

## 4.1 Introduction

When considering composite beam elements, the task of determining the beam element properties can become complex. This is especially the case when nonlinear stress-strain diagrams describe the materials comprising the cross section.

One way to capture most of the complexity ignored by the simplified finite element model is by performing a cross section analysis. By analysing the cross section at both ends of a beam element, approximate beam element properties are obtained and used in deflection calculations. The cross section analysis formed the core of this FE formulation around which the software is designed.

The *Model Column Method* is a method that can analyse cross sections consisting of multiple materials, with each material having its own nonlinear stress-strain relationship. The Model Column Method is a method based on first principles, and is equivalent to the “method based on nominal curvature”, described in Eurocode 2: Design of concrete structures (EN 1992-1-1:2004, 2004).

## 4.2 The Model Column Method

The Model Column Method methodology is an adoption of the methodology described in BetonKalender – Concrete Structures for Wind Turbines (Grünberg & Göhlmann, 2013). It is used to simplify the calculations according to second-order theory into a cross-sectional analysis based on the strain distribution resulting from the applied forces. The Bernoulli hypothesis is assumed during the cross section analysis, which states that plane sections remain plane, up until failure.

In a study conducted by Walls (2016), a cross section analysis method was implemented and tested with similar assumptions to what is assumed in this study. These case studies revealed that even when Euler-Bernoulli assumptions were violated, the cross section analysis method yielded favourable results, especially in the case of statically determinate structures. WTG towers are cantilever structures, and can thus be classified as statically determinate. Tall WTG towers can also generally be classified as slender structures, and as such it is deemed reasonable not to consider shear deformations in this study.

Failure of the cross section occurs either when the reinforcing steel or the concrete reaches its ultimate strain limit in the longitudinal direction. BetonKalender uses the strain limits specified by Eurocode 2: Design of concrete structures (EN 1992-1-1:2004, 2004). BetonKalender specifies the concrete and steel failure limits to be  $-0.0035$  m/m and  $0.025$ m/m, respectively (Grünberg & Göhlmann, 2013). The negative strain limit for concrete indicates shortening of the material fibres.

This strain limit can thus be interpreted as the crushing limit of the concrete. The positive reinforcing strain limit represents excessive lengthening of the material fibres, so that the reinforcing can no longer provide any tensile resistance.

#### 4.2.1 Model Column Method Algorithm

A WTG can generally be represented by a statically determinate cantilever structure, which implies that the internal axial forces and first order moments can be obtained before the commencement of the deflection and internal stress analysis. The Model Column Method is however designed to calculate the moment for an assumed curvature and axial load, and is thus not sufficient in calculating the properties of a cross section on its own. The Model Column Method is merely a single step in the algorithm developed in this study to solve for the cross section properties. This algorithm is iterative and requires multiple Model Column Method analyses to obtain the final cross section properties. The process describing the developed algorithm is discussed in detail in Section 4.5.

The process presented below describe the implemented Model Column Methodology only, and is summarised by the steps below.

- Step 1: Specify the curvature ( $\kappa_z$ ) for which the bending moment ( $M_z$ ) is to be found. Also specify the axial force ( $N_x$ ) acting on the cross section.
- Step 2: Calculate or assume the start value of the concentric strain. The concentric strain is the strain caused by the axial force. The accuracy of the initially assumed concentric strain is not important, as this value will be updated iteratively until convergence is achieved.
- Step 3: Calculate the total strain distribution over the cross section. From these strains, the stress and the secant Young's modulus variation over the cross section can be calculated.
- Step 4: Calculate the updated (shifted) neutral axis position and cross section properties.
- Step 5: Calculate the internal forces.
- Step 6: Convergence is achieved when the calculated internal forces (internal axial force and moment) are within the desired tolerance, else repeat from Step 3.

#### 4.2.2 Discretization of the cross section

In order to compute the variation of strain, stress and Young's modulus over the cross section, the cross section has to be discretised. Two apparent methods were identified that can be used to discretise a circular hollow section. A cross section can either be divided up into radial elements or horizontal, unidirectional strip elements (see Figure 4.1). Radial discretization might be advantageous when a three dimensional model is required that can accommodate bi-axial bending. It does however have the disadvantage of only being compatible with circular cross sectional shapes. Another disadvantage associated with radial discretization is that integration must always be used to calculate the stresses over a single element, regardless of the element size. This is because

strains will always vary significantly across radial elements that are far away from the horizontal axis that runs through the centre point of the cross section.

The comparison between radial and horizontal elements on a circular hollow section is illustrated in Figure 4.1. Here it can be seen that the strains across a horizontal element with roughly the same thickness as the radial element varies less over the thickness of the element. By specifying thinner horizontal elements, more accuracy can be obtained in internal stress calculations. Various numerical integration procedures can however be included to increase the accuracy of the internal force calculations and reduce the number of elements required.

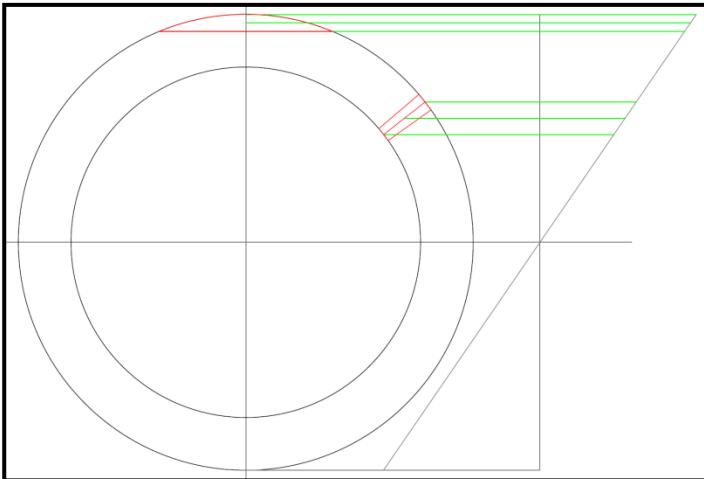


Figure 4.1: Comparison between radial and horizontal elements on a circular hollow section

For analysis results verification purposes, structural elements comprising of cross sections other than circular shapes have also been analysed. All of the structures and structural elements analysed for this study have been simplified to two-dimensional models. Due to horizontal strip elements being compatible with any shape of cross section, all of the cross sections analysed in this study are discretised using horizontal strip elements.

### 4.2.3 Calculating the strain distribution over the cross section

The strain at every element is a combination of the strain caused by the assumed curvature and the calculated concentric strain. The effectiveness of this method is achieved by keeping the curvature constant and only updating the concentric strain caused by the axial force. This is acceptable due to the Bernoulli hypothesis being assumed. This assumption enables the slope of the strain distribution over the cross section to remain constant throughout the Model Column Method procedure. By adding or reducing the concentric strain accordingly, the balance point is found where the calculated internal forces and the internal forces resulting from the applied axial load and assumed curvature are equal.

The updated concentric strain for every iteration is calculated by interpolation. This is expressed by the following equation:

$$\varepsilon_{k+1} = \varepsilon_k + \frac{(\varepsilon_k - \varepsilon_{k-1})}{(N_k - N_{k-1})} (N_x - N_k) \quad (4.1)$$

Where:

- $\varepsilon_k$  and  $N_k$  is the concentric strain and internal axial force in the  $k^{th}$  iteration, respectively; and
- $N_x$  is the applied axial force over the cross section.

For the first iteration ( $k = 1$ ), take  $\varepsilon_{k-1}$  and  $N_{k-1}$  as equal to 0.

#### 4.2.4 Calculating the updated neutral axis and cross section properties

When nonlinear materials are present in the cross section, the neutral axis of the cross section shifts from its original position due to the difference of stiffness over the cross section. When concrete cracks, for example, the neutral axis will shift to the stiffer, uncracked side of the cross section so that equilibrium is maintained. The shift in the neutral axis needs to be taken into account by calculating the updated cross section bending stiffness about the shifted neutral axis. A study done by Walls (2016) demonstrated that if the shift of the neutral axis is not taken into account, the error in deflection calculations could be significant. The updated neutral axis position is calculated using the following expression:

$${}^{i+1}c' = \frac{\int {}^iE(y)y dA}{\int {}^iE(y)dA} = \frac{\sum_{k=1}^n {}^iE_k A_k y_k}{\sum_{k=1}^n {}^iE_k A_k} \quad (4.2)$$

Where,

- $c'$  refers to the updated neutral axis position, measured relative to the datum position;
- $i$  refers to the current iteration number;
- $E_k$  is modulus of elasticity for the  $k^{th}$  element;
- $A_k$  is the area of a specific element; and
- $y_k$  is the distance measured from the point about which the internal moment is being calculated, to the neutral axis of the element being investigated.

The bending stiffness about the shifted neutral axis is calculated using the following expression:

$${}^{i+1}(EI) = \int {}^iE(y)y^2 dA + \frac{Pc'}{k} = \sum_{k=1}^n {}^iE_k (A_k y_k^2 + I_k) + \frac{N_x c'}{k} \quad (4.3)$$

Where:

- $I_k$  is the second moment of inertia of the element being investigated;
- $N_x$  is the external axial force on the cross section; and

- $k$  is the curvature.

It is recommended that the datum axis be chosen to coincide with the original, unshifted neutral axis. When this assumption is made, the applied axial force acts on the datum axis throughout the Model Column Method procedure. As the neutral axis shifts, the axial force will have an effect on the bending stiffness calculation and will have to be taken into account. This effect is taken into account by the second term in Equation (4.3). It is important to note that the curvature in this term is the *total* curvature, resulting from the total internal moment on the cross section. The total internal moment is comprised of the moment resulting from the external wind force and the P-delta effects resulting from large lateral deflections. The total moment also includes the moment caused by the eccentricity of the axial force, which is a result of the shifted neutral axis. When there is no moment caused by the lateral wind forces or P-delta effects, the last term of Equation (4.3) can be discarded, since the neutral axis will not shift in this case.

An alternative to calculating the bending stiffness of the cross section is to make use of the Euler-Bernoulli beam theory. From this, a relationship between moment, bending stiffness and curvature is obtained. When using the Model Column Method to analyse a cross section, the curvature is assumed for which the moment needs to be found. The moment and the curvature is thus known after the completion of the analysis. The bending stiffness is then simply found by dividing the moment by the curvature. Once again, the total moment is used in this relationship. The alternative relationship that is used to calculate the bending stiffness can be expressed as follows:

$$EI = \frac{M_{total}}{k_{total}} = \frac{(M_{wind} + M_{P-delta} - N_x c')}{k_{total}} \quad (4.4)$$

Where:

- $M_{wind}$  is the moment caused by the external lateral wind force;
- $M_{P-delta}$  is the moment caused by the own weight of the TWG when subject to lateral displacements; and
- $N_x c'$  is the term that takes account of the eccentricity of the axial force due to the shift of the neutral axis.

The  $N_x c'$ -term in Equation (4.4) above is subtracted from the other two moment terms because an upward shift of the neutral axis would cause the axial force to decrease the total internal moment. Figure 4.2 is provided below to demonstrate this situation.

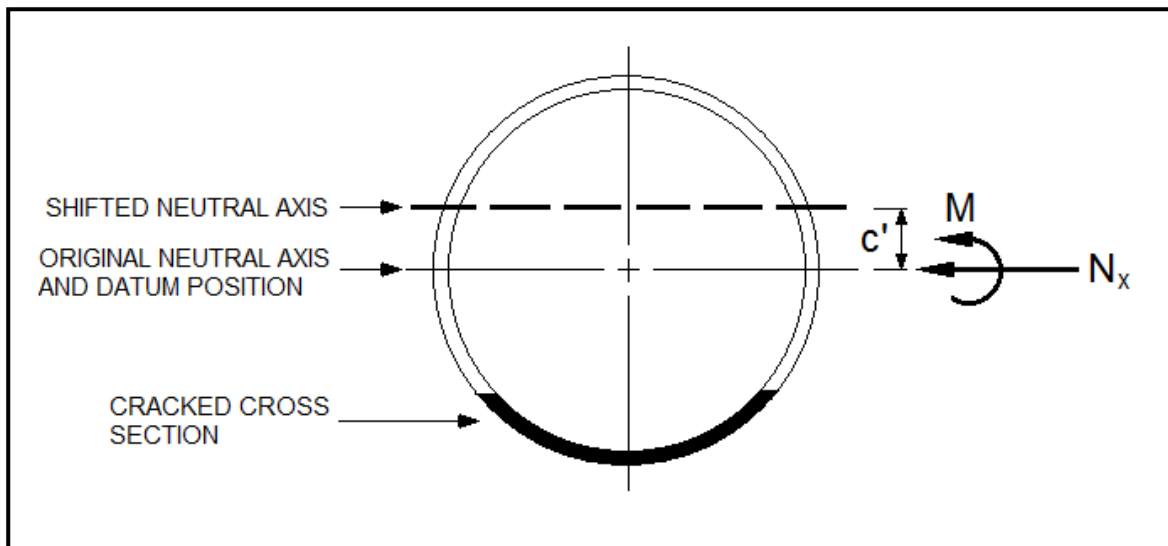


Figure 4.2: Typical cross section subject to a moment and axial load

To clarify the process of how the neutral axis migrates when a cross section is subject to an axial load and moment, consider Figure 4.2. The moment acting on the cross section in Figure 4.2 comprises the moment caused by lateral loads and P-delta effects. This moment causes tension strains at the bottom of the cross section to occur, which results in cracking of the concrete. The reduction of stiffness at the bottom of the cross section results in the neutral axis to migrate upward, to the stiffer part of the cross section. Due to the axial force,  $N_x$ , still acting through the original neutral axis position, a restoring moment is generated. This moment is equal to the axial force multiplied by the distance that the neutral axis shifts, which is denoted as  $c'$ . The effect of the restoring moment on the bending stiffness is considered by the inclusion of the last term in Equation (4.3) and Equation (4.4) above.

#### 4.2.5 Calculating internal forces

The internal forces are calculated using a simple finite element implementation. As discussed in Section 4.2.2, the cross section is discretised into multiple horizontal strip elements. Once the strain distribution over the cross section is known, it is relatively simple to calculate and add every element's force contribution. The following equations would yield the cross section's internal normal force and moment, respectively:

$$N = \int \sigma(y) dA = \sum_{k=1}^n \sigma_k A_k \quad (4.5)$$

$$M = \int \sigma(y)y dA = \sum_{k=1}^n \sigma_k A_k y_k \quad (4.6)$$

Where,

- $N$  is the internal normal force;
- $M$  is the internal moment;
- $\sigma_k$  is the stress of a specific element;
- $A_k$  is the area of a specific element; and
- $y_k$  is the distance measured from the point about which the internal moment is being calculated to the midpoint of the element being investigated.

The area of each element is calculated by the following integral:

$$A_k = \int 2\sqrt{r^2 - y^2} dy = y\sqrt{r^2 - y^2} + r^2 \tan^{-1}\left(\frac{y}{\sqrt{r^2 - y^2}}\right) \quad (4.7)$$

Where,

- $r$  is the radius of the circle; and
- $y$  is the position from the centre point of the circle.

The integral is evaluated between the top and bottom of a specific horizontal strip of the circle (see Section 4.2.2). The average stress in each element is found by the material's stress-strain diagram, which is programmed into the model as a subroutine.

Equations (4.5) and (4.6) above can only be applied to a single material at a time. For this reason, the materials present in the reinforced concrete section (steel and concrete) are modelled separately. The composite properties are then computed by the use of superposition.

As stated in the Section 4.2.4, it is assumed that the axial force always acts through the datum position of the cross section. It is thus recommended that the internal moment always be calculated around the datum position of the cross section. This is so that the effect that the axial force has on the internal moment calculation due to the shift of the neutral axis does not need to be accounted for.

### 4.3 Modelling of the reinforced concrete circular hollow section

Considering a reinforced concrete circular hollow section, it has been deemed appropriate to model the section as a series of circles. For a concrete circular cross section consisting of inner and outer longitudinal reinforcing, the cross section is modelled with two continuous steel rings. By assuring that the two rings' centrelines coincide with the reinforcing centrelines, a realistic representation of the reinforcing is maintained. In addition to this, the area of the continuous steel rings is also calculated to be equal to the sum of the actual cross section's reinforcing steel.

Considering once again the example of a concrete circular hollow section reinforced with inner and outer longitudinal steel. This section is modelled with ten circles. Six circles represent the concrete and four represent the steel.

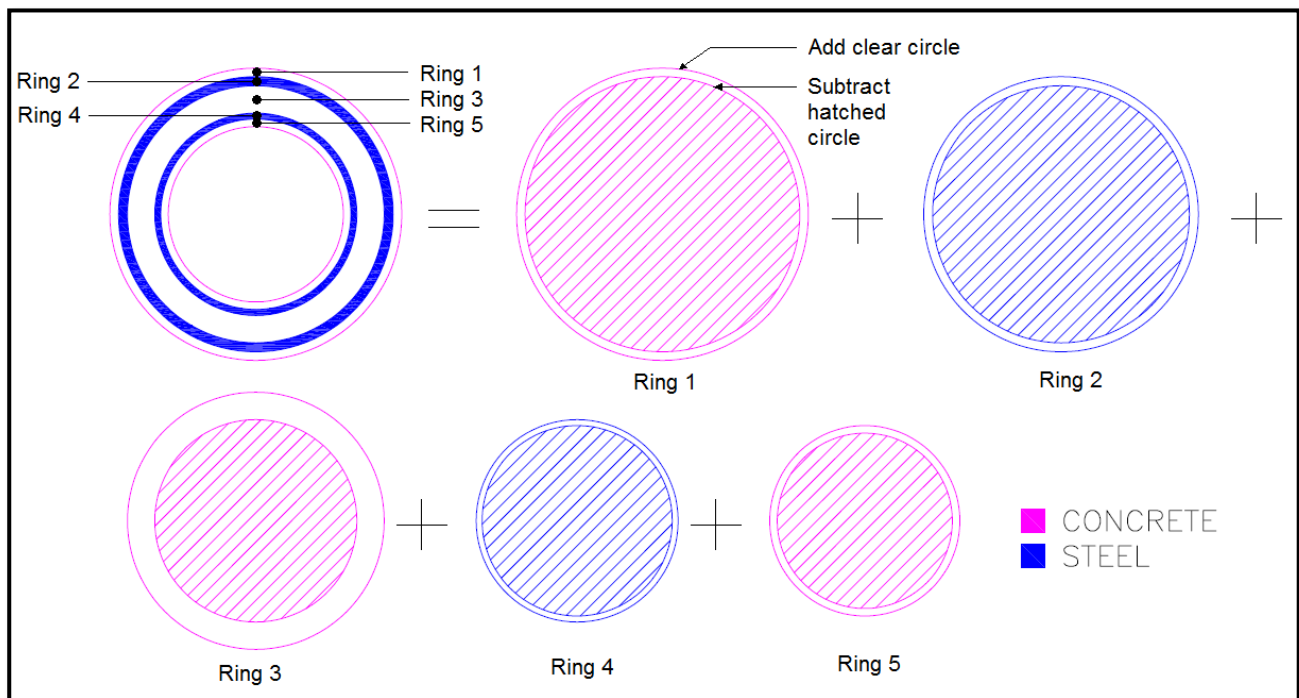


Figure 4.3: Modelling of a reinforced concrete CHS

Figure 4.3 illustrates how a reinforced concrete circular hollow section is simplified by discretizing the section into multiple circles. The first figure (top left corner) represents a circular hollow section including the “smeared area” of steel reinforcing. The figures after the equals sign represent the concrete and steel (magenta and blue respectively) that make up the cross section. The internal forces in the cross section are calculated by adding and subtracting the contributions of the bigger and smaller (clear and hatched) circles, respectively.

#### 4.4 Implemented nonlinear material models

A structure’s physical nonlinear properties are usually taken into account by implementing nonlinear stress-strain diagrams, which describe the behaviour of the associated nonlinear materials. By implementing nonlinear materials, the accuracy of the structural analysis is improved. This is particularly important when analysing concrete WTG towers due to the low tensile resistance of concrete. Some simple finite element software, however, approximate the Young’s modulus of concrete as a single value, independent of the stress state of the concrete. For concrete under relatively small internal stresses, this is a reasonable assumption. However, when a concrete cross section is exposed to larger internal stresses, a more accurate approximation of the material properties is required.

A concrete cross section's stiffness can be reduced by either large compression stresses or tensile stresses. Large compression stresses cause crushing of the concrete. On the other hand, when the axial compressive force is not big enough to counteract the tensile stresses caused by the bending moment, the cross section is subject to net tensile stresses in some areas. If it is assumed that the concrete cannot withstand any tensile stresses, the concrete is assumed to have cracked in the tension zones. This is a common assumption in structural analyses.

Both crushing and cracking in a concrete cross section can cause a significant reduction in the concrete axial and bending stiffness. If this is not taken into account, the deflections of the tower can be significantly underestimated.

The assumed material laws thus play a vital role in a structural analysis. For this study, the guidelines presented by Grünberg & Göhlmann (2013) are followed. Not only are these models suitable for implementation and testing of the software, but also demonstrate that any realistic material model can be incorporated using the software.

Both the concrete and the reinforcing steel are assumed to have nonlinear stress-strain curves. It is assumed that the concrete cannot withstand any tensile stresses. The tension capacity of the concrete is however taken into account by tension stiffening effects between the concrete and reinforcing steel.

#### 4.4.1 Tension stiffening

Tension stiffening describes the phenomenon where considerable stiffness capacity is maintained within the reinforced concrete section after the appearance of the first crack. This is because concrete does not crack suddenly and completely, but progresses as tensile stresses within the cross section increases (Behfarnia, 2009). The intact concrete adjacent to the crack still has significant tensile capacity, which when neglected could result in an overestimate of the deflection of the structure. The tension-stiffening phenomenon is illustrated in Figure 4.4.

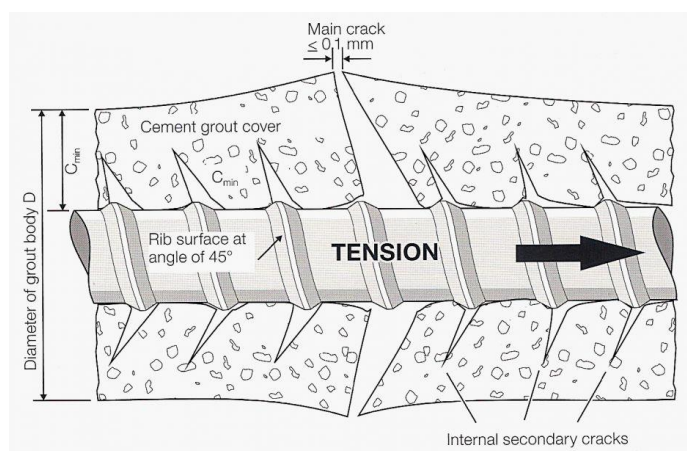


Figure 4.4: Tension stiffening effect (Piles Machinery, 2013)

Due to tension stiffening being dependent on the concrete adjacent to the cracks, the effect of tension stiffening in the concrete increases as the percentage of reinforcing steel decreases. This should not be confused with the tension capacity or stiffness of the cross section, which increases as the percentage of reinforcing steel increases.

The effect of tension stiffening within a reinforced concrete cross section is demonstrated in Figure 4.5. From this figure, it is seen that a cross section consisting purely of steel has a linear stress strain curve, which indicates the absence of tension stiffening. As the steel is replaced by concrete, the tension stiffening effect increases, making the cross section stiffer, but less ductile. Reducing the reinforcing steel enough would ultimately result in the cross section being under-reinforced. A reinforced concrete cross section which is under-reinforced would fail suddenly upon the appearance of the first crack. This is due to the tensile stress limit of the steel being reached before the tensile stress limit of the concrete (Grünberg & Göhlmann, 2013).

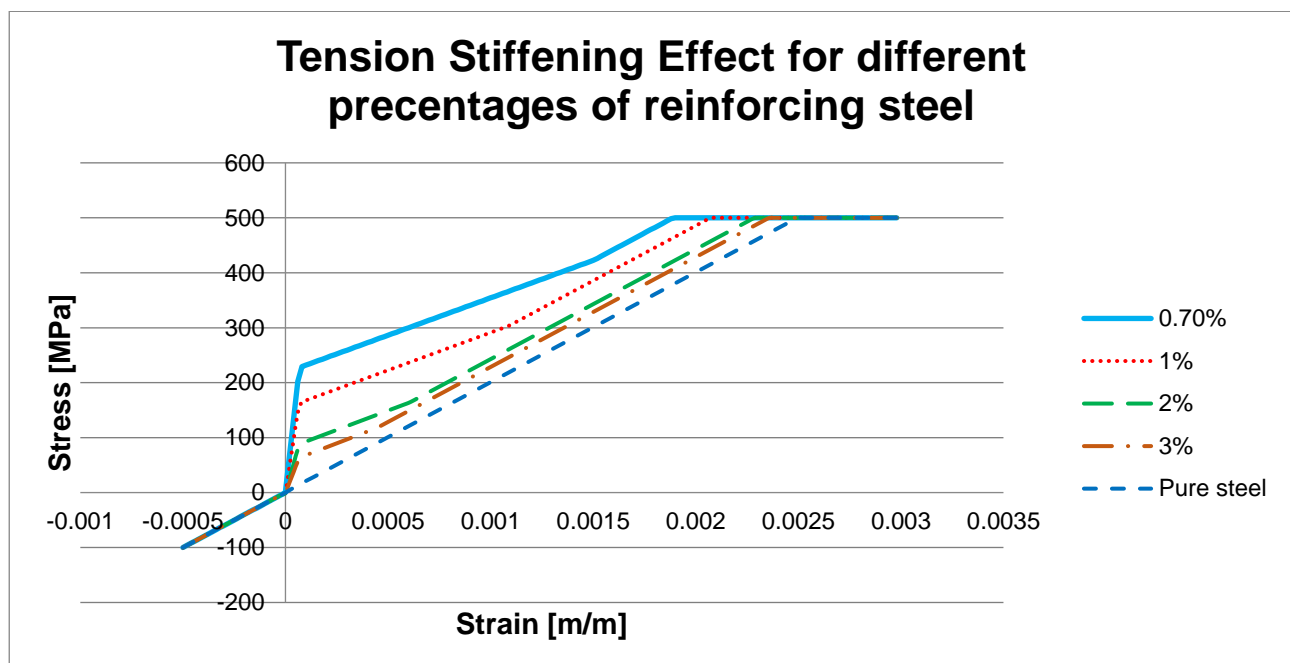


Figure 4.5: Tension Stiffening effect for different percentages of reinforcing steel (Grünberg & Göhlmann, 2013)

#### 4.4.2 Stress-strain relationship for concrete

The nonlinear stress-strain relationship used to model the concrete within the cross section is based on the guidelines given in Eurocode 2 (EN 1992-1-1:2004, 2004). This model represents the relationship between the compressive stress and shortening strain for short term uniaxial bending, and is described by the following expression:

$$\frac{\sigma_c}{f_{cm}} = \frac{k\eta - \eta^2}{1 + (k - 2)\eta} \quad (4.8)$$

Where:

- $f_{cm}$  is the mean value of the concrete cylinder compressive stress in MPa (see Table 4.1 below);
- $k$  can be determined by Equation (4.9); and
- $\eta = \varepsilon_c / \varepsilon_{c1}$ , where  $\varepsilon_c$  is the concrete strain resulting from the stress state and  $\varepsilon_{c1}$  is the strain in the concrete associated with the peak compression stress.

$$k = 1.05E_{cm} \times |\varepsilon_{c1}| / f_{cm} \quad (4.9)$$

Where:

- $E_{cm}$  is the secant modulus of elasticity of concrete in GPa (see Table 4.1 below); and
- $|\varepsilon_{c1}|$  is the absolute value of the strain in the concrete associated with the peak compression stress (see Table 4.1 below).

The expression specified in Eurocode 2 to calculate the secant modulus of elasticity is reproduced as Equation (4.10) below. By multiplying the secant modulus of elasticity,  $E_{cm}$ , by 1.05, the tangent modulus of elasticity is obtained (EN 1992-1-1:2004, 2004).

$$E_{cm} = 22000 \left( \frac{f_{cm}}{10} \right)^{0.3} \quad (4.10)$$

Table 4.1: Strength and deformation characteristics for concrete (EN 1992-1-1:2004, 2004)

Strength classes for concrete															Analytical relation / Explanation
$f_{ck}$ (MPa)	12	16	20	25	30	35	40	45	50	55	60	70	80	90	
$f_{ck,cube}$ (MPa)	15	20	25	30	37	45	50	55	60	67	75	85	95	105	2.8
$f_{cm}$ (MPa)	20	24	28	33	38	43	48	53	58	63	68	78	88	98	$f_{cm} = f_{ck} + 8$ (MPa)
$f_{ctm}$ (MPa)	1,6	1,9	2,2	2,6	2,9	3,2	3,5	3,8	4,1	4,2	4,4	4,6	4,8	5,0	$f_{ctm} = 0,30 \times f_{ck}^{(2/3)} \leq C50/60$ $f_{ctm} = 2,12 \cdot \ln(1 + (f_{cm}/10)) > C50/60$
$f_{ctk,0.05}$ (MPa)	1,1	1,3	1,5	1,8	2,0	2,2	2,5	2,7	2,9	3,0	3,1	3,2	3,4	3,5	$f_{ctk,0.05} = 0,7 \times f_{ctm}$ 5% fractile
$f_{ctk,0.95}$ (MPa)	2,0	2,5	2,9	3,3	3,8	4,2	4,6	4,9	5,3	5,5	5,7	6,0	6,3	6,6	$f_{ctk,0.95} = 1,3 \times f_{ctm}$ 95% fractile
$E_{cm}$ (GPa)	27	29	30	31	33	34	35	36	37	38	39	41	42	44	$E_{cm} = 22((f_{cm})/10)^{0,3}$ ( $f_{cm}$ in MPa)
$\epsilon_{c1}$ (‰)	1,8	1,9	2,0	2,1	2,2	2,25	2,3	2,4	2,45	2,5	2,6	2,7	2,8	2,8	see Figure 3.2 $\epsilon_{c1}^{(0/100)} = 0,7 \cdot f_{cm}^{0,31} \leq 2,8$ (‰)
$\epsilon_{cu1}$ (‰)	3,5									3,2	3,0	2,8	2,8	2,8	see Figure 3.2 for $f_{ck} \geq 50$ Mpa $\epsilon_{cu1}^{(0/100)} = 2,8 + 27((98 - f_{cm})/100)^4$
$\epsilon_{c2}$ (‰)	2,0									2,2	2,3	2,4	2,5	2,6	see Figure 3.3 for $f_{ck} \geq 50$ Mpa $\epsilon_{c2}^{(0/100)} = 2,0 + 0,085(f_{ck} - 50)^{0,53}$
$\epsilon_{cu2}$ (‰)	3,5									3,1	2,9	2,7	2,6	2,6	see Figure 3.3 for $f_{ck} \geq 50$ Mpa $\epsilon_{cu2}^{(0/100)} = 2,6 + 35((90 - f_{ck})/100)^4$
$n$	2,0									1,75	1,6	1,45	1,4	1,4	for $f_{ck} \geq 50$ Mpa $n = 1,4 + 23,4((90 - f_{ck})/100)^4$
$\epsilon_{c3}$ (‰)	1,75									1,8	1,9	2,0	2,2	2,3	see Figure 3.4 for $f_{ck} \geq 50$ Mpa $\epsilon_{c3}^{(0/100)} = 1,75 + 0,55((f_{ck} - 50)/40)$
$\epsilon_{cu3}$ (‰)	3,5									3,1	2,9	2,7	2,6	2,6	see Figure 3.4 for $f_{ck} \geq 50$ Mpa $\epsilon_{cu3}^{(0/100)} = 2,6 + 35((90 - f_{ck})/100)^4$

Figure 4.6 demonstrates a typical nonlinear stress-strain relationship for concrete subject to compression. For C40/50 grade concrete, it can be seen from Table 4.1 that the peak compression stress and strain are 48MPa and 0.0023 respectively.

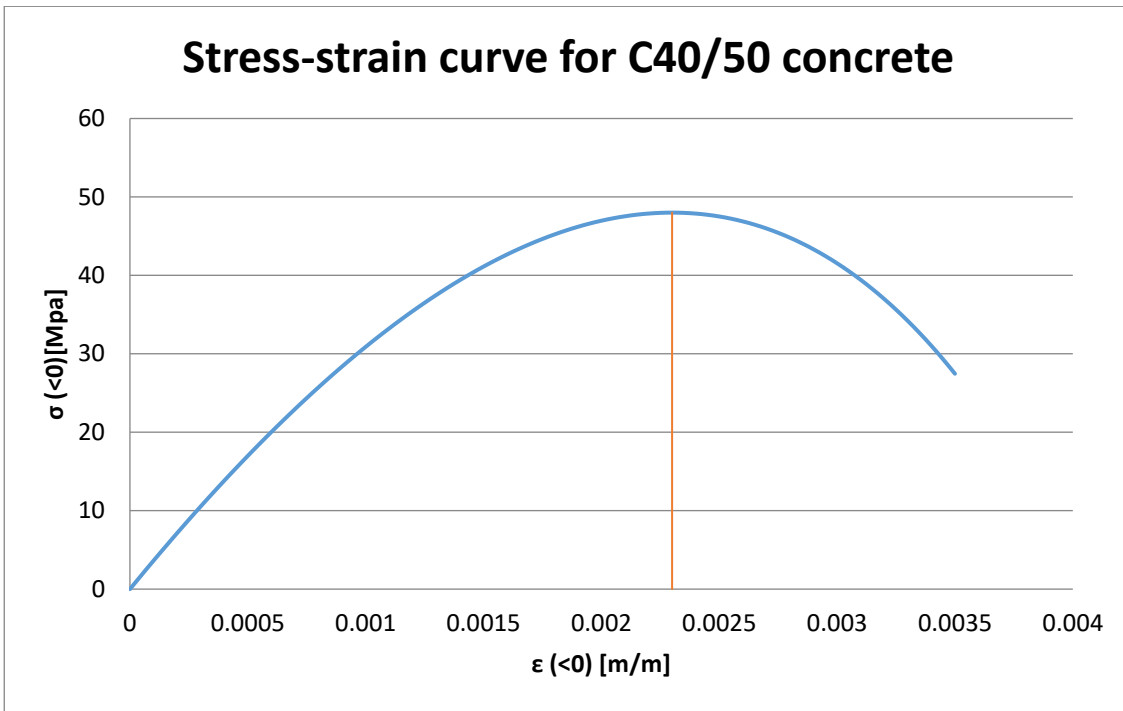


Figure 4.6: Nonlinear stress-strain curve for concrete, according to Eurocode 2

### 4.4.3 Stress-strain relationship for reinforcing steel

For reinforcement exposed to compression stresses, the bilinear stress-strain diagram according to Eurocode 2: Design of concrete structures, is assumed. This diagram is illustrated in Figure 4.7. The parameters on the diagram are normally obtained from the country’s national design code. Guidelines to obtain these parameters are also given in Eurocode 2, Annex C.

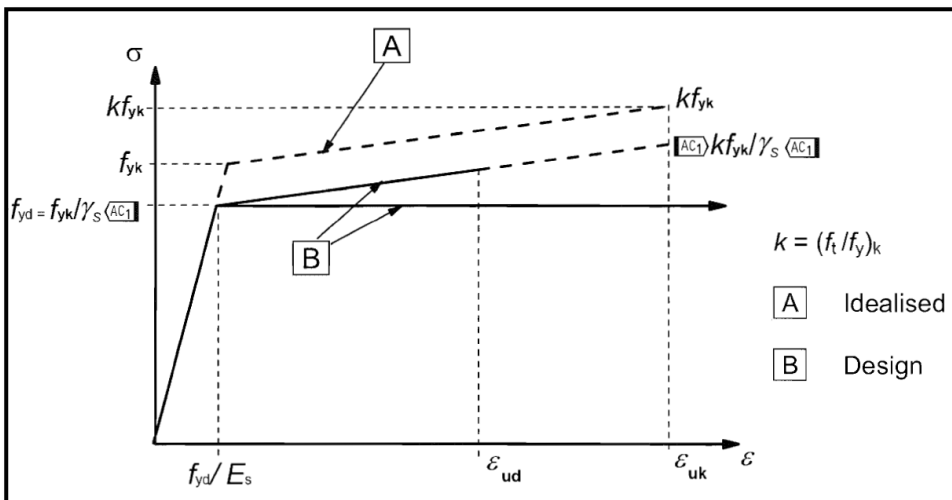


Figure 4.7: Idealized and design stress-strain diagrams used for reinforcing steel in compression (EN 1992-1-1:2004, 2004)

For reinforcing exposed to tensile stresses, a model obtained from BetonKalender: Concrete Structures for Wind Turbines is implemented (Grünberg & Göhlmann, 2013). It is chosen for its complexity, so that the behaviour of the cross section analysis, comprised of materials whose physical properties are described by nonlinear stress-strain graphs, can be tested.

This model comprises of multiple straight-line segments and includes the effects of tension stiffening. Tension stiffening increases the stiffness of the structure and causes a reduction in the tower deflections. To be conservative, BetonKalender specifies the inclusion of a partial safety factor of concrete,  $\gamma_C$ , which is taken as equal to 1.50 (Grünberg & Göhlmann, 2013).

The stress-strain curve associated with the reinforcing subject to tensile stresses can be divided into 4 intervals. These intervals represent different stress states within the cross section. The methodology used in this study to model the tensile stress-strain curve of the reinforcing steel is discussed in the following paragraphs.

**Uncracked** ( $0 < \varepsilon_s \leq \varepsilon_{srd;0.7}$ ):

The concrete is assumed to be in the uncracked state until the tensile stress in the concrete coincides with the design tensile strength of the concrete,  $f_{ctd}$ .  $f_{ctd}$  is calculated using the following expression:

$$f_{ctd} = \frac{f_{ctk;0.05}}{\gamma_C} = \frac{0.7 \times f_{ctm}}{\gamma_C} \quad (4.11)$$

Where:

- $f_{ctk;0.05}$  is the characteristic tensile stress of concrete, which has a 5% chance of being exceeded;
- $\gamma_C$  is the partial factor of safety for concrete, which can be taken as 1.50; and
- $f_{ctm}$  is the mean tensile stress of concrete, which can be found in Table 4.1.

The strain that corresponds to the appearance of the first crack,  $\varepsilon_{srd;0.7}$ , is determined using the following relationship:

$$\varepsilon_{srd;0.7} = \frac{f_{ctk;0.05}}{E_{c0m}} = \frac{0.7 \times f_{ctm}}{E_{c0m}} \quad (4.12)$$

Where  $E_{c0m}$  is the tangent Young's modulus of elasticity of concrete.  $E_{c0m}$  is calculated by multiplying the secant Young's modulus of elasticity,  $E_{cm}$ , with a factor of 1.05 (Grünberg & Göhlmann, 2013).

The stress leading to the appearance of the first crack,  $\sigma_{sr}$ , is determined using the following expression:

$$\sigma_{sr} = f_{ctm} \times \frac{1 + \alpha_{Ed}\rho_s}{\rho_s} < \frac{f_{yk}}{\gamma_s} \quad (4.13)$$

Where:

- $\alpha_{Ed}$  is the design modular ratio ( $\alpha_{Ed} = \gamma_C \frac{E_s}{E_{com}}$ );
- $\rho_s$  is the ratio of the area of reinforcing steel to the area of the concrete ( $\rho_s = \frac{A_s}{A_c}$ ); and
- $f_{yk}$  is the characteristic yield strength of the reinforcing steel; and
- $\gamma_S$  is the partial factor for reinforcing steel, which Eurocode 2 recommends to be taken as 1.15 (EN 1992-1-1:2004, 2004).

The stress leading up to the first crack,  $\sigma_{sr}$ , is limited by the characteristic yield strength of the reinforcing steel,  $f_{yk}$ , so that ductile cross section behaviour is insured.

When the reinforced concrete cross section is still in the uncracked state, the stiffness of the reinforcing steel is increased by taking the tensile capacity of the concrete into account. The increase of the stiffness depends on the ratio of reinforcing steel to concrete within the cross section as well as the ratio of the reinforcing stiffness to the concrete stiffness. As stated in Section 4.4.1, the effective modulus of elasticity of the steel will increase as the amount of reinforcing in the cross section is decreased. The effective modulus of elasticity of the steel corresponding to the uncracked section is calculated using the following expression:

$$E_{s,eff} = E_s \frac{1 + \alpha_{Ed} \rho_s}{\alpha_{Ed} \rho_s} \quad (4.14)$$

The effective stress,  $\sigma_{s,eff}$ , which corresponds to the strain in the uncracked state, is calculated using the following expression:

$$\sigma_{s,eff} = E_{s,eff} \varepsilon_s \leq \sigma_{s,eff;0.7} = \frac{0.7 \sigma_{sr}}{\gamma_C} \quad (4.15)$$

It must be checked that the calculated effective stress,  $\sigma_{s,eff}$ , is less than the limit specified in Equation (4.15) to ensure that the cross section is uncracked.

#### **Formation of cracks** ( $\varepsilon_{srd;0.7} < \varepsilon_s \leq \varepsilon_{srd;1.3}$ ):

After cracks have formed in the cross section, the effective modulus of elasticity of the steel decreases to a value lower than the characteristic modulus of elasticity of the steel,  $E_s$ . This phenomenon can be seen in Figure 4.5, where the gradient of the stress-strain curve in the region where cracks start to form is less steep than that of pure steel.

The effective modulus of elasticity of the steel in the region where cracks start to form is calculated using the following equations:

$$E_{s,eff} = \frac{0.6E_s(1 + \alpha_{Ed}\rho_s)}{1.3 + 0.6\alpha_{Ed}\rho_s - \beta_t} = \frac{\sigma_{s,eff;1.3} - \sigma_{s,eff;0.7}}{\varepsilon_{srd;1.3} - \varepsilon_{srd;0.7}} \quad (4.16)$$

$$\sigma_{s,eff;1.3} = \frac{1.3\sigma_{sr}}{\gamma_C} \quad (4.17)$$

$$\varepsilon_{srd;1.3} = \frac{f_{ctm}}{E_{c0m}} \times \frac{1.3(1 + \alpha_{Ed}\rho_s) - \beta_t}{\alpha_{Ed}\rho_s} \quad (4.18)$$

$\beta_t$  is a coefficient that takes the influence of the duration of the loading or repeated loading into account.  $\beta_t$  is taken as 0.50 for sustained loads or many cycles of repeated loading (EN 1992-1-1:2004, 2004).

**Stabilized cracking** ( $\varepsilon_{srd;1.3} < \varepsilon_s \leq \varepsilon_{smy}$ ):

The strain associated with the characteristic value of the yield point of the reinforcing steel,  $f_{yk}$ , is calculated using the following expression:

$$\varepsilon_{smy} = \frac{f_{yk}/\gamma_S}{E_s} - \frac{f_{ctm}}{E_{c0m}} \times \frac{\beta_t}{\alpha_{Ed}\rho_s} = \frac{f_{yk}}{E_s} - \frac{f_{ctm}}{E_s} \times \frac{\beta_t}{\gamma_C\rho_s} \quad (4.19)$$

The effective stress in the steel when stabilized cracking occurs,  $\sigma_{s,eff}$ , is calculated using the following expression:

$$\sigma_{s,eff} = \sigma_s + \frac{f_{ctm}\beta_t}{\gamma_C\rho_s} \quad (4.20)$$

During the stabilized cracking phase, the effective modulus of elasticity,  $E_{s,eff}$ , is equal to the modulus of elasticity of the pure reinforcing steel,  $E_s$ .

**Yielding of the steel** ( $\varepsilon_s > \varepsilon_{smy}$ ):

After the steel yields, the effective stress in the steel is equal to the characteristic value for the yield point,  $f_{yk}$ , of the reinforcing steel. This relationship does not include the effects of strain hardening.

## 4.5 Algorithm developed to calculate the cross section properties

As mentioned in Section 4.2, the Model Column Method is merely a single step in calculating the properties of a cross section subjected to an applied axial load and moment. After the completion of every Model Column Method analysis, the bending moment for a specified curvature is obtained. The specified curvature is then incremented to obtain the next moment-curvature pair. By combining all of the calculated moment-curvature pairs, a moment-curvature diagram is constructed, specific to the cross section and dependent on the axial force. From this diagram, the curvature associated with the applied bending moment is obtained. Although the main goal of this algorithm is to obtain the curvature, the other cross section properties are also obtained in the process, as well as the internal normal stresses.

The algorithm developed to calculate the curvature for a given applied bending moment is summarised below.

- Step 1: Increment the curvature with a logical amount and find the associated moment for every increment, using the Model Column Method discussed in Section 4.2.
- Step 2: After every iteration, test whether two moment-curvature pairs on the moment-curvature diagram have been found that surrounds the actual applied bending moment.
- Step 3: If the actual applied bending moment lies between two moment-curvature pairs on the moment-curvature diagram, use linear interpolation to find the curvature associated with the actual applied bending moment.
- Step 4: Use the Model Column Method to find the moment associated with the curvature obtained in Step 3.
- Step 5: Test whether the moment found in Test 4 falls within the desired tolerance when it is compared to the actual bending moment. If this test holds, the desired moment-curvature pair has been found. If not, return to Step 1, but start to increment the curvatures from the closest lower bound point on the moment-curvature diagram, and use smaller increments.

After every iteration of the algorithm, the amount by which the curvature is incremented is reduced. In this way, convergence is guaranteed for any specified tolerance. It has been found that by reducing the curvature increment by a factor of 10 after every iteration, the algorithm performed well.

Figure 4.8 demonstrates how the developed software obtains a curvature for a given moment using the process described above. For this demonstration, the applied bending moment is 25.0 MNm. It can be seen from Figure 4.8 that the graph becomes denser as the algorithm attempts to converge near the 25.0 MNm gridline. For this demonstration, the algorithm took 202 iterations, including the iterations of the Model Column Method, to find the curvature associated with the specified moment to an accuracy of  $1 \times 10^{-6}$ .

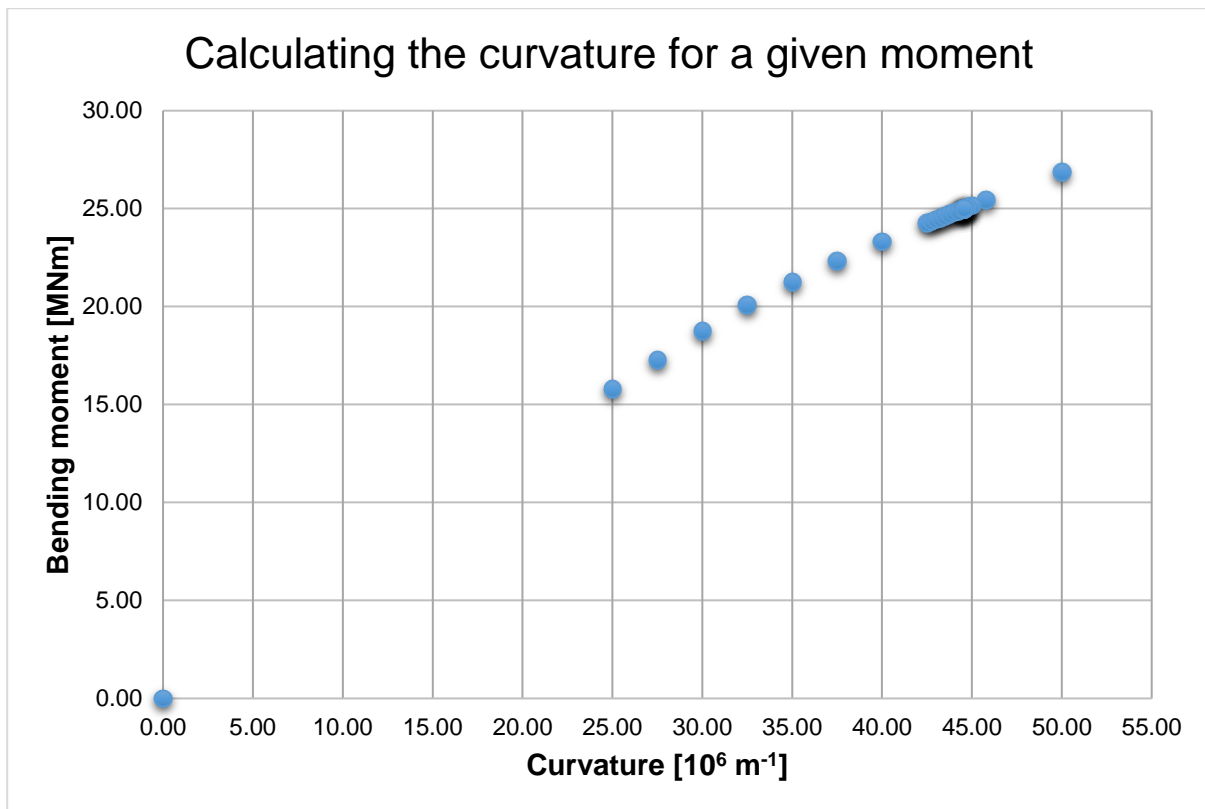


Figure 4.8: Demonstration of how the developed software finds the curvature for a given moment

When performing a structural analyses of a WTG tower, the algorithm discussed above is applied to the cross section at every node along the height of the tower. When dealing with second-order analyses, all of the cross section nonlinear properties have to be calculated after every iteration. This is discussed in Chapter 7: Deflection and Internal Stress Analysis.

The iterative nature of the algorithm described above is computationally expensive, but the complexity is linear. Consequently, the computations for a complete tower analysis when considering physical and geometric nonlinear properties require less than 10 seconds on a standard personal computer.

## 4.6 Verification of cross section analysis results

The accuracy of the cross section analysis results are verified by comparing it to an example given in BetonKalender (Grünberg & Göhlmann, 2013). BetonKalender produced a moment-curvature relationship for an annular reinforced concrete cross section with a diameter of 5m and wall thickness of 500mm. The parameters specified in the example are duplicated in this study in the attempt to reproduce the same moment-curvature relationship. The results of this test are illustrated in Figure 4.9.

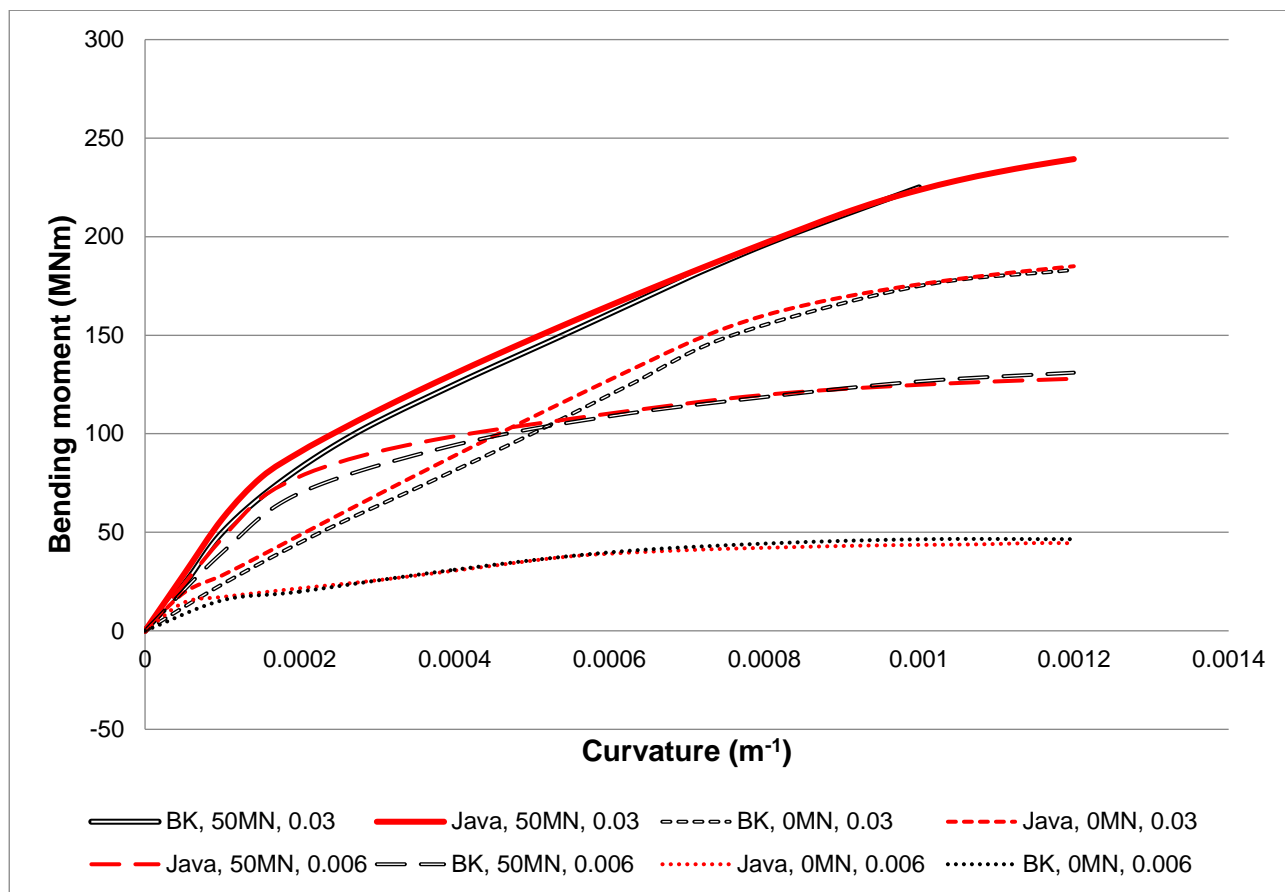


Figure 4.9: Comparison of the cross section analysis results generated by the developed software to the example found in *BetonKalender* (Grünberg & Göhlmann, 2013)

Figure 4.9 illustrates four variations of the cross section analysis, with each variation being compared to the example obtained from *BetonKalender*. In the legend above, “BK” and “Java” denoted the curves obtained from *BetonKalender* and the developed software, respectively. The values following these notations represent the applied axial force and the fraction of reinforcing steel included in the cross section, respectively.

In the example presented by *BetonKalender*, the annular reinforced concrete cross section is discretised into radial elements. This is different from the way the cross section is modelled in the developed algorithm. As discussed in Section 4.2.2, the cross section is discretised into horizontal, unidirectional strip elements. Another difference to take note of is how the reinforcing is modelled. The example presented by *BetonKalender* models the reinforcing steel as circular areas in discrete locations (Grünberg & Göhlmann, 2013). For this study, the reinforcing is modelled as continuous rings, which could explain the increased stiffness when the cross section is exposed to small moments in Figure 4.9.

The example presented by *BetonKalender* excludes detailed information regarding the distribution of inner and outer reinforcing and the cover used in the cross section model. The internal and external concrete cover are thus assumed to both be 70mm. It is also assumed that a bigger percentage of reinforcing is placed near the outer edge of the shaft compared to the internal edge.

The accuracy of the results from the cross section analysis is verified by the fact that similar moment-curvature relationships are produced when compared to the example presented by BetonKalender. The maximum deviation from the curves in BetonKalender is approximately 18%. The differences in the results are believed to be adequately explained above.

# Chapter 5: Vibration Analysis

## 5.1 Introduction

The structural analysis of a WTG begins with a dynamic analysis to determine the natural frequencies of the structure. It is important to verify that the first natural frequency of the WTG does not coincide with the blade excitation frequencies of the tower (Manwell, et al., 2009). If it is found that the first natural frequency is too close to an excitation frequency, the design of the tower should be modified so that the natural frequency falls within an acceptable range.

The important blade passing excitation frequencies to consider are the 1P and 3P frequencies (one and three blade passing frequencies, respectively). The 'P' is an abbreviation for 'per revolution'. Whole multiples of the 1P frequency (also known as the rotor frequency) should also be considered.

For variable speed wind turbines, it has been established that if the first natural frequency of the tower does not fall within the ranges of  $\pm 10\%$  of the 1P and 3P frequencies respectively, there will normally not be any problems due to load amplification arising from vibrations (DNV/Risø, 2002). A more recent report by ASCE/AWEA (2011) has stated that general wind energy experience has increased the minimum limit to a preferred range of 15%. At this percentage, there has been no recorded resonance effects on wind turbine towers.

One way to verify that the tower's first natural frequency does not coincide with the blade excitation frequencies is by the use of a Campbell diagram. This diagram plots the rotor and blade frequencies for different rotation speeds. Points where the excitation frequencies coincide with the tower's fundamental frequency should be avoided. An example of a Campbell diagram is illustrated in Figure 5.1.

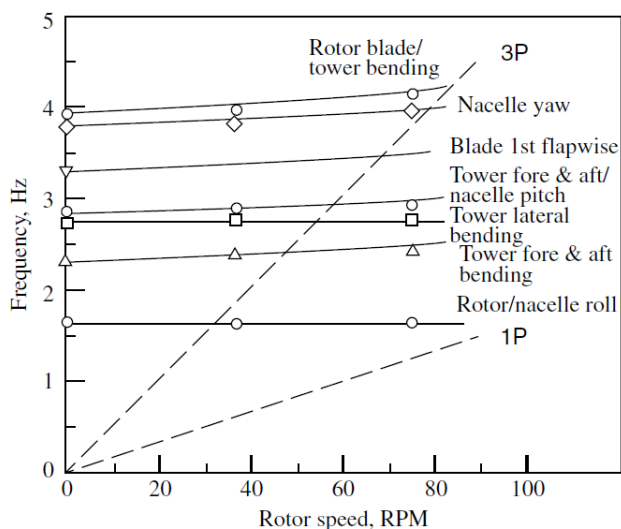


Figure 5.1: Example of a Campbell diagram for a three bladed wind turbine (Manwell, et al., 2009)

The calculation of the gust effects caused by wind loads on the WTG is also dependent on the fundamental vibration frequency. Wind gust effects are irregular variations in wind speeds along the height of the tower. Wind gust effects are discussed in Chapter 6: Wind Loading.

Various approximate analytical methods could be used to determine the fundamental frequency of a WTG. These methods could either be based on the principal of conservation of energy or they could incorporate classical vibration theory. Classical vibration theory is based on the differential equation developed for a mass-spring system with a single degree of freedom (Grünberg & Göhlmann, 2013). Some approaches that are based on the principal of conservation of energy are the energy method and Rayleigh's energy method. Approximate analytical methods could provide relatively accurate results when calculating the natural frequency and eigenmode of the fundamental vibration. Due to the assumption that WTGs are dynamically sensitive structures, higher eigenmodes and frequencies might be required to analyse vortex shedding transverse vibrations. Approximate analytical methods can thus be seen as good approaches to verify the first natural frequency of the WTG, but should generally not be used as a primary method when performing vibration calculations (ASCE/AWEA, 2011).

A modal analysis using the finite element method can be used to calculate any number of eigenmodes and eigenvalues with great accuracy and speed. For these reasons, it has been decided to implement this method.

It should be noted that the modal analysis is performed with the assumption that the tower foundation is fixed against rotation and translation. This assumption simplifies the analysis and the implementation thereof, but could result in an overestimate of the frequency. As a rule of thumb, the fixed base frequency calculation would typically result in 0 – 5 percent higher frequencies, but could result in as much as a 20% overestimate of the frequency under special conditions (DNV/Risø, 2002). It is therefore advisable to take the stiffness of the foundation and underlying geological conditions into account when calculating final vibrations, as well as for final deflection calculations (GL, 2010).

An approach that is regularly followed to take account of the foundation and soil stiffness, is to model the foundation as a rigid body, supported by a set of springs. For this method, it is generally assumed that the flexibility of the foundation could be neglected, due to its relatively small flexibility compared to the underlying soil (DNV/Risø, 2002). In reality, the soil underneath the foundation would exhibit nonlinear properties. To accurately simulate the nonlinear soil, the springs should ideally be modelled as nonlinear springs as well.

## 5.2 FEM modal analysis

The FE model discussed in Section 3.3 is used to perform the FEM modal analysis discussed in this section. The FEM modal analysis is used to generate the mode shapes and associated frequencies

of the tower. The following section presents an overview of the derivation of the eigenvalue equation used to solve for the eigenvalues and eigenvectors of the WTG tower.

### 5.2.1 Derivation of the eigenvalue problem

The generalized form of the equation of motion is given by:

$$[M]\{\ddot{U}\} + [C]\{\dot{U}\} + [K]\{U\} = \{F\} \quad (5.1)$$

Where:

- $[M]$  is the system mass matrix;
- $\{\ddot{U}\}$  is the second derivative of the displacement vector (acceleration vector);
- $[C]$  is the damping matrix;
- $\{\dot{U}\}$  is the first derivative of the displacement vector (velocity vector);
- $[K]$  is the system stiffness matrix;
- $\{U\}$  is the system displacement vector; and
- $\{F\}$  is the system force vector.

When performing a free vibration modal analysis, zero damping and zero external forces on the system are generally assumed. By applying these assumptions, the quadratic eigenvalue problem in Equation (5.1) reduces to the following:

$$[M]\{\ddot{U}\} + [K]\{U\} = \{0\} \quad (5.2)$$

Equation (5.2) represents the general eigenvalue problem used to determine a structure's free vibration frequencies and mode shapes. If it is assumed that the structure vibrates in harmonic oscillations, the displacement vector can be substituted by the following equation:

$$\{U\} = \{a\}e^{j\{\omega\}t} \quad (5.3)$$

Where:

- $\{a\}$  is the vector of displacement amplitudes;
- $\{\omega\}$  is the vector of angular frequencies (in radians per second) which needs to be determined; and
- $t$  is the time.

Substituting Equation (5.3) into Equation (5.2) yields the following:

$$[K]\{U\} = [M]\omega^2\{U\} \quad (5.4)$$

Multiplying Equation (5.4) by the inverse of the mass matrix ( $[M]^{-1}$ ) yields the standard form of an eigenvalue problem, which is solved using linear algebra theory. Equation (5.4), rewritten in the standard eigenvalue problem, looks as follows:

$$[A]\{U\} = \omega^2\{U\} \quad (5.5)$$

Where  $[A] = [M]^{-1}[K]$ .

Various software packages could be used to perform an eigenvalue decomposition on  $[A]$  in the expression above. From the eigenvalue decomposition, the eigenvectors and eigenvalues are obtained. The eigenvector represents the deformed shape of the specific mode of vibration, whereas the eigenvalue represents the angular frequency squared (radians per second squared). To obtain the linear frequency (Hz), the square root of the eigenvalue ( $\omega^2$ ) is divided by  $2\pi$ . This relationship is expressed in Equation (5.6) below.

$$f = \frac{\sqrt{\omega^2}}{2\pi} \quad (5.6)$$

Where  $f$  is the linear frequency in cycles per second (Hz).

## 5.2.2 Stiffness and mass matrix formulation

The 4DOF beam element stiffness and mass matrices are represented by Equation (5.7) and Equation (5.8), respectively. These are used to formulate the system global matrices. The use of a 4DOF beam element is considered to be acceptable for this formulation, as the axial frequencies are generally significantly higher than the turbine blade passing frequencies.

$$[K] = EI \begin{bmatrix} \frac{12}{L^3} & \frac{6}{L^2} & -\frac{12}{L^3} & \frac{6}{L^2} \\ \frac{6}{L^2} & \frac{4}{L} & -\frac{6}{L^2} & \frac{2}{L} \\ -\frac{12}{L^3} & -\frac{6}{L^2} & \frac{12}{L^3} & -\frac{6}{L^2} \\ \frac{6}{L^2} & \frac{2}{L} & -\frac{6}{L^2} & \frac{4}{L} \end{bmatrix} \quad (5.7)$$

$$[M] = \frac{m}{420} \begin{bmatrix} 156 & 22L & 54 & -13L \\ 22L & 4L^2 & 13L & -3L^2 \\ 54 & 13L & 156 & -22L \\ -13L & -3L^2 & -22L & 4L^2 \end{bmatrix} \quad (5.8)$$

Where:

- $EI$  is bending stiffness of the beam element;
- $L$  is the length of the beam element; and
- $m$  is the mass of the beam element.

### 5.3 Vortex induced transverse vibrations

In fluid dynamics, bodies subject to fluid flow can either be classified as streamlined or bluff. A bluff body can be defined as a body that causes the flow to separate over a substantial part of its surface. This is a result of the body's shape (Naval Studies Board; National Research Council, 1997). The shape of a bluff body can be defined as a body in which the dimension in the direction of the flow is close or equal to the dimension normal to the flow. A wind turbine tower can generally be categorised as a bluff body.

When substance such as water or wind flows over a bluff body, the flow separates and creates vortices behind the body. The vortices break away from the body in a phenomenon called vortex shedding. This creates alternating high and low-pressure zones on opposite sides of the body. Due to the fluctuating load resulting from the alternating pressure zones on opposite sides of the body, the body will tend to oscillate in the plane normal to the mean flow direction (EN 1991-1-4:2005, 2005).

Vortex shedding is an important topic in structural dynamics. When considering slender structures that can be defined as having a bluff shape, the structure may be susceptible to fatigue resulting from excessive oscillating. When the induced transverse vibrations coincide with one of the structure's natural frequencies, the structure could also undergo excessive deformation due to resonance.

In a publication by Grünberg & Göhlmann (2013), it is stated that vortex-induced transverse vibrations are normally of minor significance when considering reinforced concrete and pre-stressed towers. Due to the slenderness and shape of wind turbine towers, it is still necessary to verify that vortex-induced vibrations would not have a significant effect on the structure. In a publication by DNV/Risø (2002), it is stated that vortex-induced vibrations could have a significant effect on wind turbine towers before the rotor and nacelle have been mounted on the tower.

In order to verify that vortex shedding will not have a significant effect, it is necessary to compare the vortex shedding frequency to the natural frequencies of the wind turbine tower. Another, more popular way to analyse the tower for vortex shedding, is to calculate the wind speed at which resonance effect will occur. This wind speed is termed the critical wind speed, and is calculated using Equation (5.9) below (DNV/Risø, 2002).

$$V_{cri} = \frac{D\omega_i}{St} \quad (5.9)$$

Where:

- $D$  is the diameter of the tower (m);
- $\omega_i$  is the  $i^{th}$  natural frequency of the tower (Hz); and
- $St$  is the Strouhal number described below.

For tapered towers, it is clear that the critical wind speed will vary along the height of the tower. This results in a range of critical wind speeds that should be avoided as far as possible to reduce the possibility of resonance effects. The range of critical wind speeds can be expressed by the following equation:

$$\frac{D_{min}\omega_i}{St} \leq V_{cri} \leq \frac{D_{max}\omega_i}{St} \quad (5.10)$$

Where  $D_{min}$  and  $D_{max}$  are the smallest and largest tower diameters, respectively.

The Strouhal number,  $St$ , depends on the Reynolds number of the cross section. This relationship is illustrated in Figure 5.2.

Annex E in Eurocode 1 provides a table that can be used to determine Strouhal numbers for various cross sections. This table is reproduced below as Table 5.1, and proposes that a Strouhal number of 0.18 be used for bodies with a circular cross section. In a publication by DNV/Risø (2002), a relationship is made between the Strouhal number and the ratio of the tower height to the top diameter. This figure is reproduced as Figure 5.3.

A Strouhal number of 0.2 is sometimes used as a first approximation. From Figure 5.2 it can be seen that this is a good approximation at the preliminary design stage. For very high or low Reynolds numbers, however, it might be necessary to perform a more accurate calculation to determine the Strouhal number (Van Zyl, 2014).

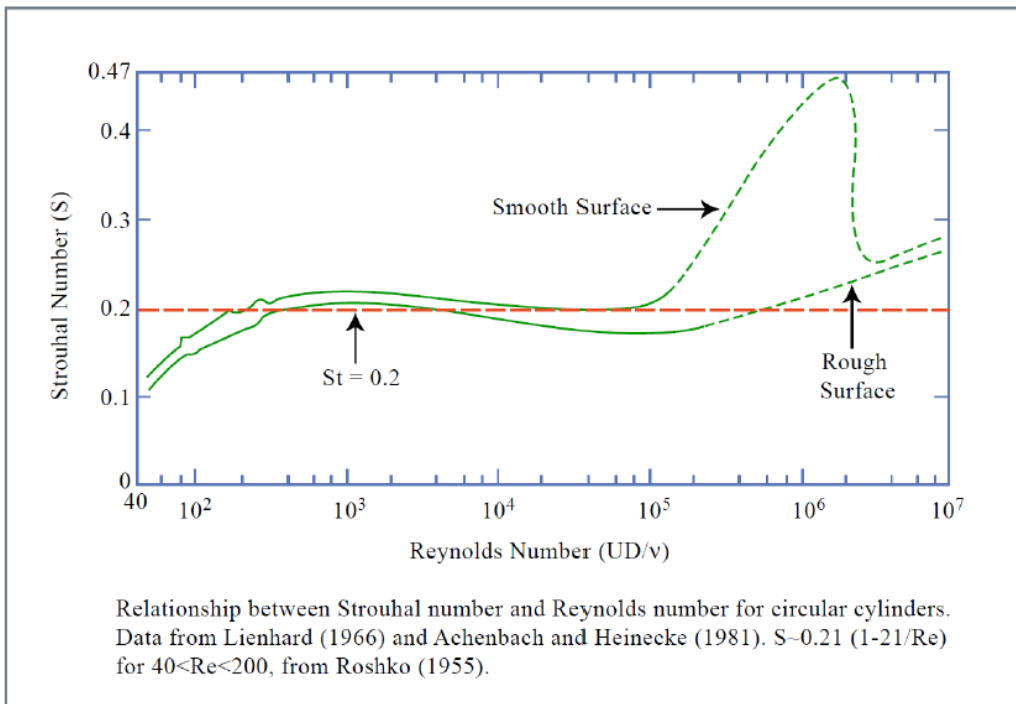


Figure 5.2: Relationship between the Strouhal number and Reynolds number (Tchet, 2005)

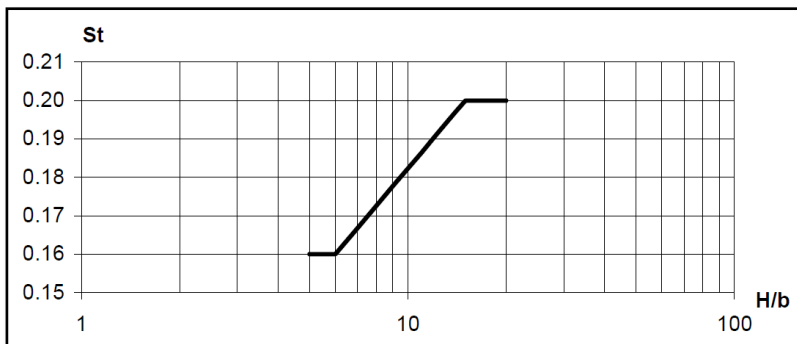
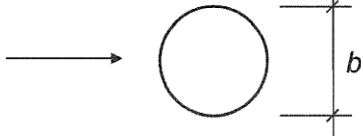
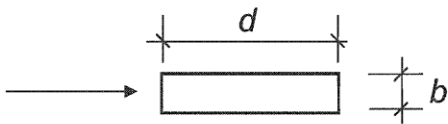
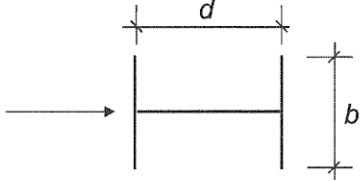
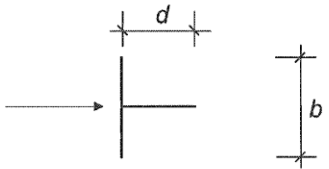
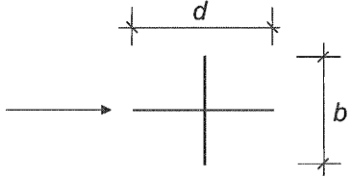
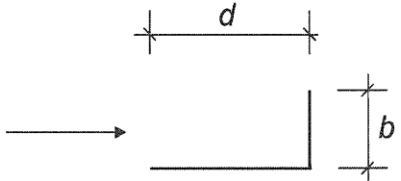


Figure 5.3: Relationship between the Strouhal number and the ratio of the tower height to the tower top diameter (DNV/Risø, 2002)

If it is found that the mean wind speed falls within the critical wind speed range, it might be necessary to temporarily stiffen the structure, especially during the erection of the tower. This could be done by guy wiring the tower or by mounting a temporary mass near the top of the tower. Normally vortex-induced vibrations are not a major concern when the WTG is operational. After the rotor and nacelle have been mounted, the added mass at the top of the structure will lower the critical wind speed of the tower. The blades will also interfere with the wind flow around the tower, which will obstruct the formation of vortices (DNV/Risø, 2002).

Table 5.1: Strouhal numbers for various cross sections (EN 1991-1-4:2005, 2005)

Cross-section	St
 for all Re-numbers	0,18
 $0,5 \leq d/b \leq 10$	from Figure E.1
 linear interpolation	$d/b = 1$ 0,11 $d/b = 1,5$ 0,10 $d/b = 2$ 0,14
 linear interpolation	$d/b = 1$ 0,13 $d/b = 2$ 0,08
 linear interpolation	$d/b = 1$ 0,16 $d/b = 2$ 0,12
 linear interpolation	$d/b = 1,3$ 0,11 $d/b = 2,0$ 0,07
NOTE Extrapolations for Strouhal numbers as function of $d/b$ are not allowed.	

## 5.4 Verification of frequency analysis output

The accuracy of the developed FEM modal analysis results is verified by comparing it to the results generated by software developed by Prokon Software Consultants (Prokon Software Consultants, 2016). Prokon software is sufficient in performing analyses where linear material properties are assumed, which is generally the case when performing modal analyses.

Four relatively simple models are tested. The first modal analysis test is conducted using a solid steel rod with a uniform circular cross section. The second test model consists of a uniform reinforced concrete circular hollow cross section. The third test model is made up of two reinforced concrete tower segments, each consisting of different cross section dimensions and height. Test 4 compares a 20m high concrete-steel hybrid column. This test delivered the closest results to that obtained by Prokon. Further details of the test models are given in Table 5.2 below.

Table 5.2: Deflection analysis test model details

	Description
<b>Test 1</b>	12m high, 100mm DIA S355JR steel solid circular section (12 beam elements)
<b>Test 2</b>	120m high, 7x6m RC circular hollow section (12 beam elements)
<b>Test 3</b>	Tower segment 1: 50m high, 7x6m RC CHS (5 beam elements) Tower segment 2: 70m high, 6x5 RC CHS (7 beam elements)
<b>Test 4</b>	Tower segment 1: 14m high, 0,9m RC solid circular section (14 beam elements) Tower segment 2: 6m high, 508x12mm S355JR steel CHS (6 elements)

The comparison between the output generated by Prokon and the developed software is illustrated in Table 5.3. Generally, only the lower modes and frequencies are important for design and analysis. Higher structural mode shapes and frequencies, however, can become relevant when considering vortex-induced transverse vibrations (Giosan).

Table 5.3: Frequency modal analysis output verification

	Mode	Prokon (Hz)	Developed Software (Hz)	% Difference
<b>Test 1</b>	1	70.520	70.614	0.13
	2	438.360	442.545	0.95
	3	1214.490	1239.414	2.05
	4	2352.610	2430.453	3.31
	5	3813.360	4024.005	5.52
<b>Test 2</b>	1	0.300	0.297	1.01
	2	1.850	1.860	0.54
	3	5.140	5.210	1.36
	4	9.950	10.214	2.65
	5	16.230	16.897	4.11
<b>Test 3</b>	1	0.310	0.312	0.65
	2	1.690	1.695	0.30
	3	4.720	4.767	1.01
	4	9.020	9.212	2.13
	5	14.800	15.302	3.39
<b>Test 4</b>	1	1.890	1.886	0.19
	2	9.260	9.276	0.17
	3	17.700	17.761	0.35
	4	37.320	37.663	0.92
	5	65.730	66.668	1.43

The accuracy of the developed software is verified by the fact that the highest %-difference between the Prokon and the developed software output is 5.52%. This is the result obtained from the first test, where the 5<sup>th</sup> mode shape is compared. The relatively large difference in this case may be due to very high frequency outputs, which are approximately 4000Hz. For test 2 and 3, which test models that better approximate reinforced concrete wind turbine towers, results closer to that generated by Prokon are obtained.

Figure 5.4 and Figure 5.5 compare the first five mode shapes of Test 4, generated by the developed software and Prokon, respectively.



Figure 5.4: Test 4 mode shapes generated by the developed software

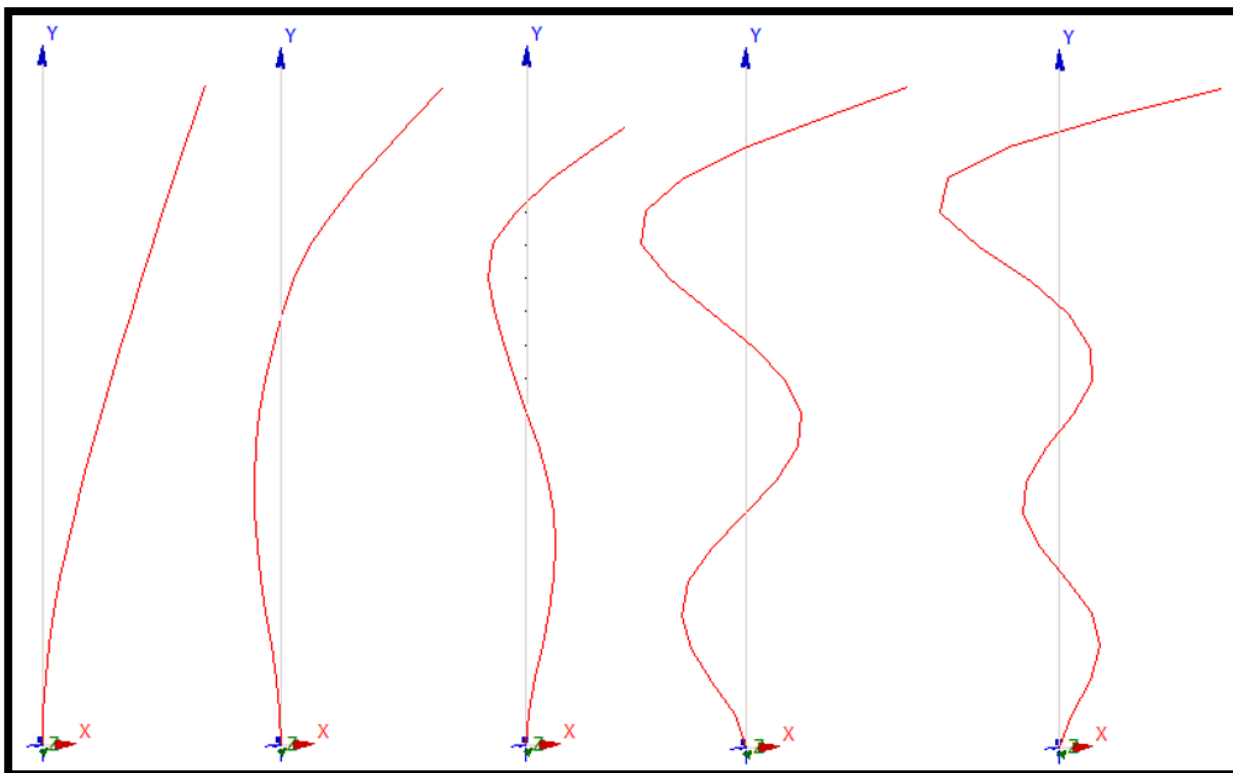


Figure 5.5: Test 4 mode shapes generated by Prokon

The time elapsed during each frequency test is presented in Table 5.4. This is presented to provide an idea of the speed in which a modal analysis can be completed using the modal analysis methodology implemented for this study.

Table 5.4: Time required to perform modal analysis tests

Test	Time elapsed (s)	
	Prokon	Developed Software
1	1.916	0.053
2	0.247	0.059
3	0.149	0.054
4	0.283	0.105

# Chapter 6: Wind Loading

## 6.1 Introduction

There are various codes and guidelines which can be followed to determine the wind loads acting on a wind turbine tower. There is currently no design codes dealing exclusively with the detailed design of post-tensioned reinforced concrete wind turbine towers (Van Zyl, 2014). It is thus expected of the design engineer to find a suitable design code or a combination thereof to aid in the design of a wind turbine support structure that is safe and economical. This chapter identifies and investigates various methods of calculating external wind loads on a wind turbine tower.

The first step in applying wind loads to a structure is to determine the basic average wind speed and terrain conditions of the prospective site. The basic average wind speed is usually measured at a height of 10 meters above ground level. It is obtained by measuring a site's average wind speed during 10-minute time intervals. Multiple of these measurements are usually carried out over a time period of a year. The average of these measurements are then obtained to determine the basic average wind speed, specific to the site in question. SANS 10160-3:2011, for example, uses a map of South Africa to represent the fundamental values of the basic wind speeds across the country (SANS 10160-3:2011, 2011).

Once the basic average wind speed and terrain conditions are obtained, a suitable mathematical model must be used to calculate the wind speed distribution along the height of the structure. After the wind distribution along the height of the structure is obtained, the wind speed can be converted into external and internal wind pressures. The wind pressure, multiplied with an area, along with various equation factors, yields the design wind force acting on the structure.

Regarding the multiple step process to obtain wind loads on a structure, it is common that multiple design codes and guidelines are used in combination. Some codes and guidelines might only be partially applicable to a specific design situation. A more "general" design standard could then be consulted to fill the gaps. The South African wind loading code, SANS 10160-3:2011, for example, refers the designer to other appropriate standards or specialist literature when the structure being analysed falls outside the scope of SANS 10160-3 (SANS 10160-3:2011, 2011).

Care should be taken with the units of the terms used in the wind load calculations. The reference wind speed,  $V_{ref}$ , used in the IEC 61400-1 calculations, for example, could be in terms of the 10-minute average or the 3-second gust wind speed. Wind speeds could also be measured from various heights above ground level. Wind speeds can be converted from a 3-second gust to a 10-minute average wind speed and by dividing the value by 1.4. This conversion factor is consistent throughout

various design codes, such as SANS 10160-3:2011 (SANS 10160-3:2011, 2011), EN 1991-1-4:2005 (EN 1991-1-4:2005, 2005) and IEC 61400-1:2005 (IEC 61400-1:2005, 2005). A wind speed measured from a specific height above the ground can be converted to represent a wind speed at a different height above the ground by using the power law (IEC 61400-1:2005, 2005). The power law is represented as Equation (6.1).

## 6.2 Summary of implemented codes and guidelines

Various design codes and guidelines, which can be used to calculate the wind loading on structures such as wind turbine towers, are discussed in the remainder of this chapter. For this study, the guidelines presented by IEC 61400 to determine the reference wind speed,  $V_{ref}$ , are followed. The IEC extreme wind speed model is then used to determine the 3-second gust wind speed, measured at a height of 10 meters above ground level. ASCE 7-10 is used in all further calculations to determine the external design wind pressures and forces acting on the tower. The reasons for choosing these codes are discussed in the following sections of this chapter.

## 6.3 SANS 10160-3:2011

SANS 10160-3:2011 is the standard most commonly used in South Africa to calculate wind actions on structures. It is based on the guidelines given by Eurocode (EN 1991-1-4:2005, 2005). For this study, SANS 10160-3 was investigated to determine whether it is suitable to predict wind actions on WTG structures.

The first remark is on what is written in the scope of SANS 10160-3. In clause 1.2.3, it states that SANS 10160-3: 2011 does NOT cover structures and buildings higher than 100m tall. It also states that it does NOT cover or take account of dynamic effects or the design of dynamically sensitive structures (SANS 10160-3:2011, 2011). In a publication by Grünberg and Göhlmann (2013), it is stated that wind turbines should generally be assumed dynamically sensitive structures. It is thus important to take account of dynamic wind pressures, arising from wind turbulence and wind gust effects.

As mentioned earlier, the first step in obtaining the external wind loading on a structure is to determine basic fundamental wind speed of the region. This value is independent on the structure height or the interaction between the wind and the structure. The map of the fundamental value of the basic wind speed in SANS 10160-3:2011 is thus an acceptable source to determine the basic wind speed for a region in South Africa. The equations used to determine the wind distribution along the height of the tower, however, should be used only if it can be justified that these equations yield accurate wind regimes for structures taller than 100 meters.

Eurocode 1, which deals with actions on structures, is a good alternative to use when the structure that needs to be designed falls outside the scope of SANS. It is stated in the scope of EN 1991-1-

4:2005, that this standard is applicable to include the design of buildings and engineering works with heights up to 200m (EN 1991-1-4:2005, 2005).

The structural factor is an important factor, which is incorporated in the external wind force calculation. It is used in Eurocode 1: Actions on Structures, to take account of the dynamic sensitivity of wind turbine towers. For structures falling in the scope of SANS 10160-3, however, this factor is simply assumed to be equal to 1.0 (SANS 10160-3:2011, 2011). The following is stated in SANS 10160-3 regarding the structural factor:

*“The structural factor,  $C_s C_d$ , takes into account the combined effects of*

- a) The disorganized distribution, i.e. non-simultaneous occurrence of peak pressures over the external surfaces of the building or structures, and*
- b) The dynamic effects due to resonance between the turbulence of the flow and vibration of the structure” (SANS 10160-3:2011, 2011).*

The structural factor calculation procedure is excluded from this study due to its tediousness and length. Annex B and C in EN 1991-1-4:2005, however, provide two alternative approaches for calculating the structural factor.

It has been decided that for wind turbine towers of heights 100m and taller, it is reasonable to use SANS 10160-3:2011 to obtain the fundamental value of the basic wind speed in South Africa. It is however recommended that the wind speeds along the height of the structure be determined by an alternative design code, such as Eurocode, when tower heights exceed 100m.

## 6.4 IEC 61400-1 (2005)

The IEC 61400-1 is an alternative design guideline that could be used to determine the wind speeds along the height of a wind turbine tower. The IEC 61400-1 is an international standard published by the International Electrotechnical Commission (IEC). It was published with the intent to provide an outline for the minimum design requirements of onshore wind turbines and is not intended for the use as a complete design specification or instructional manual (IEC 61400-1:2005, 2005). The IEC 61400-1 is very useful guide, which could be used to consider various load combinations and wind loading models. The wind loading models (wind regimes) discussed in IEC 61400-1 can generally be divided into two categories, namely: normal and extreme wind conditions. Normal wind conditions are conditions that will occur frequently during normal operation of a wind turbine. Extreme wind conditions are defined as having a 1-year or 50-year recurrence period (IEC 61400-1:2005, 2005).

The effect of external conditions are taken into account by the identification of various turbine classes. Each turbine class represents different reference wind speed and turbulence parameters. A note under the definition of the reference wind speed in IEC 61400-1, clause 3.42, states the following:

“A turbine designed for a wind turbine class with a reference wind speed  $V_{ref}$ , is designed to withstand climates for which the extreme 10 min average wind speed with a recurrence period of 50 years at turbine hub height is lower than or equal to  $V_{ref}$ .”

Stated differently, the designer can design a particular WTG for a specific wind turbine class (class I, II or III) only if it can be verified that the extreme 10 min average wind speed with a recurrence period of 50 years is lower or equal to the IEC reference wind speed at the tower hub height. This can usually be verified by a regional design code. In South Africa, for example, regional wind speeds can be determined by the South African wind loading code, SANS 10160-3 (SANS 10160-3:2011, 2011). In a study conducted by Way (2014), a comparison is made between the design wind speeds calculated by the IEC 61400-1 and SANS 10160-3: 2011 design codes, respectively. This study revealed that the IEC code yielded larger extreme wind speeds at hub height for all the towers investigated in the report, the tallest being 120m tall.

Due to the South African wind loading code falling outside the scope of tall WTG towers (100m or taller), and the findings of Way, the design approach proposed by IEC 61400-1 for the design of a class III wind turbine has been found to be acceptable for this study. If it had been found that the South African code yielded a higher extreme wind speed at hub height compared to the IEC class III reference wind speed, the tower could have been designed as an IEC class II or I wind turbine. If it had been found that the external wind conditions had not been covered by any of the normal turbine classes (turbine class I, II or III), then the turbine could have been designed as an IEC special wind turbine (IEC turbine class S design).

The different IEC wind turbine classes and their parameters are expressed in Table 1 in IEC 61400-1. For convenience, this table is reproduced as Table 6.1.

Table 6.1: Basic parameters for wind turbine classes (IEC 61400-1:2005, 2005)

Wind turbine class		I	II	III	S
$V_{ref}$ (m/s)		50	42.5	37.5	Values specified by the user
$I_{ref}$ (-)	A	0.16			
	B	0.14			
	C	0.12			

Where:

- $V_{ref}$  is the reference wind speed average over 10 minutes (in m/s) at the tower hub height;
- $I_{ref}$  is the expected value of the turbulence intensity at 15 m/s; and

- A, B and C designates the categories for higher, medium and lower turbulence characteristics, respectively.

It is worth noting that all the reference wind speed values specified in Table 6.1 apply at hub height, irrespective of the height of the tower.

There are various normal and extreme wind models described in IEC 61400-1. There are two normal wind condition models, which are the normal wind speed profile model (NWP) and the normal turbulence model (NTM). There are six extreme wind condition models, which are as follows: The extreme wind speed model (EWM), extreme operating gust (EOG), extreme turbulence model (ETM), extreme direction change (EDC), extreme coherent gust with direction change (ECD) and extreme wind shear (EWS).

Due to the specific aims of this study, it is deemed acceptable to only implement the extreme wind speed model. If needed, the software can later be extended to include additional wind loading models. Once the wind loads are added to the WTG model, the external force vector can be computed, which is then used in the deflection analysis. This is further discussed in Chapter 7: Deflection and Internal Stress Analysis.

#### 6.4.1 Extreme wind speed model

The extreme wind speed model can be divided into either a steady or turbulent wind model. For both the steady and turbulent wind models, one can either calculate the wind speed with a recurrence period of 1 year or 50 years. The wind speed with a recurrence period of 1 year can be calculated by multiplying the 50 year wind speed by a factor of 0.8 (IEC 61400-1:2005, 2005). The turbulent extreme wind speed model is calculated by the use of Equation (6.1) below, but excluding the factor of 1.4 (IEC 61400-1:2005, 2005).

The steady extreme wind speed model with a recurrence period of 50 years at height,  $z$ , along the tower, can be computed by the following equation:

$$V_{e50} = 1.4V_{ref} \left( \frac{z}{z_{hub}} \right)^{0.11} \quad (6.1)$$

Where:

- $V_{ref}$  is the reference wind speed average over 10 minutes (in m/s) at the tower hub height;
- $z$  is the height at which the wind speed needs to be determined; and
- $z_{hub}$  is the tower hub height.

The factor of 1.4 in Equation (6.1) converts the 10-minute average reference wind speed ( $V_{ref}$ ) into a 3-second gust wind speed at hub height. The factor of 1.4 is also used in SANS 10160-3 for the same conversion (SANS 10160-3:2011, 2011).

## 6.5 ASCE 7-10 (2010)

The ASCE 7-10 was published by the American Society of Civil Engineers. It provides yet another alternative to obtain the wind speed distribution along the height of structures, such as wind turbine towers. As discussed in Section 6.2, Eurocode 1 takes the dynamic effects into account by the calculation of the structural factor. ASCE 7-10 takes similar effects into account by the inclusion of the *gust effect factor*. The gust effect factor is included to take account of loading effects in the along-wind direction resulting from turbulence-structure interaction. Similar to the structural factor, the gust effect factor also accounts of load amplifications arising from the dynamic effects of flexible structures (ASCE 7-10, 2010).

The calculation procedure associated with the gust effect factor is found to be less complex and time consuming, compared to the calculation procedure of the structural factor presented by Eurocode. The incorporation of the gust effect factor is also recognized in *BetonKalender* (Grünberg & Göhlmann, 2013). It has thus been deemed reasonable to implement the gust effect factor methodology in this study to consider the WTG tower's sensitivity to vibration.

Chapter 29 in ASCE 7-10 deals with the calculation of wind loads on appurtenances and other structures not covered in the preceding chapters of the code. In particular, the code specifies "other structures" to include structures such as solid freestanding walls and solid signs, *chimneys*, tanks, open signs, lattice frameworks and trussed towers (ASCE 7-10, 2010). It is common that reinforced concrete chimney design methodology is adopted by procedures used to design reinforced concrete wind turbine towers. This is due to concrete wind turbine towers and concrete chimneys having similar geometry and slenderness characteristics. It is thus assumed that Chapter 29 of ASCE 7-10 provides a procedure that is adequate in determining the external wind loading on a wind turbine tower (Van Zyl, 2014).

### 6.5.1 Velocity pressure calculation procedure

Equation (6.2) is used to calculate the velocity pressure distribution along the height of the tower. It can be found in clause 29.3.2 in ASCE 7-10 as Equation (26.3-1). This calculation is dependent on the basic (fundamental) wind speed, as well as other factors, which incorporate terrain and wind direction conditions (ASCE 7-10, 2010).

The velocity pressure at height  $z$  above the ground can be calculated as follows:

$$q_z = 0.613K_zK_{zt}K_dV^2 \text{ (Pa)} \quad (6.2)$$

Where:

- $K_z$  is the velocity pressure exposure coefficient;
- $K_{zt}$  is the topographic factor;

- $K_d$  is the directionality factor; and
- $V$  is the basic wind speed in m/s.

It is important to note that the basic wind speed ( $V$ ) in the above equation is defined as the 3-second gust wind speed, measured at a height of 10 meters above ground level. As stated in Section 6.4, the reference wind speed given in IEC 61400-1 is the 10-minute average wind speed, measured at hub height. If it is decided to use the reference wind speed given in IEC 61400-1, it must first be converted to the correct format specified for Equation (6.2).

**The directionality factor**,  $K_d$ , is a factor which takes account of the shape of the structure. It is specified in ASCE 7-10 that the directionality factor should only be included in the wind calculations if the ASCE 7-10 load combinations are used. These load combinations can be found in clause 2.3 and 2.4 in ASCE 7-10. The directionality factor can be taken as equal to 0.95 for structures with a round cross section, such as concrete chimneys and wind turbine towers. (ASCE 7-10, 2010).

**The topographic factor**,  $K_{zt}$ , is included in the wind calculations to take account of wind speed-up effects resulting from the topography of the specific region. Topographic features that would cause wind speed-up effects are ridges, hills or escarpments. Wind turbines are usually constructed in relatively flat areas with low vegetation. For this reason, the topographic factor can be taken as equal to 1.0 (ASCE 7-10, 2010).

**The velocity pressure exposure coefficient**,  $K_z$ , is the only variable in Equation (6.2) that is dependent on the height of measurement. It is calculated by the following equation:

$$K_z = \begin{cases} 2.01 \left( \frac{z}{z_g} \right)^{2/\alpha} & \text{for } 4.6 \leq z \leq z_g \\ 2.01 \left( \frac{15}{z_g} \right)^{2/\alpha} & \text{for } z < 4.6 \end{cases} \quad (6.3)$$

Where:

- $z$  is the height of interest;
- $z_g$  is the gradient height; and
- $\alpha$  is an empirical exponent.

The two terms,  $z_g$  and  $\alpha$ , in Equation (6.3) can be obtained from Table 26.9-1: Terrain Exposure Constants in ASCE 7-10. For ease to the reader, this table has been reproduced here as Table 6.2.

Table 6.2: Terrain Exposure Constants (ASCE 7-10, 2010)

*In metric*

Exposure	$\alpha$	$z_g$ (m)	$\hat{\alpha}$	$\hat{b}$	$\bar{\alpha}$	$\bar{b}$	$c$	$\ell$ (m)	$\bar{\epsilon}$	$z_{min}$ (m)*
<b>B</b>	7.0	365.76	1/7	0.84	1/4.0	0.45	0.30	97.54	1/3.0	9.14
<b>C</b>	9.5	274.32	1/9.5	1.00	1/6.5	0.65	0.20	152.4	1/5.0	4.57
<b>D</b>	11.5	213.36	1/11.5	1.07	1/9.0	0.80	0.15	198.12	1/8.0	2.13

\* $z_{min}$  = minimum height used to ensure that the equivalent height  $\bar{z}$  is greater of  $0.6h$  or  $z_{min}$ .  
For buildings with  $h \leq z_{min}$ ,  $\bar{z}$  shall be taken as  $z_{min}$ .

**The exposure categories** listed in Table 6.2 above are used to define the type of exposure due to vegetation (surface roughness) encountered on the site in question. The different surface roughness categories, which are used to define the exposure categories in ASCE 7-10, are defined in the following paragraph.

Surface roughness B is defined as urban and suburban areas, wooded areas, or other terrain with numerous closely spaced obstructions having the size of single-family dwellings or larger. Surface roughness C is defined as areas with open terrain with scattered obstructions, generally having heights less than 9.1m (30ft). This category includes flat, open country and grasslands. Surface roughness D would cause the most extreme wind loading on the structure. It is defined as flat, unobstructed areas and water surfaces. This category also includes smooth mud flats, salt flats and unbroken ice (ASCE 7-10, 2010).

### 6.5.2 Design wind force calculation procedure

This section deals with the calculation procedure of the design wind force along the height of the tower, which is dependent on the velocity pressure calculated in the previous section.

The equation that is used to calculate the design wind force for “other structures” is given in Chapter 29.5 in ASCE 7-10 (2010). This equation is reproduced as Equation (6.4) below.

$$F = q_z G_f C_f A_f \quad (N) \quad (6.4)$$

Where:

- $q_z$  is the velocity pressure, measured in Pa (see Section 6.5.1);
- $G_f$  is the gust effect factor;
- $C_f$  is a force coefficient; and
- $A_f$  is the projected area normal to the wind, measured in  $m^2$ .

The **gust effect factor** for flexible or dynamically sensitive structures and other buildings is calculated using the following equation:

$$G_f = 0.925 \left( \frac{1 + 1.7I_{\bar{z}} \sqrt{g_Q^2 Q^2 + g_R^2 R^2}}{1 + 1.7g_V I_{\bar{z}}} \right) \quad (6.5)$$

Where:

- $g_V$  is the peak factor for wind response, which is taken as 3.4 in ASCE 7-10;
- $g_Q$  is the peak factor for background response, which is taken as 3.4 in ASCE 7-10;
- $g_R$  is the peak factor for resonance and can be calculated using Equation (6.6);
- $I_{\bar{z}}$  is the turbulence intensity at height  $\bar{z}$  and can be calculated using Equation (6.7);
- $Q$  is background response and can be calculated using Equation (6.8); and
- $R$  is the resonant factor and can be calculated using Equation (6.10).

The **peak factor for resonance**,  $g_R$ , is calculated as follows:

$$g_R = \sqrt{2 \ln(3600n_1)} + \frac{0.577}{\sqrt{2 \ln(3600n_1)}} \quad (6.6)$$

The symbol,  $n_1$ , represents the first natural frequency of the tower.

The **turbulence intensity at height  $\bar{z}$** ,  $I_{\bar{z}}$ , is calculated as follows:

$$I_{\bar{z}} = c \left( \frac{10}{\bar{z}} \right)^{1/6} \quad (6.7)$$

Where:

- $c$  is a constant, which can be obtained from Table 6.2; and
- $\bar{z}$  is defined as the equivalent height of the structure. The equivalent height of the structure is defined as being equal to 0.6 times the height of the structure, but not less than  $z_{min}$ . The value of  $z_{min}$  can be found in Table 6.2.

The **background response**,  $Q$ , is calculated as follows:

$$Q = \sqrt{\frac{1}{1 + 0.63 \left( \frac{B+h}{L_{\bar{z}}} \right)^{0.63}}} \quad (6.8)$$

Where:

- $B$  is die horizontal dimension normal to the wind direction. For wind turbine towers, this is equal to the diameter;
- $h$  is the hub height of the tower; and
- $L_{\bar{z}}$  is the integral length scale of turbulence (in meters), and can be calculated using Equation (6.9).

The **integral length scale of turbulence**,  $L_{\bar{z}}$ , is calculated as follows:

$$L_{\bar{z}} = l \left( \frac{\bar{z}}{10} \right)^{\bar{\epsilon}} \quad (6.9)$$

The two terms in Equation (6.9),  $l$  and  $\bar{\epsilon}$ , are constants listed in Table 6.2.

The **resonant factor**,  $R$ , is calculated as follows:

$$R = \sqrt{\frac{1}{\beta} R_n R_h R_B (0.53 + 0.47 R_L)} \quad (6.10)$$

Where:

- $\beta$  is the damping ratio; and
- $R_n$ ,  $R_h$ ,  $R_B$  and  $R_L$  can be calculated using the following equations:

$$R_n = \frac{7.74 N_1}{(1 + 10.3 N_1)^{5/3}} \quad (6.11)$$

$$N_1 = \frac{n_1 L_{\bar{z}}}{V_{\bar{z}}} \quad (6.12)$$

$V_{\bar{z}}$  in Equation (6.12), is defined as the mean hourly wind speed in m/s, and is calculated as follows:

$$V_{\bar{z}} = \bar{v} \left( \frac{\bar{z}}{10} \right)^{\bar{\alpha}} \quad (6.13)$$

The two terms in Equation (6.13),  $\bar{v}$  and  $\bar{\alpha}$ , are constants listed in Table 6.2.

$$R_h = \frac{1}{4.6 n_1 \frac{h}{V_{\bar{z}}}} - \frac{\left( 1 - e^{-2(4.6 n_1 \frac{h}{V_{\bar{z}}})} \right)}{2 \left( 4.6 n_1 \frac{h}{V_{\bar{z}}} \right)^2} \quad (6.14)$$

$$R_B = \frac{1}{4.6 n_1 \frac{B}{V_{\bar{z}}}} - \frac{\left( 1 - e^{-2(4.6 n_1 \frac{B}{V_{\bar{z}}})} \right)}{2 \left( 4.6 n_1 \frac{B}{V_{\bar{z}}} \right)^2} \quad (6.15)$$

$$R_L = \frac{1}{15.4 n_1 \frac{L}{V_{\bar{z}}}} - \frac{\left( 1 - e^{-2(15.4 n_1 \frac{L}{V_{\bar{z}}})} \right)}{2 \left( 15.4 n_1 \frac{L}{V_{\bar{z}}} \right)^2} \quad (6.16)$$

The **force coefficient**,  $C_f$ , for chimneys, is calculated using Figure 29.5-1 in ASCE 7-10. For ease to the reader, this figure is reproduced as Table 6.3.

Table 6.3: Calculation procedure of the structural factor,  $C_f$ , for chimneys, tanks, rooftop equipment and similar structures (ASCE 7-10, 2010)

Cross-Section	Type of Surface	h/D		
		1	7	25
Square (wind normal to face)	All	1.3	1.4	2.0
Square (wind along diagonal)	All	1.0	1.1	1.5
Hexagonal or octagonal	All	1.0	1.2	1.4
Round ( $D\sqrt{q_z} > 2.5$ ) ( $D\sqrt{q_z} > 5.3$ , $D$ in m, $q_z$ in $N/m^2$ )	Moderately smooth	0.5	0.6	0.7
	Rough ( $D'/D = 0.02$ )	0.7	0.8	0.9
	Very rough ( $D'/D = 0.08$ )	0.8	1.0	1.2
Round ( $D\sqrt{q_z} \leq 2.5$ ) ( $D\sqrt{q_z} \leq 5.3$ , $D$ in m, $q_z$ in $N/m^2$ )	All	0.7	0.8	1.2

For Table 6.3 above, the following apply:

- $D$  is the diameter of the tower (m);
- $D'$  is the depth of protruding elements such as ribs and spoilers (m); and
- $h$  is the height of the structure.

## 6.6 Sensitivity to vibration according to BetonKalender

According to a publication by Grünberg & Göhlmann (2013), wind turbine towers' sensitivity to vibration should be taken into account by the inclusion of the gust response factor. The gust response factor, however, should only be included in the case when the WTG is non-operational. When the WTG is in the non-operational stage, it is assumed that the WTG is vulnerable to vibration. A publication by DNV/Risø (2002) stated that vortex-induced vibrations are normally not a problem when the WTG is operational, as the blades obstruct the generation of vortices behind the tower. In addition to this, aerodynamic damping of the blades and nacelle also reduce vortex induced vibrations when the WTG is operational.

The turbulent extreme wind speed model (EWM) is one of the IEC load cases that considers the wind loads on the WTG in the non-operational condition. As such, EWM should be applied with the inclusion of the gust response factor (Grünberg & Göhlmann, 2013). As stated in Section 3.3.1 above, the turbulent extreme wind speed model uses the 10-minute average wind speed.

If it can be verified that the WTG is not susceptible to vibration, the steady extreme wind speed model should be applied without the inclusion of the gust response factor (Grünberg & Göhlmann, 2013). The steady extreme wind speed model uses the 3-second gust wind speed, as expressed in Equation (6.1).

It should be noted that the ASCE 7-10 code has different specifications regarding which type of wind speed should be used with the gust effect factor. ASCE 7-10 specifies that the velocity pressure should be calculated using the 3-second gust wind speed, measured at a height of 10 meters above ground level. The velocity pressure is then used in Equation (6.4) above, along with the gust effect factor, to calculate the external force acting on the tower. ASCE 7-10 therefore specifies that the design wind force should be calculated with the inclusion of both the 3-second gust wind speed and the gust effect factor. This would generally yield more conservative designs, as bigger lateral wind loads would act on the tower. For this reason, the approach presented by ASCE 7-10 is implemented for this study, to account for uncertainties regarding the tower's sensitivity to vibration.

# Chapter 7: Deflection and Internal Stress Analysis

## 7.1 Introduction

Although deflections are traditionally calculated for the Serviceability Limit State (SLS), a critical deflection analysis of a WTG must be carried out to verify that no excessive deflections shall occur that might affect the structural integrity of the tower. For this reason, WTG deflections are also calculated for the Ultimate Limit State (ULS), considering both physical and geometric nonlinearities.

It is also important to verify that no mechanical interference between blade and tower will occur (IEC 61400-1:2005). When the tower is exposed to critical wind loading, the tower and blade tip deflections may be out of phase. This could increase the chances of the tower interfering with the rotation of the blades (DNV/Risø, 2002).

This chapter discusses two methods that could be used to solve for the deflections of WTG towers with varying cross section properties. Both the methods, i.e. the Moment Area Method and the Direct Stiffness Method, use the cross section analysis developed for this study to calculate the parameters required to perform the deflection calculations. The integration with the cross section analysis algorithm not only results in accurate deflection calculations, but also results in obtaining the stress state of the cross sections at every nodal position. The two methods discussed in this chapter thus focus on calculating the deflections, whereas the cross section analyses calculate internal normal stresses and cross section properties.

Due to the Bernoulli assumption that plane sections remain plane, the only stresses that are calculated are in the longitudinal direction, i.e. the normal stresses. These stresses are regarded as the most important, especially during initial design stages, as these stresses are associated with the crushing limit of concrete and the yield limit of the reinforcing. The torsion and shear stresses of the cross sections are not considered in this study. According to Nicholson (2011), these stresses are usually insignificant compared to the stresses caused by the axial loads and moments when dealing with concrete WTG towers. The longitudinal reinforcing designed for the internal moments usually provide adequate shear resistance to the cross sections. In addition to this, post-tensioning is usually applied to concrete WTG towers, thus minimizing cracking in the concrete. The uncracked concrete would also increase the shear resistance of the cross sections (Grünberg & Göhlmann, 2013). Although these findings motivate the exclusion of torsion and shear stresses in this study, it is however still recommended that the designer verifies that torsion and shear stresses are within the allowable limits throughout the tower. The reader is referred to a study conducted by Van Zyl (2014) and ACI 318, which is a design code published by the American Concrete Institute (ACI 318, 2011), for further reading on shear strength and torsion resistance calculations.

Internal moments and shear forces are however calculated throughout the height of the tower. The internal moments are considered in the cross section analysis but the shear forces are left for the designer to analyse.

## 7.2 Internal Moment and Shear Force calculations

The Internal moments and shear forces throughout the height of the tower are calculated by similar numerical approaches. The moment at height  $h$  is be calculated using the following expression:

$$M(h) = \int_h^H F_w(y)(y - h)dy + F_T(H - h) = \sum (F_w)_i(h_i - h) + F_T(H - h) \quad (7.1)$$

$$V(h) = \int_h^H F_w(y)dy + F_T = \sum (F_w)_i + F_T \quad (7.2)$$

Where:

- $H$  is the hub height of the tower;
- $h$  is the height where the moment needs to be calculated;
- $F_w(y)$  is the lateral wind force acting at height  $y$ ; and
- $F_T$  is the lateral wind force acting on the tower hub and blades.

The integrals in the equations above can also be calculated numerically. It should be noted that Equation (7.1) only accounts for the internal moment caused by the lateral wind loads. During second order and nonlinear analyses, the moments caused by P-delta effects and the shift in neutral axis are also be included.

## 7.3 Moment Area Method for deflection calculation

Due to the varying stiffness throughout the tower, an analytical deflection calculation method, which involves integration over the height of the tower, is considered. One such a method is the Moment Area Method. This method is advantageous when working with irregular bending moment diagrams and towers with varying section properties. It is based on two theorems called the moment area theorems.

Theorem 1 states that the change in slope between any two points on a continuous elastic curve equals the area under the  $M/EI$  (moment over bending stiffness) curve between these points. Theorem 1 is illustrated in Figure 7.1. Mathematically, this can be written as:

$$\theta_{AB} = \int_A^B \frac{M}{EI} dx \quad (7.3)$$

Where,

- $M$  is the moment;
- $EI$  is the bending stiffness;
- $\theta_{AB}$  is the change in slope between points A and B; and
- A and B are two points on the continuous elastic curve.

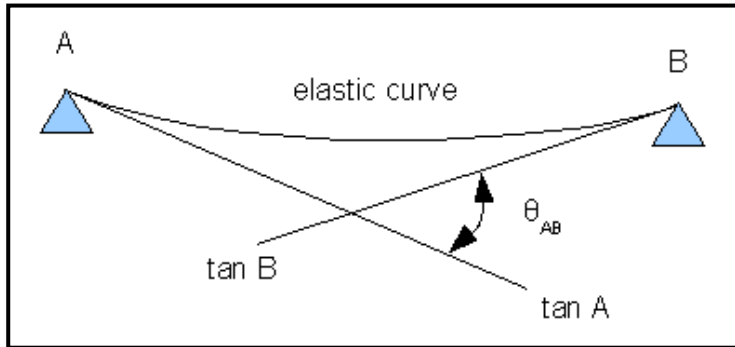


Figure 7.1: Moment Area Method Theorem 1 visualisation (BridgeArt.net, 2016)

Theorem 2 states the following: Consider two points A and B on a continuous elastic curve. The vertical deviation of point A measured from the tangent, which is extended from point B, equals the moment of area under the  $M/EI$  curve between these points. Theorem 2 is illustrated in Figure 7.2. Mathematically, Theorem 2 can be stated as follows:

$$t_{AB} = \int_B^A \frac{M}{EI} x \, dx \quad (7.4)$$

Where,

- $t_{AB}$  is the vertical deviation of the tangent at point B relative to the tangent at point A; and
- $x$  is the distance from the infinitesimal area under the  $M/EI$  curve to point A (i.e. the lever arm of the infinitesimal area under the  $M/EI$  curve).

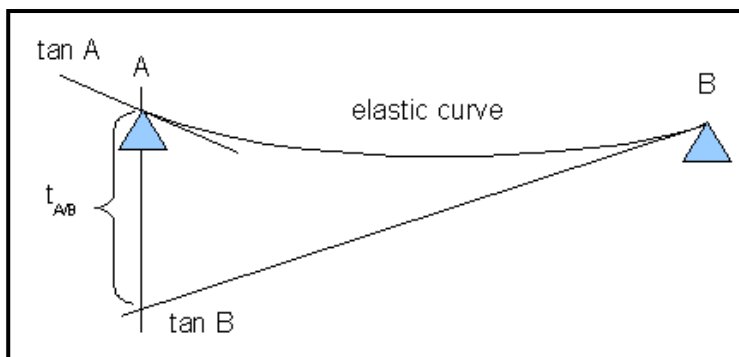


Figure 7.2: Moment Area Method Theorem 2 visualisation (BridgeArt.net, 2016)

Mathematically it can also be shown that:

$$\frac{M}{EI} = \frac{1}{R} = \kappa \quad (7.5)$$

Where  $R$  can be defined as the radius of curvature (m) and  $\kappa$  as the curvature ( $\text{m}^{-1}$ ). The relationship illustrated in Equation (7.5) is useful when performing deflection calculations because it creates a direct relationship between curvature and the total applied moment acting on a particular cross section of the tower.

Substituting  $\kappa$  into Equation (7.4) above yields the following equation:

$$t_{AB} = \int_B^A \kappa x \, dx \quad (7.6)$$

Equation (7.6) illustrates that the deflection at any point along the height of the tower can be found if the curvature curve throughout the tower is known. The deflection anywhere along the height of the tower can be found using the following equation:

$$\Delta(h) = \int_0^h \kappa(y) (h - y) \, dy \quad (7.7)$$

Where,

- $\Delta(h)$  is the lateral deflection at height  $h$  measured from the base of the tower;
- $\kappa(y)$  is the curvature at height  $y$  measured from the base of the tower; and
- $(h - y)$  is the lever arm of the area under the curvature curve.

The moment area method is illustrated in Figure 7.3.

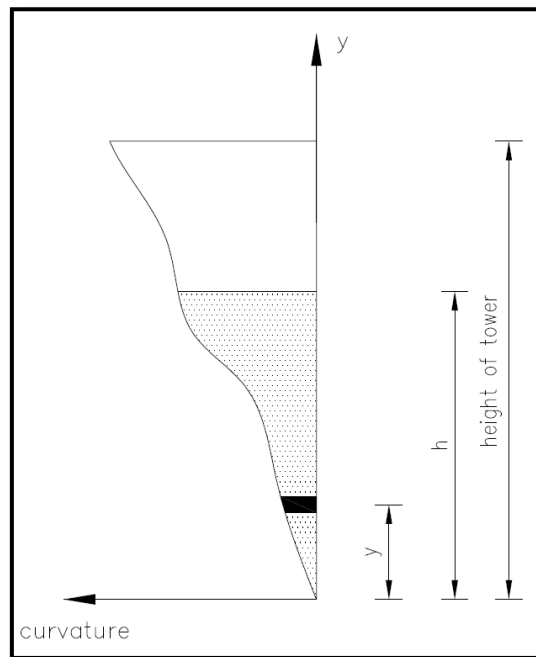


Figure 7.3: Moment area method

Due to the irregular shape of the curvature curve, it is worth carrying out a numerical integration method such as the trapezoidal rule or Simpson's integration method. Special attention should be given at discontinuous or steep gradient positions on the curve (Grünberg & Göhlmann, 2013). It might be necessary to divide the tower up into more elements at these positions.

## 7.4 Direct Stiffness Method for deflection calculations

The accuracy of the Moment Area Method greatly depends on the number of bar elements along the height of the tower and the numerical integration technique used to calculate the deflections. In some cases, it might be necessary to discretise the tower into a substantial number of bar elements before reasonably accurate results are obtained. This could result in a considerable increase in computation time. When performing second order analyses, the computation time is further multiplied by the number of iterations required to achieve convergence.

The Direct Stiffness Method (or Matrix Stiffness Method) for the use in tower deflection calculations is an alternative which yields very accurate results, even when modelling the tower with less finite elements. The Stiffness Method formulation makes use of the same beam element that is used in the FEM modal analysis. For convenience, this matrix is reproduced here as Equation (7.8).

$$[K] = EI \begin{bmatrix} \frac{12}{L^3} & \frac{6}{L^2} & -\frac{12}{L^3} & \frac{6}{L^2} \\ \frac{6}{L^2} & \frac{4}{L} & -\frac{6}{L^2} & \frac{2}{L} \\ -\frac{12}{L^3} & -\frac{6}{L^2} & \frac{12}{L^3} & -\frac{6}{L^2} \\ \frac{6}{L^2} & \frac{2}{L} & -\frac{6}{L^2} & \frac{4}{L} \end{bmatrix} \quad (7.8)$$

Where,

- $EI$  is bending stiffness of the beam element; and
- $L$  is the length of the beam element.

## 7.5 Geometric and Physical Nonlinear Analysis

According to Eurocode 2 (EN 1992-1-1:2004, 2004), second order effects must be taken into account if these effects are likely to have a significant impact on the overall stability of a structure. Second order effects should also be included for the attainment of stresses in critical cross sections for the ultimate limit state. More specifically, Eurocode 2 states that second order effects should be taken into account if they are more than 10% of first order effects. Due to the long, slender geometry of a wind turbine tower, this situation should generally be assumed (Grünberg & Göhlmann, 2013).

The deflection analysis methods explained in the preceding sections only deal with first order analyses, which neglect geometric nonlinearities. One of the most common second order effects is known as the P-delta effect (Van Zyl, 2014). This effect refers to increased deflections and internal stresses due to own weight or gravity forces acting at an eccentricity in the deformed state of the structure. This phenomenon is demonstrated in Figure 7.4.

A second order analysis due to P-delta effects requires an iterative procedure, and is continued until convergence is achieved. The increased moment due to the P-delta effects are taken into account by adding an additional component to the applied moment acting on the cross section. The moment caused by the external wind pressure is assumed to stay constant, while the P-delta moment component is recalculated after every iteration until convergence is achieved.

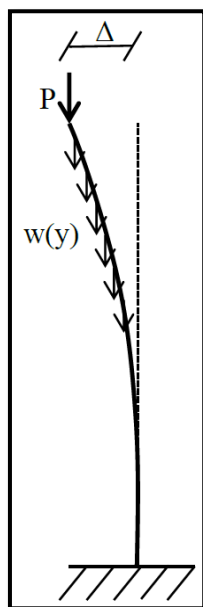


Figure 7.4: Additional moment due to P-delta effects (Van Zyl, 2014)

The P-delta moment component at height  $h$  is recalculated after every iteration using the following expression, which is obtained from research done by Van Zyl (2014):

$$M_{P-\text{delta},h} = \int_h^H w(y)\Delta(y)dy + P\Delta \quad (7.9)$$

Where:

- $H$  is the hub height of the WTG;
- $w(y)$  is the weight of the finite element at height  $y$ ;
- $\Delta(y)$  is the lateral displacement of the finite element at height  $y$ ;
- $\Delta$  is the lateral displacement at the top of the tower; and
- $P$  is the own weight of the turbine generator.

For this study, second order analyses are performed by considering either linear or nonlinear material stress-strain relationships. When the analysis is performed that considered both geometric and physical nonlinear effects, an updated additional moment due to the P-delta effects is calculated, as well as updated cross section properties. This is done because of the dependence of the nonlinear materials on the applied moment. An increase in the moment on the cross section changes the stress distribution over the cross section and thus influence the cross section properties.

When the second order analysis is performed using the Direct Stiffness Method, the geometric stiffness matrix is used to take account of geometric nonlinearities. The geometric stiffness matrix has the following layout:

$$[k_{geo}] = \frac{P}{10} \begin{bmatrix} \frac{12}{L} & 1 & -\frac{12}{L} & 1 \\ 1 & \frac{4L}{3} & -1 & -\frac{L}{3} \\ -\frac{12}{L} & -1 & \frac{12}{L} & -1 \\ 1 & \frac{-L}{3} & -1 & \frac{4L}{3} \end{bmatrix} \quad (7.10)$$

Where,

- $P$  is the axial load in the beam element; and
- $L$  is the length of the beam element.

Due to the simple geometry of a WTG tower, the axial loads resulting from the tower and generator own weight are calculated prior to the analysis. The geometric stiffness matrix is then obtained from the known axial loads and added to each beam element's stiffness matrix. The final beam element stiffness matrix is obtained by the addition of the element stiffness matrix and the geometric stiffness matrix. The final beam element stiffness matrices are then used to formulate the tower global stiffness matrix.

When the second order analysis is performed using the Moment Area Method, the geometric nonlinearities are taken into account by the increase of the total applied moment on the cross section. The increase in the total applied moment changes the curvature curve over the height of the tower and results in an increase in the tower deflections.

## 7.6 Verification of Analysis results

Various studies are presented in this section to compare the results obtained from the implemented analyses performed in this study. The first order analysis results are verified by comparing it to existing structural analysis software, known as Prokon. For analyses where geometric and physical nonlinearities are considered, more advanced methods and software are used for verification. A case study is also included at the end of this section to compare the results of the various techniques implemented for this study.

### 7.6.1 Linear Material Properties Analysis Comparison and Verification

The first set of tests conducted compare a relatively simple 30m hybrid cantilever structure. Only linear material properties are considered for these tests. The model comprises of three tower segments with constant cross sectional properties and shape. The bottom tower segment is comprised of a 900mm diameter solid circular cross section made from 40MPa concrete. This tower segment is discretised into five 3m beam elements. The middle tower segment is similar to the bottom tower segment, except that it comprises of a 750mm diameter solid circular cross section and is discretised into three 3m beam elements. The top tower segment comprises of a 508x8mm

CHS made from S355JR structural steel. It is discretised into two 3m beam elements. The lateral wind loads are simulated by 5kN lateral point loads, which are placed on every node. A 10kN lateral point load and a 20kNm point moment simulate the generator loads. The base is modelled as a fully fixed connection. Two alternatives are tested. The first alternative excludes the generator mass of 34027.44kg. The second alternative includes this mass, which is used to test the sensitivity of the second order analysis. A schematization of the model is illustrated in Figure 7.5.

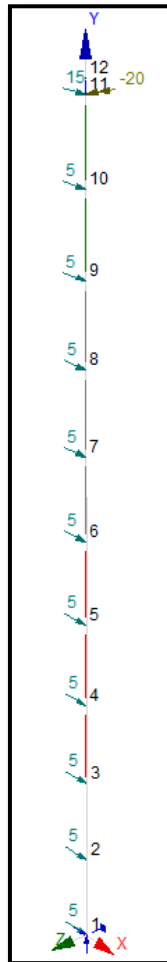


Figure 7.5: Schematization of the test model used to verify the analysis results when only linear material properties are considered

For verification purposes, the deflections obtained from the Prokon analysis are compared to the deflections obtained from both the Stiffness Method and Moment Area Method. These results are summarised in Table 7.1 below.

Table 7.1: Comparison of the deflections (in mm) obtained from the Prokon analysis to the implemented analysis techniques

		Developed Software		
		Prokon	Stiffness method	Moment Area Method
Test 1: Excluding generator mass	First order	370.99	370.83	370.83
	Second order	379.88	379.38	379.31
Test 2: Including generator mass of 36027.44kg	First order	370.99	370.83	370.83
	Second order	469.88	467.39	466.96

Table 7.2: % Difference of the results obtained from the implemented analysis techniques to the results obtained by Prokon

		% -Difference	
		Stiffness method	Moment Area Method
Test 1: Excluding generator mass	First order	0.043137149	0.043137149
	Second order	0.131707189	0.150160039
Test 2: Including generator mass of 36027.44kg	First order	0.043137149	0.043137149
	Second order	0.531330353	0.623372187

Table 7.2 illustrates the %-difference of the results obtained from the implemented analysis techniques to the results that are obtained from the Prokon analysis. From this table, it can be seen that the biggest %-difference is only 0.62%.

## 7.6.2 Geometric and Physical Nonlinear Analysis Comparison and Verification

Two tests are conducted in the attempt to verify the analysis results when geometric and physical nonlinearities are considered. In both tests, a theoretical material model is implemented where the material used hardened in compression and softened in tension. The tests and the theoretical material model are obtained from research done by Walls (2016).

The following equation describes the implemented theoretical material model, and is used to find the stress associated with a specific strain:

$$\sigma(\epsilon) = \frac{E_0(e^{\beta\epsilon} - 1)}{\beta} \quad (7.11)$$

Where:

- $E_0$  is the initial tangent modulus of elasticity; and
- $\beta$  represents the rate of change of the tangent stiffness with changing stress.

Two configurations of the material model are tested, each with a different  $E_0$  and  $\beta$  value. The first model is implemented with  $E_0 = 200\text{GPa}$  and  $\beta = -1000$ . The second material model represents a much softer material with  $E_0 = 20\text{GPa}$  and  $\beta = -50$ . The second configuration is implemented so

that large deflections are guaranteed. Figure 7.6 demonstrates the two configurations of the implemented material model.

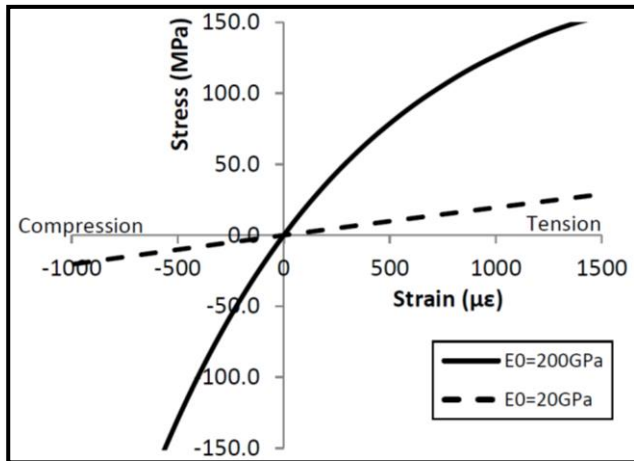


Figure 7.6: Two configurations of the implemented material models (Walls, 2016)

The beam that is analysed is illustrated in Figure 7.7. Both tests consider a 3-meter cantilever beam comprising a 200 IPE cross section. The cross section of the beam model is discretised into 200 equal horizontal elements. The number of elements over the cross section can however be reduced significantly without causing significant changes in the results. Twelve 4DOF beam elements are used to construct the model.

When only a moment is applied to the end of the cantilever beam, a closed form analytical solution exists with which the maximum tip deflection can be calculated (Walls, 2016). This is because the constant moment results in a constant bending stiffness throughout the beam. The nonlinear bending stiffness must however be calculated about the shifted neutral axis. This is done using the cross section analysis, which is discussed in Section 4.5. The analytical solution is expressed in the following equation:

$$\delta = \frac{EI}{M} \left( 1 - \cos\left(\frac{ML}{EI}\right) \right) \quad (7.12)$$

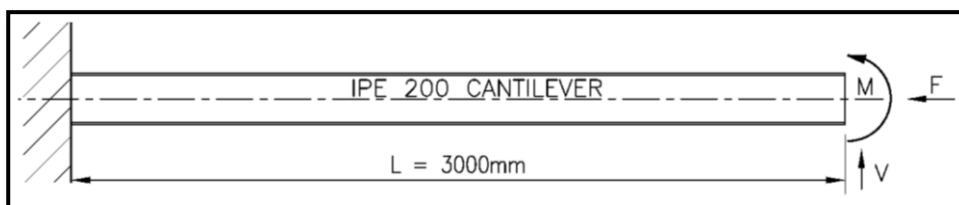


Figure 7.7: Implement test model (Walls, 2016)

For the first test, only a moment is applied to the end of the beam. By doing this, the results obtained from the implemented deflection techniques are verified using the analytical solution shown in

Equation (7.2). The comparison of the results for the first test with the two alternative material models are illustrated in Figure 7.8 and Figure 7.9. The graphs are created by incrementing the applied loading and finding the associated tip deflection. As can be seen from these figures, the results from the analytical solution are nearly indistinguishable from the results obtained from the implemented Stiffness and MA (Moment Area) Methods.

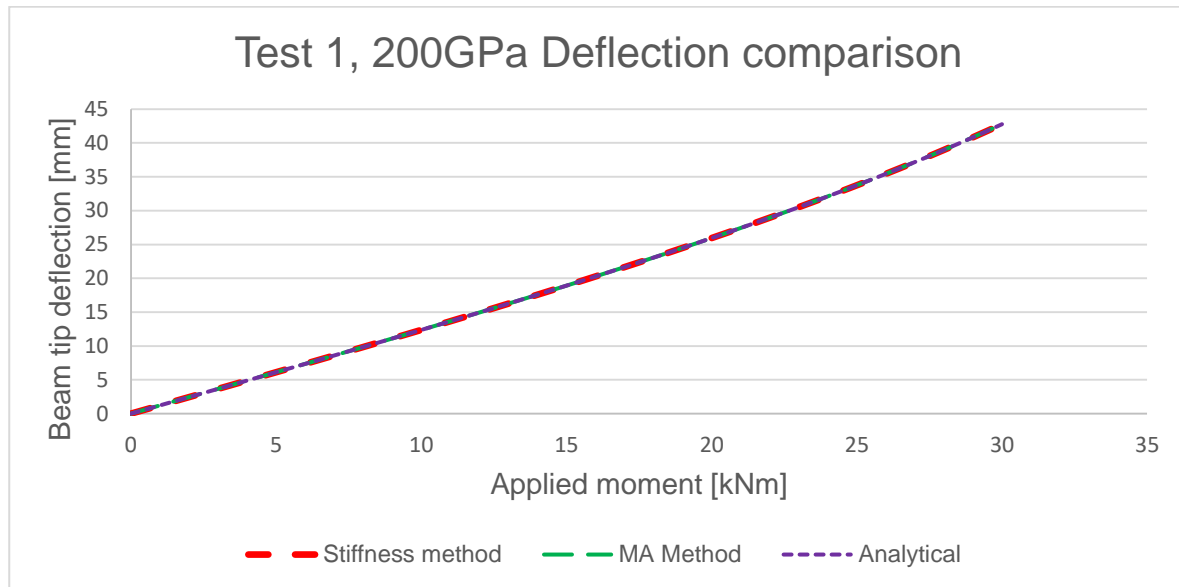


Figure 7.8: Deflection comparison of Test 1 with increasing end moment with  $E_0 = 200\text{GPa}$  and  $\beta = -1000$

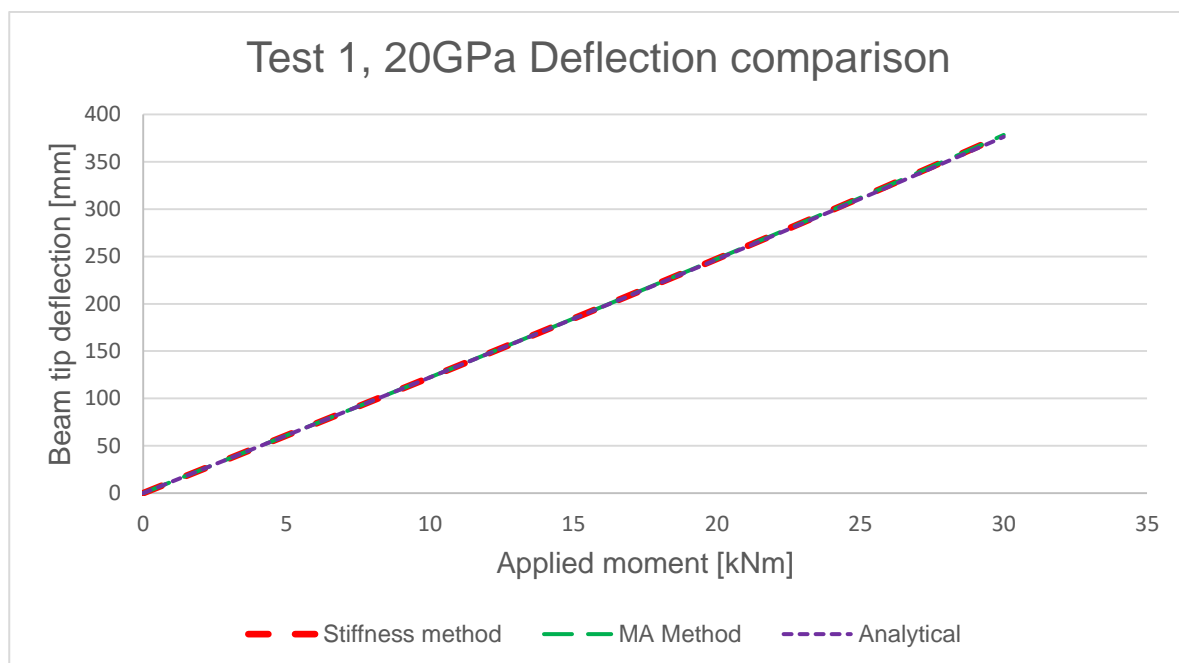


Figure 7.9: Deflection comparison of Test 1 with increasing end moment with  $E_0 = 20\text{GPa}$  and  $\beta = -50$

For the second test, a lateral and axial load are applied to the end of the cantilever. The lateral load is mainly applied to increase the nonlinearity of the material model, whereas the applied compressive axial load causes geometric nonlinear effects. The size of the lateral and axial loads are calculated as functions of the moment, which is incremented as in the first test. The lateral load is calculated

as  $V = \frac{3M}{L} = M$  kN and the axial loads as  $F = \frac{30M}{L} = 10M$  kN, where  $M$  refers to the applied moment. The results of the implemented Stiffness and MA methods are illustrated in Figure 7.10 and Figure 7.11. These are compared to results from existing FEM software, Abaqus, which is obtained from research done by Walls (2016). The model used in the Abaqus analysis was meshed using 3D shell elements. In total, 1920 shell elements were used, which resulted in 116886 DOFs throughout the model. This is significantly more compared to this study, which equated to a total of 26 DOFs.

The fourth set of results included in the figures below is from an analysis using the stiffness method, but excluding the geometric stiffness matrix. This is included to demonstrate that even though the increase in moment due to the P-delta effects are taken into account, the analysis underestimates the deflections when large enough forces are applied to cause geometric nonlinearities. The implemented MA Method takes both the physical and geometric nonlinearities of the structure into account. The MA Method thus generates very similar results to the Abaqus model and the Stiffness Method when the geometric stiffness matrix is included in the analysis.

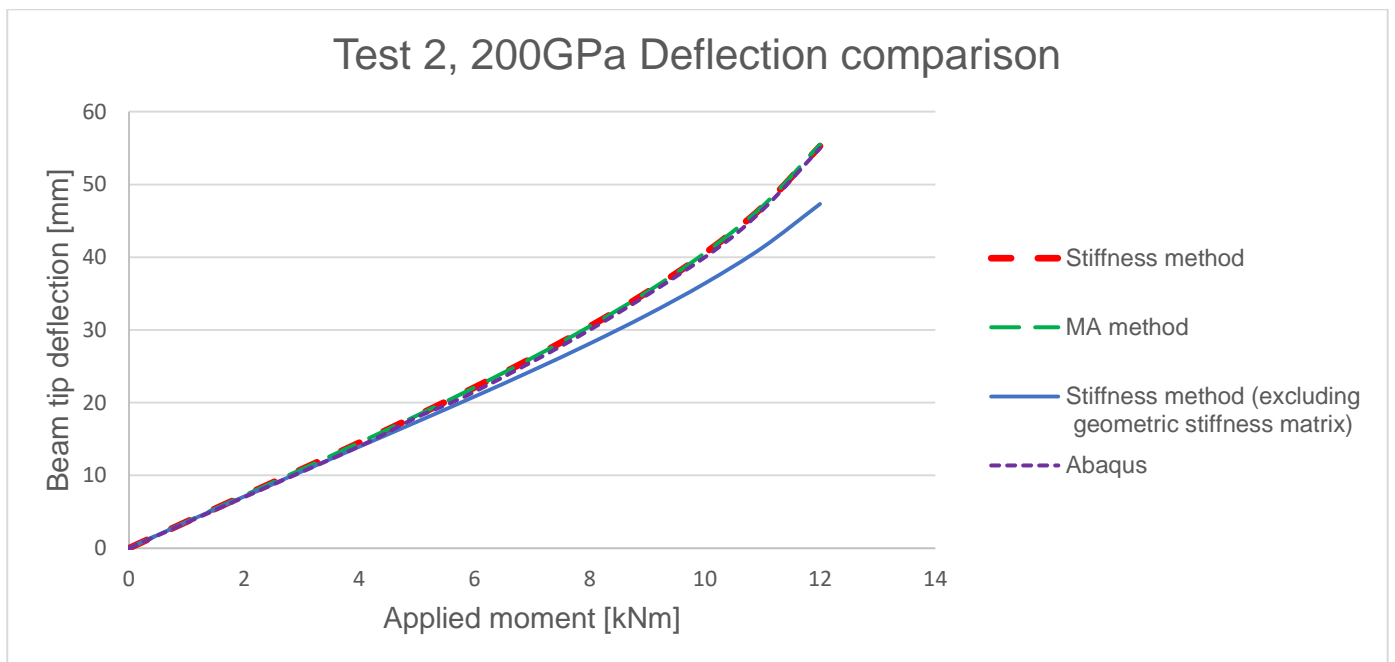


Figure 7.10: Deflection comparison of Test 2 with increasing end moment, lateral and axial loads with  $E_0 = 200\text{GPa}$  and  $\beta = -1000$

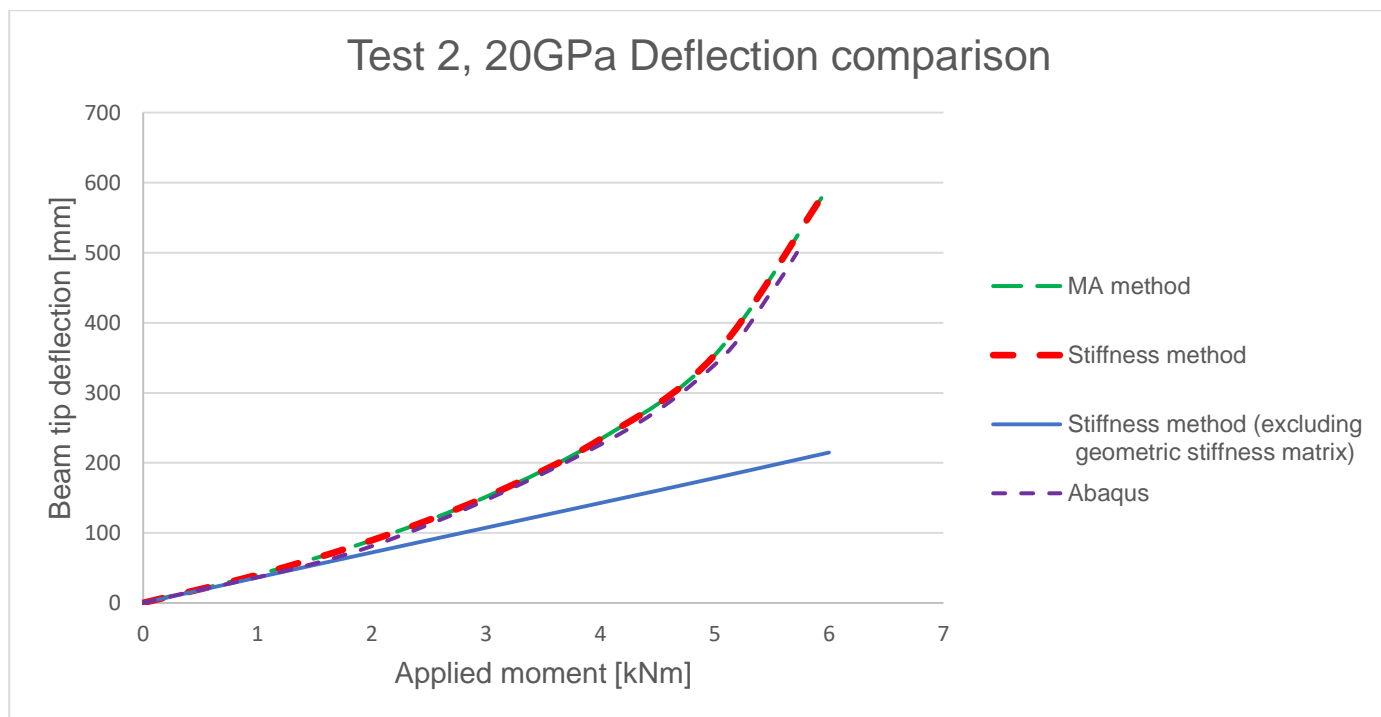


Figure 7.11: Deflection comparison of Test 2 with increasing end moment, lateral and axial loads with  $E_0 = 20\text{GPa}$  and  $\beta = -50$

It is reassuring to see that the methodology implemented for this study yields very similar results than that obtained from the Abaqus analysis, especially because Abaqus uses a significantly different analysis approach.

## 7.7 Case study: 120m High RC Tower

A short case study is included to provide an idea of the difference in outputs from the various types of analyses implemented in this study. The test model consists of three reinforced concrete tower segments. The generator used has a mass of 315 ton and induces a lateral force on the tower of 800kN due to the wind loading. Table 7.3 summarises the lateral wind loading acting on the tower. Table 7.4 summarises the input parameters used to set up the three tower segments.

Table 7.3: Lateral wind loads acting on the tower

Node height(m)	Lateral wind load (kN)
0	17.30031
5	34.4526
10	38.12712
15	40.11698
20	41.33602
25	42.09666
30	42.54679
35	42.76922
40	42.81544
45	42.71988
50	42.50681

Node height(m)	Lateral wind load (kN)
55	42.19404
60	41.79508
65	41.98369
70	42.12535
75	42.22552
80	42.28866
85	42.31849
90	42.31813
95	42.29024
100	42.2371
105	39.9702
110	37.62505
115	35.20384
120	16.35416

Table 7.4: Input parameters of the model used in the case study

	Input parameters	Tower Segment 1	Tower Segment 2	Tower Segment 3
	Concrete	C35/45	C35/45	C35/45
	Reinforcing	Ysteel	Ysteel	Ysteel
Tower segment specifications	Bottom height (m)	0	60	100
	Top height (m)	60	100	120
	Bottom outer diameter (m)	7	5	4.5
	Bottom inner diameter (m)	6.2	4.3	4
	Top outer diameter (m)	5	4.5	3
	Top inner diameter (m)	4.3	4	2.7
	No. of beam elements	12	8	4
Cross section specifications	Outer cover (m)	0.07	0.06	0.05
	Inner cover (m)	0.07	0.06	0.05
	Outer bar diameter (m)	0.03	0.025	0.02
	Inner bar diameter (m)	0.02	0.02	0.016
	Area of outer longitudinal reinforcing (m <sup>2</sup> )	0.12	0.09	0.03
	Area of inner longitudinal reinforcing (m <sup>2</sup> )	0.11	0.08	0.025
	Reinforcing percentage (Bottom of tower segment)	2.77	3.42	1.65
	No. of cross section elements	300	300	300

Table 7.5: Deflection comparison (mm) of the various implemented analysis techniques

	Linear material properties		Nonlinear material properties	
	1st order	2nd order	1st order	2nd order
Stiffness Method [mm]	809.21	848.285	1751.695	2025.89
Moment Area Method [mm]	808.497	847.493	1750.634	2024.419
Stiffness Method excluding geometric stiffness matrix [mm]	NA	NA	NA	1811.111

Table 7.6: Base moment (MNm) comparison between the various implemented analysis techniques

	Linear material properties		Nonlinear material properties	
	1st order	2nd order	1st order	2nd order
<b>Stiffness Method [MNm]</b>	154.6058	160.461	154.6058	168.807
<b>Moment Area Method [MNm]</b>	154.6058	160.456	154.6058	168.795
<b>Stiffness Method excluding geometric stiffness matrix [MNm]</b>	NA	NA	NA	167.327

Table 7.5 and Table 7.6 compare the tower tip deflections and base moments obtained from the various implemented analysis techniques, respectively. It is interesting to see that the analysis where physical and geometric nonlinearities are taken into account yields a tower tip deflection that is approximately 2.5 times higher compared to the simple first order linear analysis. When the geometric stiffness matrix is excluded from the Stiffness Method analysis, the deflection is calculated to be approximately 10% lower compared to the case where the geometric stiffness matrix is included. For the case when physical and geometrical nonlinearities are assumed, the base moment increases by 9.2% compared to the first order linear material analysis.

Table 7.7: Computation time (seconds) comparison between the various implemented analysis techniques

	Linear material properties		Nonlinear material properties	
	1st order	2nd order	1st order	2nd order
<b>Stiffness Method [s]</b>	0.0021	0.0045	0.7749	4.524
<b>Moment Area Method [s]</b>	0.0013	0.0139	0.7820	7.829
<b>Stiffness Method excluding geometric stiffness matrix [s]</b>	NA	NA	NA	4.513

Table 7.7 compares the computation time, measured in execution time seconds, of the various implemented analysis techniques. It is interesting to note that the Stiffness Method outperformed the MA method by 57% when geometric and physical nonlinearities are considered.

This case study serves as confirmation that deflections and stresses of large reinforced concrete wind turbine towers can be significantly underestimated when geometric and physical nonlinearities are excluded from the analysis.

# Chapter 8: Modelling of a Post-tensioned Concrete Tower

## 8.1 Introduction

The cross section analysis described in the previous sections is implemented without the effects of post-tensioning. The results generated by the implemented cross section analysis and its integration with the Moment Area and Stiffness Method are verified in the previous chapters. Due to the success of the implemented cross section analysis, it has been deemed sensible to extend the existing methodology to consider the effects of post-tensioning as well.

By eliminating tensile stresses in the concrete, post-tensioning can increase the stiffness of a tower. It should be kept in mind that the considerable force the prestressing steel exerts on the tower could also reduce the stiffness of the concrete. This can be due to the compressive stress nearing the crushing limit of the concrete. The effect that the high compressive force has on the concrete mostly depends on the implemented concrete material model. A high-strength concrete would for example be more effective in retaining its stiffness when it is subjected to a large compressive force.

Generally, two post-tensioning systems exist. A structure can either be post-tensioned using internal or external post-tensioning. Concrete towers constructed from prefabricated segments generally employ internal grouted post-tensioning, whereas cast-in-place towers frequently make use of external unbonded post-tensioning (Grünberg & Göhlmann, 2013).

### 8.1.1 External unbonded prestressing tendons

When considering wind turbine towers consisting of an annular cross section, external prestressing is usually installed on the inside of the tower shaft. Due to the accessibility of the tendons, monitoring and maintenance can readily be carried out. Friction losses are also reduced due to wobble effects being greatly eliminated. Another significant advantage of external prestressing is that tendons can be restressed, destressed or replaced, due to the absence of bond (Structural Systems, 2016).

When external prestressing is utilised, the prestressing forces must be applied as external forces to the tower. Before any deformation occurs due to lateral wind loads, the prestressing only causes a concentric normal force throughout the tower. As lateral loads cause the tower to deflect, the tendons induce change-of-direction and anchorage forces in the tower. If the tendons are exposed over the full height of the tower, the tendons assume different orientations relative to one another in the deformed state. On the windward side of the tower, the tendons will coincide with the chord, whereas the tendons on the leeward side will touch the inside of the tower shaft (Grünberg & Göhlmann,

2013). The positioning of the tendons can be improved, however, by providing corbels through which the tendons can be guided. This will allow the tendons to follow the deformed shape of the structure and not touch the inside of the tower shaft. The disadvantage of using corbels is that the pull-out forces need to be calculated and designed for so that adequate anchorage can be provided.

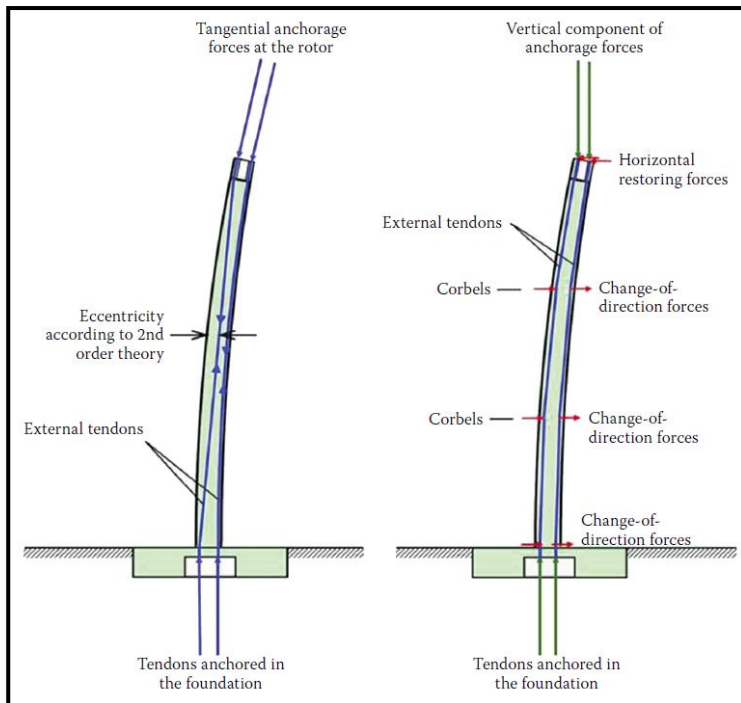


Figure 8.1: Unguided (left) vs. corbel-guided (right) external prestressing tendons according to Grünberg & Göhlmann (2013). Image obtained from a journal by Von Der Haar & Marx (2015)

### 8.1.2 Internal grouted prestressing

Internal tendons are installed by first casting ducts within the cross section. After the tower is assembled or constructed on site, the prestressing tendons are guided through the ducts and anchored. The tendons are then tensioned using jacks and grouted into place.

Internal prestressing has the advantage that the forces from the tendons only exert normal forces perpendicular to the cross section, without lateral restoring forces. This simplifies the model greatly compared to external prestressing. At every node, the post-tension force can then be included in the cross section analysis as an externally applied normal force.

Internal prestressing is normally positioned on the centreline of the annular cross section of wind turbine towers. Internal prestressing is thus more effective in providing restoring moments to the tower in the deformed state compared to external prestressing. Another advantage of internal grouted prestressing over external unbonded prestressing is that there is a reduced risk of tendon or anchorage failure or fatigue. This is due to the bond used with internal prestressing.

As a result of all of the considerations mentioned above, the internal grouted prestressing model is implemented for this study.

## 8.2 Methodology developed to consider internal grouted post-tensioning

### 8.2.1 Cross section model used to consider post-tensioning

The model of the cross section used to consider the effects of the post-tensioning is very similar to that used to model a normally reinforced concrete circular hollow section. The normally reinforced cross section model is modified so that the reduction of concrete, due to the inclusion of the post-tension ducts, is taken into account. The modified cross section is then analysed as discussed in Section 4.3.

After the completion of the cross section analysis, the normal forces required to ensure that the cross section remains entirely in compression are calculated. The process used to obtain the post-tension force is iterative, due to the nonlinear material properties present in the cross section. This force is found by performing multiple cross section analyses and incrementing the post-tension force after each analysis. This is done until the post-tension force is large enough to ensure that the entire cross section is in compression.

The post tension force is then applied to the cross section as a concentric normal force. In the deformed state, the restoring moment from the tendons is calculated and subtracted from the moments caused by lateral forces and P-delta effects. The process in finding the prestressing restoring moment is also iterative, due to the restoring moment being dependent on the existing moment acting on the cross section. The effect of the post-tensioning is thus modelled as an externally applied normal force and restoring moment, which act together with the original axial force and moment.

Due to the accurate results obtained from the cross section analysis performed in Section 4.6, it is deemed sensible to apply the “smeared area”-concept that is used to model the reinforcing steel, to the prestressing steel as well. This is also deemed sensible because the prestressing steel model is treated independently from the cross section model. Unlike the reinforcing, the prestressing steel is assumed not to contribute directly to the composite cross section properties.

### 8.2.2 Algorithm developed to consider post-tensioning

The overall structural analysis process developed to consider the effects of post-tensioning is summarised below.

- Step 1: Perform a structural analysis as discussed in Chapter 7, but with the modified cross section discussed in Section 8.2.1.
- Step 2: Find the minimum post-tension force required to ensure that the tower segments remain entirely in compression, eliminating all cracks.

- Step 3: Apply the post-tension force as an external axial force, along with the original internal forces (axial force and moment).
- Step 4: Perform another structural analysis to calculate the post-tension restoring moments and subtract it from the existing internal moments. Perform Step 4 until the restoring moment converges.

Step 4 above is repeated until the restoring moment converges because the restoring moment is dependent on the curvature of the cross section. The curvature, however, is dependent on the total applied moment on the cross section. By subtracting the restoring moment from the existing internal moment in Step 4, the curvature is reduced. If Step 4 is repeated, the calculation of the restoring moment will yield a lower value to what is obtained during the first iteration. The third iteration would yield a slightly bigger restoring moment to what is obtained in the second iteration. By repeating this process, the true restoring moment is obtained.

It should be noted that the calculation of losses associated with the post-tensioning is ignored for this study. The minimum post-tension force required to eliminate cracking is calculated with the assumption that friction losses are taken into account. It is thus left to the engineer to design the post-tensioning so that the final post-tension force (including losses) equals the post-tension force obtained from the developed software.

### 8.2.3 Implemented material model for prestressing steel

In order to calculate the post-tension restoring moment, a material model is implemented, similar to the other materials present in the cross section. The force present in each tendon is dependent on its strain state. Therefore, tendons located further away from the bending axis have a bigger contribution to the restoring moment compared to tendons located near or on the bending axis.

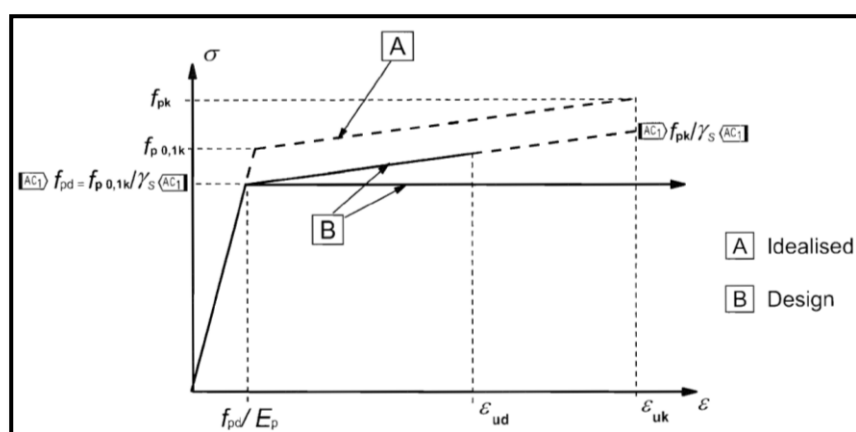


Figure 8.2: Idealized and design stress-strain diagrams for prestressing steel. Obtained from Eurocode 2 (EN 1992-1-1:2004, 2004)

The prestressing steel material model is obtained from Eurocode 2: Design of concrete structures. This is illustrated in Figure 8.2, where:

- $f_{pk}$  is the characteristic tensile strength of prestressing steel;
- $f_{p0.1k}$  is the characteristic 0.1% proof-stress of prestressing steel;
- $\gamma_s$  is the partial factor for reinforcing and prestressing steel, which can be taken as 1.15 (EN 1992-1-1:2004, 2004);
- $\varepsilon_{ud}$  and  $\varepsilon_{uk}$  are the design and characteristic strains of reinforcing or prestressing steel at maximum load, respectively; and
- $E_p$  is the design value of modulus of elasticity of prestressing steel, which can be taken as 205 GPa (EN 1992-1-1:2004, 2004).

For the prestressing tendons to achieve the required tension force, the tendons are tensioned to a specific strain. This strain can be interpreted as the initial strain of the tendons, before the tower progresses into the deformed state. The actual strain in each tendon in the deformed state is calculated as the initial strain plus the strain resulting from the curvature at the height where the cross section is analysed. The total strain within a tendon is thus composed of an initial normal strain and the strain resulting from bending.

## 8.3 Case studies

This section was included to demonstrate how the inclusion of post-tensioning influenced the tower analysis. The tower model used in the case study in Section 7.7 is modified to include internal grouted prestressing steel. All other parameters are kept constant so that the results could be compared with one another. As discussed above, the concrete area in the cross section is reduced accordingly to take account of the post-tension ducts. Before post-tensioning is applied to the tower, the reduction of concrete resulted in a reduction in stiffness. This led to a small increase in tower deflections. After the tower is post-tensioned, however, the tower deflections reduced due to the increased stiffness and elimination of cracks.

### 8.3.1 Case study A: Individual tower segment post-tensioning (C35/45 concrete)

The first case study investigated the effect of post-tensioning when the minimum post-tension force required to eliminate cracking, is calculated for every tower segment. This method utilises the prestressing steel most effectively, and should be more economical in terms of material usage. As is usually the case, however, the increase of economy of a structure also increases the complexity associated with design and construction. An alternative to calculating the post-tension force required for each tower segment, is to calculate a single post-tension force big enough to eliminate all cracks and apply this force throughout the entire tower. This technique simplifies the construction of the tower, as multiple access joints are not required as in the case where each tower segment is post-tensioned individually. Special care should however be taken not to exceed the crushing limit of the

concrete. Table 8.1 and Table 8.2 below sum up the output of a second order nonlinear analysis before and after post-tensioning is applied, respectively.

Table 8.1: Case study A: Second order nonlinear analysis results before individual tower segment post-tensioning

<b>Second order, nonlinear analysis BEFORE post tension is applied</b>		
Deflection	2038.5	mm
<b>Crack percentage at bottom of tower segments</b>		
Segment 1	65.4	%
Segment 2	65.7	%
Segment 3	67.1	%
<b>Normal stresses</b>		
Height (m)	max concrete stress (MPa)	max reinforcing stress (MPa)
0	-15.4	264.1
60	-14.0	232.6
100	-8.5	156.1
120	-1.8	-13.6
<b>Post tension force required to eliminate cracking</b>		
Segment 1	101.9	MN
Segment 2	62.3	MN
Segment 3	16.0	MN
<b>Post tension steel area [m<sup>2</sup>]</b>		
	<b>Minimum required</b>	<b>Amount installed</b>
Segment 1	0.07	0.075
Segment 2	0.04	0.045
Segment 3	0.01	0.015

Table 8.2: Case study A: Second order nonlinear analysis results after individual tower segment post-tensioning

<b>Second order, nonlinear analysis AFTER post tension is applied</b>			
Deflection	1326.3	mm	
<b>Crack percentage at bottom of tower segments</b>			
Segment 1	0	%	
Segment 2	0	%	
Segment 3	0	%	
<b>Normal stresses</b>			
Height (m)	max concrete stress (MPa)	max reinforcing stress (MPa)	max PT steel stress (MPa)
0	-20.2	-230.3	1363.6
60	-18.9	-203.3	1390.1
100	-10.0	-84.9	1104.2
120	-10.9	-95.3	1066
<b>Total time elapsed =</b>		18.7	seconds

### 8.3.2 Case study B: Individual tower segment post-tensioning (C50/60 concrete)

Case study B is included to demonstrate how the use of a concrete with a higher stiffness influences the analysis results. The tower model used in Case study B is exactly the same as the model used in case study A, except that C50/60 concrete is used instead of C35/45 concrete.

Table 8.3: Case study B: Second order nonlinear analysis results before individual tower segment post-tensioning

<b>Second order, nonlinear analysis BEFORE post tension is applied</b>		
Deflection	1718.0	mm
<b>Crack percentage at bottom of tower segments</b>		
Segment 1	69.2	%
Segment 2	69.3	%
Segment 3	66.6	%
<b>Normal stresses</b>		
Height (m)	max concrete stress (MPa)	max reinforcing stress (MPa)
0	-17.7	240.4
60	-16.2	213.8
100	-8.8	140.8
120	-2.0	-10.9
<b>Post tension force required to eliminate cracking</b>		
Segment 1	92.6	MN
Segment 2	57.6	MN
Segment 3	15.2	MN
<b>Post tension steel area [m<sup>2</sup>]</b>		
	<b>Minimum required</b>	<b>Amount installed</b>
Segment 1	0.06	0.075
Segment 2	0.04	0.045
Segment 3	0.01	0.015

Table 8.4: Case study B: Second order nonlinear analysis results after individual tower segment post-tensioning

<b>Second order, nonlinear analysis AFTER post tension is applied</b>			
Deflection	850.4	mm	
<b>Crack percentage at bottom of tower segments</b>			
Segment 1	0	%	
Segment 2	0	%	
Segment 3	0	%	
<b>Normal stresses</b>			
Height (m)	max concrete stress (MPa)	max reinforcing stress (MPa)	max PT steel stress (MPa)
0	-21.2	-143.5	1298.9
60	-20.1	-133.0	1306.7
100	-10.2	-60.3	1039.2
120	-11.4	-69.1	1012
<b>Total time elapsed =</b>		17.2	s

## 8.4 Comments on case study results

After post-tensioning is applied to the test models in Case Study A and B, the tower tip deflections are reduced by 35.3% and 51%, respectively. This demonstrates that by utilizing a concrete with higher stiffness, the effectiveness of the post-tensioning is increased in terms of reducing deflections. By utilizing a stiffer concrete, the concrete also relieves the reinforcing of some of the compressive stresses.

It takes approximately 20 seconds for each of the two tests in this chapter to complete. Each of these tests include a modal analysis, as the first natural frequency is required to determine wind loads on the tower. The modal analysis is only executed once at the start of each test, using the elastic composite stiffness. Each analysis also includes two full structural analyses where geometric and physical nonlinearities are considered. One aspect of the analysis that is found to be an expensive operation, is the determination of the post-tension force required to eliminate cracking.

# Chapter 9: Graphical User Interface

## 9.1 Introduction

In software design, an application generally consists of two parts: The back-end and the front-end. The back-end defines everything that the user cannot see when using the application. For this study, the back-end represents the network of classes developed to model a WTG tower, as well as the algorithms and code developed to implement the theory discussed in the previous chapters.

The front-end of an application defines the component(s) used to interact with the back-end. For the software developed in this study, a graphical user interface (GUI) was developed as front-end. The GUI was developed with the intent to provide user-friendly controls to guide the user during the model setup and analysis.

What follows in this chapter, aids as a user manual for the developed GUI. It includes a series of steps, describing the process of how a WTG model is set up and analysed. After the completion of an analysis, the GUI also provides results for the user to analyse.

## 9.2 User Manual

### 9.2.1 Model setup

**Step 1:** Click on Input-tab.

**Step 2:** Specify the number of tower segments and click on "Generate Segments".

**Step 3:** Specify the material properties. Create new, edit or delete materials using the buttons on the right.

**Step 4:** Complete the tower segment dimensions and other specifications.

**NOTE:** The post-tension specifications do not initially have to be entered. Later, the application will aid the user in choosing correct parameters.

Figure 9.1: How to specify input parameters using the GUI

Figure 9.1 above illustrates how the input parameters of each tower segment are entered using the GUI. By specifying the number of tower segments and clicking on the “Generate Segments”-button, the appropriate number of tower segment tabs are created in the tab pane. The user is then able to scroll through the various tower segment tabs and edit the input parameters.

The next steps are to enter the input parameters associated with the generator and the wind loading. This is illustrated in Figure 9.2 and Figure 9.3, respectively. As mentioned in Chapter 6, only the IEC steady extreme wind speed model was implemented for this study. The user has a choice on the IEC wind turbine class (class I, II or III) and the ASCE 7-10 terrain category (category A, B or D).

Wind turbine generator analysis

Input Dynamic Analysis Deflection and Stress Analysis

TowerSegments Generator Wind Loads

### Generator Specifications

Description: 3.6 MW Turbine

Mass (kg): 315000

Horizontal Point Load (N): 800e3

Point Moment (Nm): 60e3

Torsion (Pa): 0.0

One blade passing frequency (Hz): 0.22

Three blade passing frequency (Hz): 0.66

Generate example

Figure 9.2: Entering generator input parameters using the GUI

Wind turbine generator analysis

Input Dynamic Analysis Deflection and Stress Analysis

TowerSegments Generator Wind Loads

### Wind loading settings

Steady Extreme Wind Speed Model (1:50)

IEC turbine class: 3

ASCE 7-10 terrain Category: d

ASCE 7-10 terrainCategory (a, b or d, d is worst case - open, unconstructed terrains)

Figure 9.3: Entering wind loading input parameters using the GUI

After all of the input parameters are entered, the GUI displays a simple representation of the WTG tower, which also serves as confirmation that all of the input parameters were entered. This is illustrated on the right hand side of Figure 9.4.

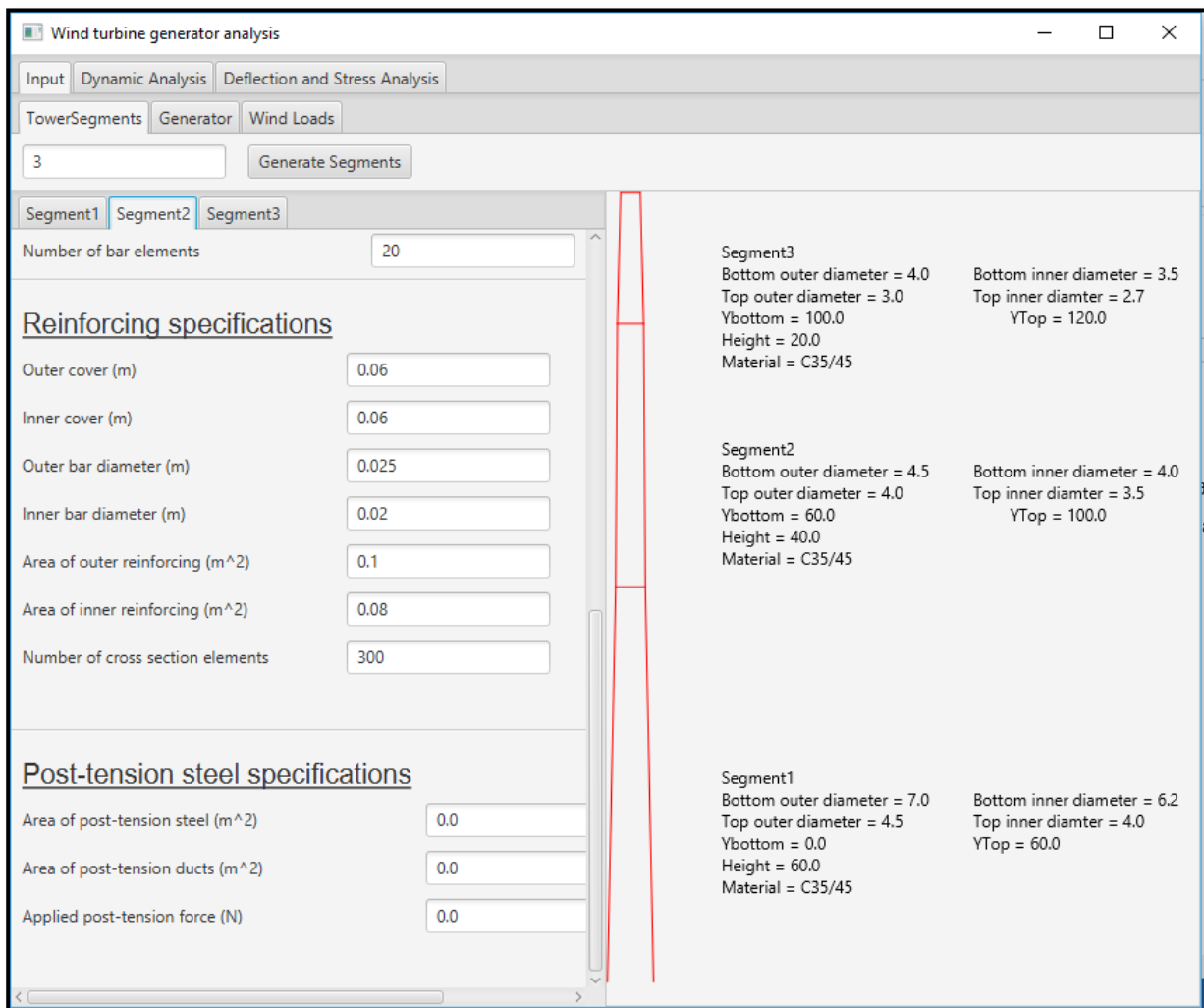


Figure 9.4: The GUI displaying a simple representation of the WTG tower and input parameters

## 9.2.2 Performing analyses

The software developed is able to perform modal and structural analyses. A modal analysis yields the tower frequencies and mode shapes, while internal stresses, moments, forces and deflections are obtained by performing a structural analysis. Due to the first natural frequency being required to calculate the wind loading on the tower, a modal analysis is performed automatically before the structural analysis commences. If only the tower frequencies need to be analysed, the user should navigate to the “Dynamic analysis” tab. By clicking on the “Calculate Frequencies” button, a modal analysis is performed and the output is illustrated on the right hand side of the GUI. This is illustrated in Figure 9.5. By clicking on the “Next mode” or “Previous mode” button, the GUI navigates to higher or lower mode shapes and their associated frequencies, respectively.

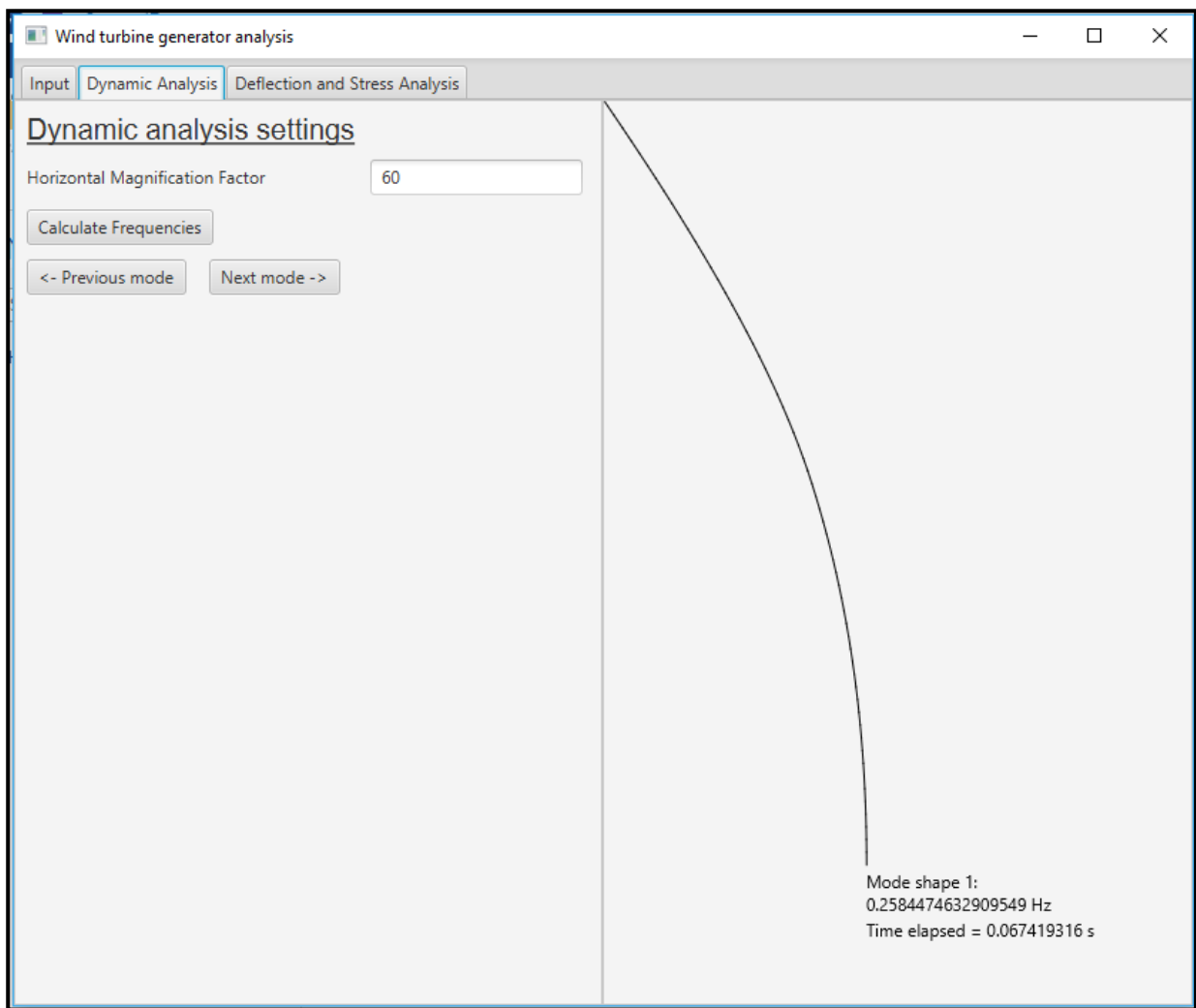


Figure 9.5: Performing a modal analysis using the GUI

Figure 9.6 demonstrates how a structural analysis is performed using the GUI. This tab provides fields to specify axial and wind load factors used in the analysis. It also provides options regarding the technique used to calculate the tower deflections and whether geometric and material nonlinearities should be taken into account. The “tolerance”-field relates to the accuracy of the second order analysis. Specifying a smaller tolerance would typically result in more iterations being performed before the tower deflections converge.

The structural analysis will commence once the “Perform Analysis!”-button is clicked. If the analysis is successful, a popup message will notify the user of the success. By clicking on the “Ok”-button on the popup, the post-tension analysis section is unlocked and a new window displaying the analysis output becomes visible. This is illustrated in Figure 9.7 Figure 9.8.

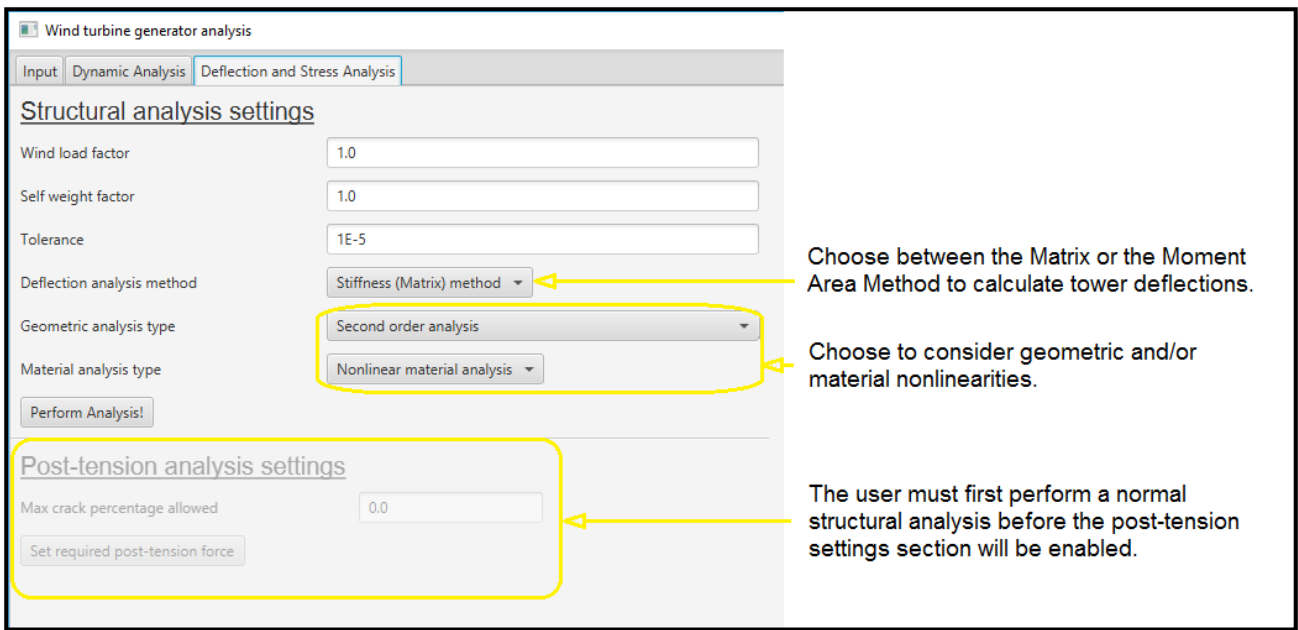


Figure 9.6: Performing a structural analysis using the GUI

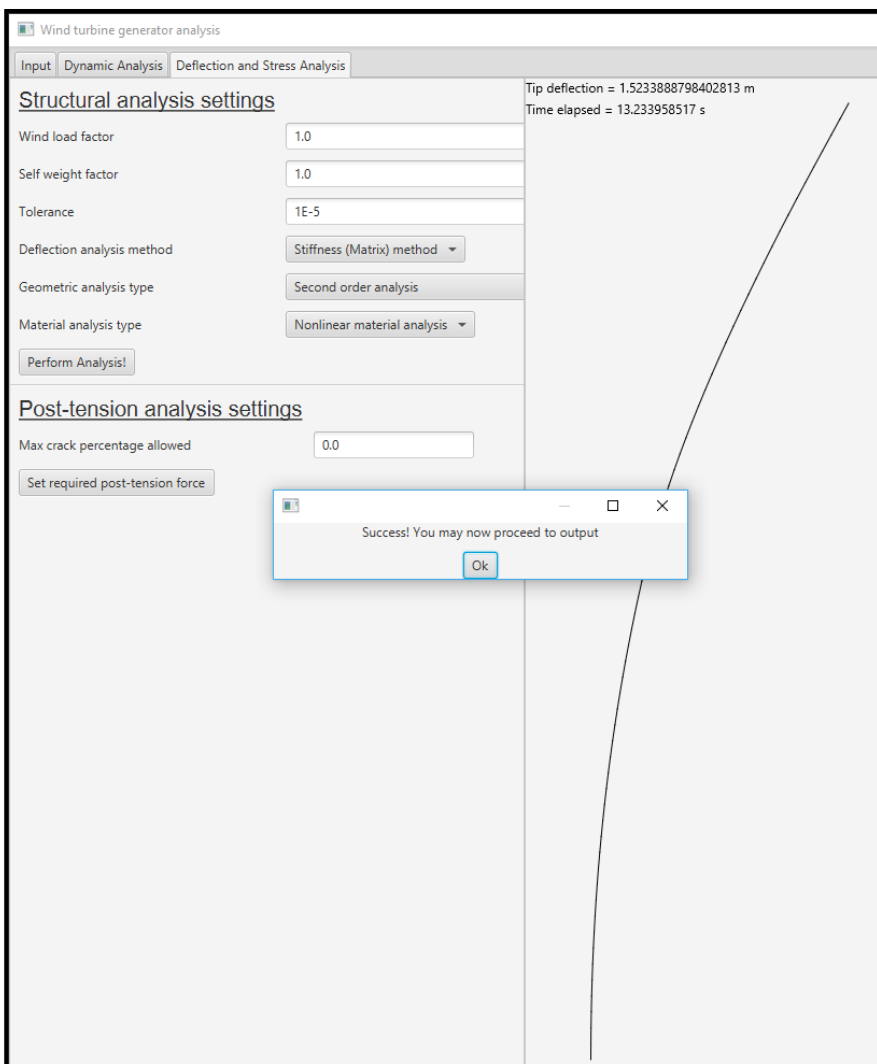


Figure 9.7: Illustration of GUI after the successful completion of a structural analysis

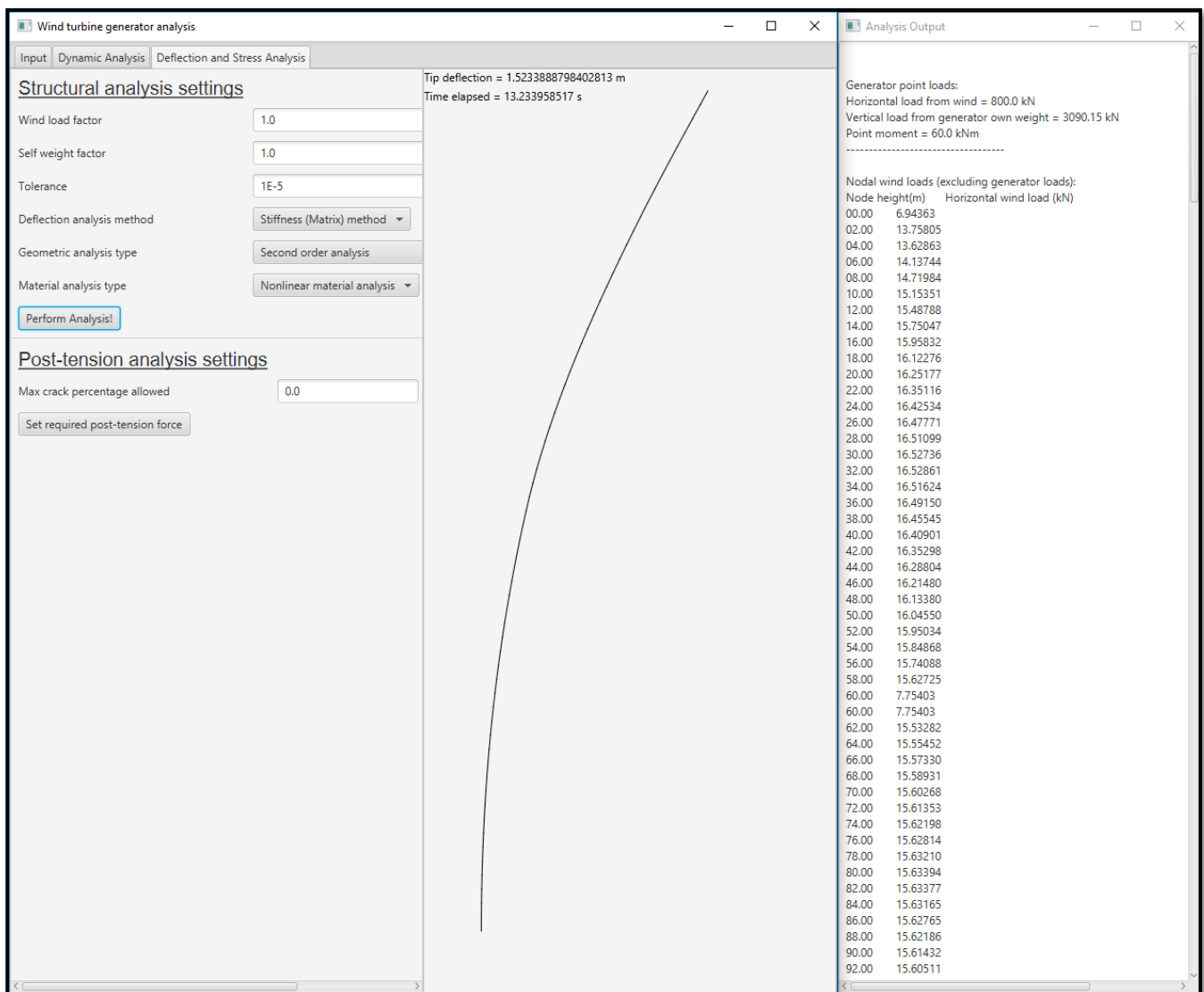


Figure 9.8: An illustration of the tower deflection along with the analysis output information

After the completion of the structural analysis, the stress state throughout the tower is known. This enables the software to calculate the post-tension force required per tower segment to achieve the desired crack percentage. This is done by clicking on the “Set required post-tension force”-button. After the required post-tension forces are calculated, a test is conducted to establish whether enough post-tension steel was specified during the input phase of the analysis. If it is found that the post-tension steel will yield, a warning message will be displayed, along with suggestions of the amount of post-tension steel required to avoid yielding. This message is illustrated in Figure 9.9.

By clicking on the “Yes”-button in Figure 9.9, the amount of post-tension steel is changed as indicated. The input information can be reviewed by navigating to the input-tab. The WTG tower has to be re-analysed, however, due to the change of input.

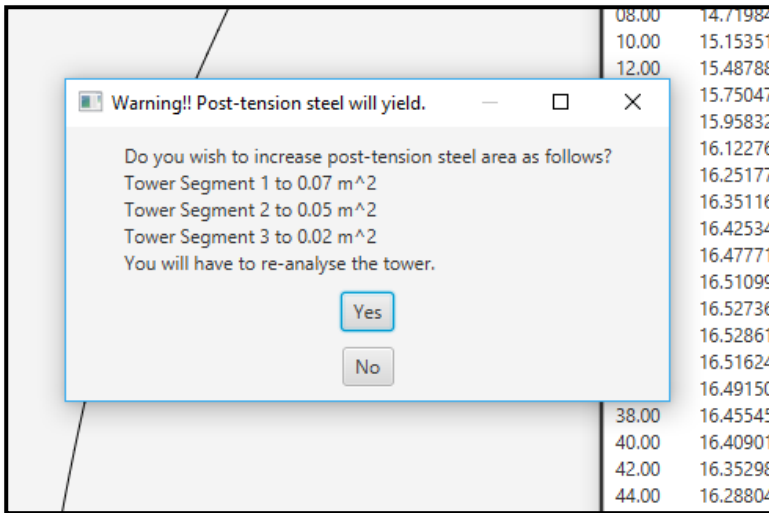


Figure 9.9: Illustration of warning message along with suggestions on the amount of post-tension steel required to avoid yielding

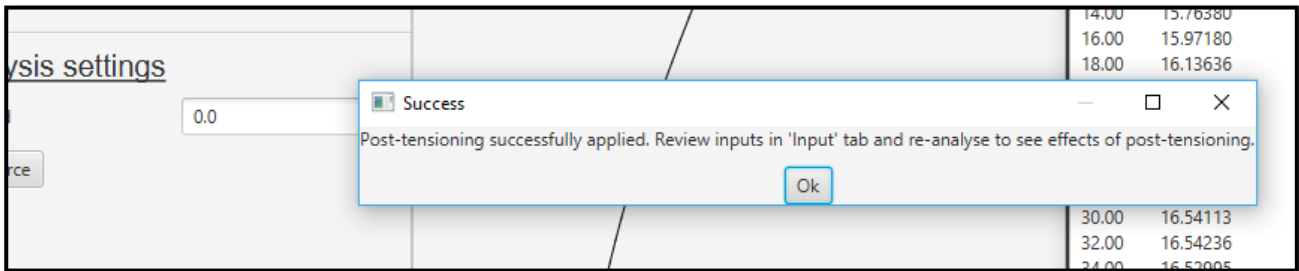


Figure 9.10: Illustration of success message after the post-tension forces have successfully been applied to the tower

Figure 9.10 illustrates the success message after the required post-tension force has been calculated and an adequate amount of post-tension steel has been provided so that no yielding will occur. The post-tensioning input can once again be reviewed and edited by navigating to the input-tab. To analyse the WTG tower while including the effects of the post-tensioning, click on the “Perform Analysis!”-button once more. The analysis output window will once again be displayed with a summary of the amount of post-tension steel provided, as well as the post-tension force applied, in each tower segment.

# Chapter 10: Conclusions and recommendations

## 10.1 Summary

This study conducts a short literature review on the transportation difficulties associated with tall wind turbine towers. The use of concrete towers is motivated as alternative to the traditional tubular steel tower. The literature review also emphasises the impracticality of using sophisticated FEM software to model and analyse wind turbine towers in the work environment. Specifically, standard FEM software is too costly and time consuming to be useful in the preliminary design stage and/or the optimisation of tower parameters such as the diameter, wall thickness, etc.

A simplified FE model, specifically designed to analyse wind turbine towers, is suggested. This model consists of 4DOF beam elements along the height of the tower. Although a simplified FE model is used, the complexity of the tower is captured by the cross section analysis methodology. The cross section analysis methodology is integrated with the Moment Area Method and Direct Stiffness (Matrix) Method. In doing so, geometric and physical (material) nonlinearities are considered during the structural analyses. The cross section analysis methodology is also extended to consider the effects of internal grouted post-tensioning applied to a concrete WTG tower.

Various design codes and guidelines are presented, which are associated with the determination of wind loads on a WTG tower. A suitable approach is then decided on and implemented for this study.

Software is designed to create a FE model of a wind turbine generator and perform modal and full structural analyses. To simplify the use of the software, a graphical user interface (GUI) is developed. The GUI is designed with the intent to aid the user during the model setup, adding loads to the model, performing analyses and generating output. Using the GUI, tests are conducted for verification purposes, as well as to compare different analysis techniques.

## 10.2 Conclusions

The cross section analysis methodology implemented for this study is verified in Chapter 4. This is achieved by duplicating an example of a cross section model and its associated set of moment-curvature diagrams, which are obtained from literature. Similar moment-curvature diagrams are obtained using the cross section analysis methodology implemented for this study, even though slightly different approaches are followed.

In Chapter 5, the accuracy of the FEM modal analysis is verified by comparing it to existing FEM software. The implemented FEM modal analysis is found to yield similar results compared to existing software, especially at lower mode shapes and frequencies, which are normally of greater importance.

It is found in Chapter 6 that by following the guidelines proposed by IEC 61400-1 in conjunction with ASCE 7-10, important aspects associated with calculating external design wind pressures on tall WTG towers, are all considered.

The Moment Area and Stiffness methods are verified in Chapter 7. It is found that the implemented methodology yielded tower tip deflections within 1% of the output generated by existing commercial FEM software, known as Prokon. It is also found that the implemented analysis techniques, when geometric and physical nonlinearities are considered, performed adequately. This is verified by the implemented techniques generating essentially the same deflections compared to analytical methods, as well as deflections generated by Abaqus.

The main finding of this study is that by developing software specific to WTGs, the efficiency of the processes associated with the model setup and analysis are significantly increased. The model setup and analysis processes, which could take weeks using sophisticated general purpose FEM, is reduced to minutes when using custom WTG software. This makes optimisation of the tower design possible, which is important given the fact that a large number of the same tower may be built for a typical wind farm.

### 10.3 Recommendations

The effects of the foundation and underlying soil parameters are not considered during this study. As mentioned in Chapter 5, the assumption of a fixed base could overestimate frequencies by 20% in extreme cases. Although it is conservative in terms of the base moment and internal stresses to assume a fixed base, the deflections could be underestimated during structural analyses.

It is thus recommended that a model of the WTG foundation should be developed and integrated with the software developed in this study. Currently, it seems sensible that the foundation and tower models should be developed independently. An algorithm could then be developed that could integrate the two models. An iterative approach, similar to that implemented to calculate the final restoring moment in Section 8.2.2, could be implemented to calculate the final base moment. In this way, the simplicity associated with the WTG tower model implemented in this study can be maintained, while more realistic analysis results can be obtained.

Due to the speed of the developed software, potential exists to extend the functionality of the software to optimise the WTG tower design. The analysis that only considers linear material and geometric properties would be ideal for optimisation purposes, as this analysis takes a fraction of a second to perform.

# References

- ACCIONA Energy, 2016. *Major projects > GOUDA WIND FARM*. [Online]  
Available at: <http://www.acciona-energia.com/areas-of-activity/wind-power/major-projects/gouda-wind-farm/>  
[Accessed 15 August 2016].
- ACI 307-98, 1998. *American Concrete Institute 307-98: Design and Constuction of Reinforced Concrete Chimneys*: American Concrete Institute.
- ACI 318, 2011. *Building Code Requirements for Structural Concrete*: American Concrete Institute.
- ASCE 7-10, 2010. *Minium Design Loads for Buildings and Other Structures*, Virginia: American Society of Civil Engineers.
- ASCE/AWEA, 2011. *Recommended Practice for Compliance of Large Land-based Wind Turbine Support Structures*, Washington, DC: American Wind Energy Association.
- Behfarnia, K., 2009. *THE EFFECT OF TENSION STIFFENING ON THE BEHAVIOUR OF REINFORCED CONCRETE BEAMS*, Isfahan: Isfahan University of Technology.
- BridgeArt.net, 2016. *Moment area method*. [Online]  
Available at: <http://www.bridgeart.net/topics/moment-area-method>  
[Accessed 13 November 2015].
- Consolis Hormifuste, 2011. *Precast Concrete Towers and Foundations: A Huge Market Coming Ahead*. Presentation at Danish Concrete Association (DBF): Beton Til Vindmøller (Concrete for Wind Turbines) Conference. URL: <http://www.slideshare.net/slides/eoi/jaime-de-rbago-precaster-concrete-wind-turbine-and-offshore-foundations-a-huge-market-coming-ahead>, s.n.
- Cook, B., 2016. *Techniques used to construct the towers of the Gouda Wind Facility* [Interview] (12 September 2016).
- Cremer media reporters, 2015. *138 MW Gouda wind farm enters commercial operations*. [Online]  
Available at: [http://www.engineeringnews.co.za/article/138-mw-gouda-wind-farm-enters-commercial-operations-2015-09-08/rep\\_id:4136](http://www.engineeringnews.co.za/article/138-mw-gouda-wind-farm-enters-commercial-operations-2015-09-08/rep_id:4136)  
[Accessed 15 August 2016].
- D.H. Blattner & Sons Inc, 2003. *A Self-Erecting Method for Wind Turbines. Phase1: Feasibility and Preliminary Design.*, Avon: D.H. Blattner & Sons, Inc..
- DCD Mining and Energy, 2016. *DCD Mining and Energy: DCD Wind Towers*. [Online]  
Available at: <http://www.dcd.co.za/miningandenergy/DCDWindTowers.aspx>  
[Accessed 15 August 2016].

Deutsches Institut für Bautechnik (DIBt), 2004. *Richtlinie Windenergieanlagen. Einwirkungen und Standsicherheitsnachweise für Turm und Gründung [wind turbine guideline - actions on and stability analyses for tower and foundation]*, Berlin: Deutsches Institut für Bautechnik (German Institute for Civil Engineering - DIBt).

Diana 9.4.4, 2012. *Diana's user manual (In Element Library Chapter 9)*, The Netherlands: TNO-DIANA.

DNV/Risø, 2002. *Guidelines for the Design of Wind Turbines*, Denmark: Det Norske Veritas, Riso National Laboratory.

Dvorak, P., 2016. *Building a better concrete wind turbine tower*. [Online]  
Available at: <http://www.windpowerengineering.com/construction/building-better-concrete-wind-turbine-tower/>  
[Accessed 19 August 2016].

EN 1991-1-4:2005, 2005. *EN 1991-1-4:2005: Eurocode 1: Actions on structures - Part 1-4: General actions - Wind actions*, Brussels: CEN (Comité Européen de Normalisation).

EN 1992-1-1:2004, 2004. *EN 1992-1-1:2004: Eurocode 2: Design of concrete structures - Part 1-1: General rules and rules for buildings*, Brussels: CEN (Comité Européen de Normalisation).

Enercon, 2015. *Enercon energy for the world*. [Online]  
Available at: [http://www.enercon.de/fileadmin/Redakteur/Medien-Portal/broschueren/pdf/en/ENERCON\\_Produnkt\\_en\\_06\\_2015.pdf](http://www.enercon.de/fileadmin/Redakteur/Medien-Portal/broschueren/pdf/en/ENERCON_Produnkt_en_06_2015.pdf)  
[Accessed 2016 September 2016].

Energy world, 2008. *Strategic alliances - Slipform Engineering*. [Online]  
Available at: <http://www.energyworldcorp.com/sa-seil.html>  
[Accessed 15 September 2015].

Fabcon, 2013. *Wind Turbine Towers*. [Online]  
Available at: <http://www.fabcon-usa.com/products/wind-turbinetowers/>  
[Accessed 12 July 2015].

Ghonim, M., n.d. *King Saud University*. [Online]  
Available at: <http://fac.ksu.edu.sa/sites/default/files/7-slip-form-construction.pdf>  
[Accessed 16 September 2015].

Giosan, I., n.d. *Vortex Shedding Induced Loads on Free Standing Structures*  
Available at:  
<http://citeseerx.ist.psu.edu/viewdoc/download?doi=10.1.1.582.3179&rep=rep1&type=pdf>.

GL, 2010. *Guideline for the Certification of Wind Turbines*, Hamburg: Germanischer Lloyd.

Grünberg, J. & Göhlmann, J., 2013. *BetonKalender*. Concrete Structures for Wind Turbines ed. Berlin: Ernst & Sohn.

IEC 61400-1:2005, 2005. *International Electrotechnical Commission 61400-1:2005: Wind Turbines - Part 1: Design Requirements*.

Jeffrey's bay wind farm, 2016. *Jeffrey's bay wind farm*. [Online]  
Available at: <http://jeffreysbaywindfarm.co.za/benefits/community-benefits/>  
[Accessed 16 September 2015].

Kahn, T., 2016. *SA has huge wind energy potential, says Nordex*. [Online]  
Available at: <http://www.bdlive.co.za/business/energy/2016/06/15/sa-has-huge-wind-energy-potential-says-nordex>  
[Accessed 15 August 2016].

LaNier, M.W.; PE Berger/ABAM Engineers Inc., 2004. *LWST Phase I Project Conceptual Design Study: Evaluation of Design and Construction Approaches for Economical Hybrid Steel/Concrete Wind Turbine Towers*, Colorado: National Renewable Energy Laboratory.

Manwell, J. F., McGowan, J. G. & Rogers, A. L., 2009. *Wind Energy Explained - Theory, Design and Application*. 2nd ed. Chichester: John Wiley & Sons Ltd.

Naval Studies Board; National Research Council, 1997. *Twenty-First Symposium on Naval Hydrodynamics*. Washington, D.C: National Academy of Sciences.

Nicholson, J. C., 2011. *Design of Wind Turbine Tower and Foundation Systems: Optimization Approach*, Iowa: University of Iowa.

NREL, 2014. *Analysis of Transportation and Logistics Challenges Affecting the Deployment of Larger Wind Turbines: Summary of Results*, Denver: National Renewable Energy Laboratory.

Piles Machinery, 2013. *Piles Machinery - Anchoring Products*. [Online]  
Available at: <http://www.piles-machinery.lv/en/anchoring-products/ischebeck-titan/for-designers>  
[Accessed 1 July 2016].

Power engineering international, 2001. *Valmont demonstrates innovative wind energy structure*. [Online]  
Available at: <http://www.powerengineeringint.com/articles/2001/12/valmont-demonstrates-innovative-wind-energy-structure.html>  
[Accessed 19 July 2016].

Prokon Software Consultants, 2016. *Prokon*. [Online]  
Available at: <https://www.prokon.com/>  
[Accessed 24 March 2016].

Renewable Energy World, 2002. *Self-Erecting Wind Turbine Designed for Remote Sites*. [Online] Available at: <http://www.renewableenergyworld.com/articles/2002/01/self-erecting-wind-turbine-designed-for-remote-sites-5785.html>

[Accessed 5 June 2016].

Robberts, J. M. & Marshall, V., 2010. *Analysis and Design of Concrete Structures*. s.l.:Nuclear Structural Engineering .

SANS 10160-3:2011, 2011. *South African National Standards 10160. Basis of structural design and actions for buildings and industrial structures. Part3: Wind actions*, Pretoria: South African Bureau of Standards (SABS).

Sharpley, N., 2013. *Windpower engineering and development*. [Online]

Available at: <http://www.windpowerengineering.com/featured/business-news-projects/whats-holding-up-tower-technology/>

[Accessed 15 September 2015].

South Africa info, 2014. *Investing in South Africa*. [Online]

Available at: <http://www.southafrica.info/business/investing/energy-140714.htm#.V9qfDih97IV>

[Accessed 3 September 2015].

South Africa info, 2016. *Investing in South Africa*. [Online]

Available at: <http://www.southafrica.info/business/investing/energy-140714.htm#.V9qfDih97IV>

[Accessed 15 September 2016].

Structural Systems, 2016. *Prestressing Technology*. [Online]

Available at: [www.structuralsystemsuk.com/downloads/PreStressing.pdf](http://www.structuralsystemsuk.com/downloads/PreStressing.pdf)

[Accessed 16 August 2016].

Techet, A., 2005. *Vortex Induced Vibrations*: Massachusetts Institute of Technology.

Trading Economics, 2016. *South Africa Unemployment Rate*. [Online]

Available at: <http://www.tradingeconomics.com/south-africa/unemployment-rate>

[Accessed 20 September 2016].

Turbines.co.za, 2016. *Wind Farms in South Africa*. [Online]

Available at: <http://www.turbines.co.za/wind-farms/wind-farms-in-south-africa/>

[Accessed 29 May 2016].

U.S. Department of Energy, 2015. *Enabling wind power nationwide*, Oak Ridge: U.S. Department of Energy.

Van Zyl, W. S., 2014. *Concrete Wind Turbine Towers in South Africa*, Stellenbosch: Stellenbosch University.

Van Zyl, W. S., 2016. *Modelling and analysis of concrete wind turbine towers in Diana* [Interview] (22 September 2016).

Von der Haar, C. & Marx, S., 2015. Design aspects of concrete towers for wind turbines. *Journal of the South African Institution of Civil Engineering*, 57(4), pp. 30-37.

Walls, R. S., 2016. *A beam finite element for the analysis of structures in fire*, Stellenbosch: Stellenbosch University.

Way, A. C., 2014. *A study on the design and material costs of tall wind turbine towers in South Africa*, Stellenbosch: Stellenbosch University.

Way, A. C., 2016. *Modelling and analysis of wind turbine towers in Abaqus* [Interview] (21 September 2016).